ASSOCIATE EDITOR: PAUL INSEL

Turn On, Tune In, Turnover! Target Biology Impacts In Vivo Potency, Efficacy, and Clearance

Johan Gabrielsson and Stephan Hjorth

MedDoor AB, Gothenburg, Sweden (J.G.) and Pharmacilitator AB, Vallda, Sweden (S.H.)

Address correspondence to: John Gabrielsson, MedDoor AB, Engelbrektsgatan 5, 41127 Gothenburg, Sweden. E-mail: Professor.Gabrielsson@gmail.com

Disclaimer: This review examines open versus closed system ligand–target response models. The new ideas present the incorporation of free target and enzyme turnover as an additional independent component to ligand–target protein binding. This does not detract from the potential of the open system, in contrast to the closed, which is influenced by other factors, such as metabolic, post-target events, feedback, etc., and external (placebo) factors that may also have an impact on the pharmacological effect.

Abstract——Even though significant efforts have been spent in recent years to understand and define the determinants of in vivo potency and clearance, important pieces of information are still lacking. By introducing target turnover into the reasoning, we open up to further the understanding of central factors important to the optimization of translational dose–concentration–response predictions. We describe (i) new (open model) expressions of the in vivo potency and efficacy parameters, which embody target turnover, binding, and complex kinetics, also capturing full, partial, and inverse agonism and antagonism; (ii) a detailed examination of open models to show what potency and efficacy parameters have in common and how they differ; and (iii) a comprehensive literature review showing that target turnover rate varies with age, species, tissue/subregion, treatment, disease state, hormonal and nutritional state, and day–night cycle. The new open model expression, which integrates system and drug properties, shows the following. Fractional turnover rates rather than the absolute target or ligand–target complex expression determine necessary drug exposure via in vivo potency. Absolute ligand–target expression determines the need of a drug, based on the transduction ρ and in vivo efficacy parameters. The free enzyme concentration determines clearance and maximum metabolic rate. The fractional turnover rate determines time to equilibrium between substrate, free enzyme, and complex. The properties of substrate, target, and the complex demonstrate nonsaturable metabolic behavior at equilibrium. Nonlinear processes, previously referred to as capacity- and time-dependent kinetics, may occasionally have been disequilibria. Finally, the open model may pinpoint why some subjects differ in their demand of drug.

Significance statement——Understanding the target turnover is a central tenet in many translational dose–concentration–response predictions. New open model expressions of in vivo potency, efficacy parameter, and clearance are derived and anchored onto a comprehensive literature review showing that target turnover rate varies with age, species, tissue/subregion, treatment, disease, hormonal and nutritional state, day–night cycle, and more. Target turnover concepts will therefore significantly impact fundamental aspects of pharmacodynamics and pharmacokinetics, thereby also the basics of drug discovery, development, and optimization of clinical dosing.

I. Introduction

In vivo potency guides at which plasma exposure a drug is active, and clearance carries information about how efficiently the body removes the medicine. Combined, they define the clinically efficacious dose range. Variability in drug potency and clearance is thus of key importance to ascertain proper dosing and assessment of risk and needs to be meticulously tested and documented in drug application filings. In recent years, these topics have started to gain traction in basic research and drug discovery, yet the understanding of components essential to the definition of in vivo potency, efficacy parameter, and clearance still remains incomplete.

A. What Is the Problem?

Traditionally, in vivo potency estimates are projected from in vitro target affinity and clearance from enzymatic breakdown data. Drug disposition processes are likewise assayed in vitro and in preclinical species and viewed as more or less fixed uptake and/or elimination elements, in line with conventional basic mass action concepts. Importantly, however, these measures are derived and modeled from closed systems, typically at constant total protein expression levels, thus in sharp contrast to the inherent dynamics of a living system.

Proteins in the body are continuously produced and degraded, with turnover half-lives ranging from a few minutes to several days, months, or even longer in vivo

ABBREVIATIONS: ACh, acetylcholine; AChE, acetylcholine esterase; ASA, acetylsalicylic acid; C, total plasma concentration; C_u, unbound (free) plasma concentration; $Cl_{(S)}$, clearance of substrate; CNS, central nervous system; COX-1, cyclooxygenase-1; D1R, D1 receptors; D2R, D2 receptors; E, free enzyme concentration; E_0, free baseline enzyme concentration; E_{max}/I_{max}, efficacy parameter for in vivo maximum drug-induced effect (stimulatory effects/inhibitory effects) fitting the Hill equation including baseline; EC_{50}, in vivo potency (stimulatory effects); EEDQ, ethoxycarbonyl-2-ethoxy-12-dihydroquinoline; E_{ss}, free enzyme concentration at equilibrium (steady state); ES_{ss}, free enzyme-substrate complex concentration at equilibrium (steady state); E(t), free enzyme concentration as a function of time (disequilibrium); FFA, free fatty acid; GABAA, GABA type A; GPCR, G-protein coupled receptors; GSECR, gamma secretase; k_{cat}, fractional catabolic rate constant; k_{deg}, fractional turnover rate (also known as k_{out}); K_d, dissociation constant; $k_{e(RL)}$, ligand–target complex elimination rate constant; k_{irr}, second-order irreversible loss rate constant; K_m, Michaelis–Menten constant; k_{off}, dissociation rate constant of ligand–target complex; k_{on}, association rate constant of ligand–target complex; k_{syn}, turnover rate constant of target; L, ligand concentration; LFTR, ligand facilitated target removal; LPS, lipopolysaccharide; L_{ss}, ligand concentration at steady-state; MABEL, minimal anticipated biological effect level; MAO-B, monoamine oxidase-B; MM, Michaelis–Menten; NiAc, nicotinic acid; NSAID, nonsteroidal anti-inflammatory drug; NT, nortriptyline; PD, pharmacodynamic; PK, pharmacokinetic; PPI, protonpump inhibitor; Q_i, blood flow through the eliminating organ; R, target concentration; RL, ligand–target complex concentration; R_{ss}, target concentration at steady-state; RL_{max}, maximum ligand–target complex concentration; RL_{ss}, ligand–target complex concentration at steady-state; S_{ss}, substrate concentration at steady state; TMDD, target-mediated drug disposition; V, volume of distribution; $V_{max}(t)$, maximum elimination (metabolic) rate during disequilibrium; $V_{max}(0)$, maximum elimination (metabolic) rate at baseline; ρ, transduction parameter for conversion of a ligand–receptor complex concentration to a pharmacological response, unique for each compound, target, and response.

(Boisvert et al., 2012). The turnover rates vary greatly among different organs and tissues, nutritional status, time of day, between sexes, across species, and also depending on age and lifespan (for a review, see Waterlow, 1984). Fig. 1 schematically shows how turnover is addressed in this review.

Furthermore, the synthesis and degradation of drug and metabolic targets (k_{syn} and k_{deg} of receptor or enzyme protein) differ depending on the overall energy (heat) turnover in a particular species. In general, the smaller the species, the faster the loss of heat, and therefore the higher energy turnover to maintain a 37°C homeostasis (Adolph, 1949; Waterlow, 1984). Even more crucial from the individual patient perspective is that the disease and/or treatment context may significantly influence protein/target degradation k_{deg} (and synthesis k_{syn}) compared with normal healthy conditions. Examples include altered protein synthesis and degradation in fever or hyperinflammatory states (Waterlow, 1984; Fearon et al., 1988) or after chronic drug treatment (Pich et al., 1987). Factors like the aforementioned may give rise to systematic deviations when predicting drug in vivo potency and clearance from in vitro binding/metabolism data (Jansson-Lofmark et al., 2020). The insufficient power of applied methods is also a challenge to interspecies in vivo extrapolations of pharmacological and metabolic data (Gabrielsson et al., 2018b). This is a contrast to reductionist approaches that define/assess mechanisms of drug action with ligands, cells, or tissues (in vitro or ex vivo, and perhaps purified targets versus in vivo studies in experimental animals or humans.

B. What Is Lacking?

A more complete and mechanistic description of the determinants of potency, the efficacy parameter, and clearance properties is required to optimize predictions
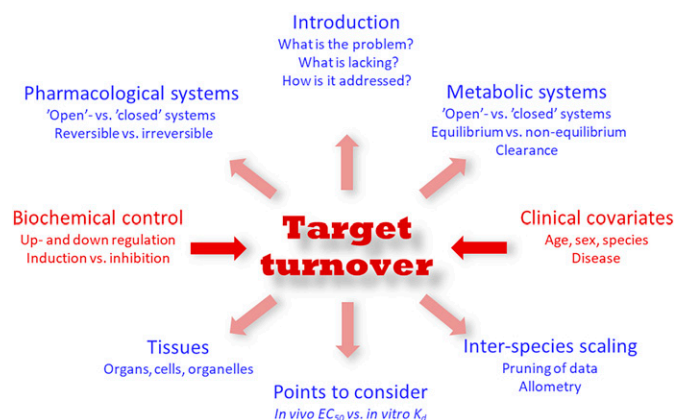
of in vivo pharmacologic effectiveness toward clinical use. Not least, there is a crucial need for further insight into and quantification of the impact of turnover rates of corresponding target protein entities. Thus, taken together, a greater focus on target biology properties relative to drug features (such as binding affinity) is warranted.

C. How Can We Address the Problem?

The time-dependent and varying turnover rates of target proteins across species are typically not captured by most contemporary in vitro assay systems or in preclinical profiling. Recently, we have therefore introduced new mathematical expressions of in vivo potency and the efficacy parameter derived in part from target-mediated drug disposition (TMDD) reasoning (Gabrielsson and Peletier, 2017; Gabrielsson et al., 2018a) and have shown how variations in target synthesis and loss might impact pharmacodynamic (PD) variability (Gabrielsson et al., 2018a). The present account builds further on these ideas, expanding the open system concept and accompanying expressions to describe and consider the dynamics of in vivo potency–, efficacy-, and clearance-related parameters, with representative literature examples included to illustrate their impact. Among these, we discuss in particular drug target and metabolic enzyme turnover within the context of chronic treatment, aging, disease, and nutritional state influences. Fig. 2 illustrates schematically the background and key differences between closed and open drug target and metabolic systems along with their corresponding parameters. By *open*, we mean that all major determinants of the pharmacological response and/or of clearance have input (synthesis, dosing, binding) and loss (elimination, dissociation, transport, clearance) terms.

II. Pharmacologic Systems and Ligand–Target Interactions

While in vitro ligand–target binding and functional preparations remain useful for the purpose of identifying fundamental drug properties, the impact of the target on drug responses in an integrated living organism can only be addressed by an open in vivo system approach. Ranking of test compounds based on their in vitro binding affinities (K_d or in vitro potencies) and preclinical in vivo profiles is standard practice in the drug discovery context. However, in the in vivo situation, several factors (see the Introduction) pertaining to the synthesis and degradation rates (turnover) of corresponding target proteins may significantly influence the pharmacodynamic outcome of a drug.

To this end, turnover models and target turnover have been introduced to rejuvenate modeling and pharmacodynamic analysis, thereby expanding the

Fig. 1. Schematic outline of various topics related to turnover concepts in this review. The strategy is to cover turnover from both a pharmacological and a metabolic (clearance) point of view. The review also covers how turnover is controlled and what potential covariates (age, sex, species, disease) are related to the topic. The review covers how turnover may differ across different tissues and proposes means for interspecies scaling. Finally, a set of points to consider related to experimental design, interpretation of data, and translational issues are listed.
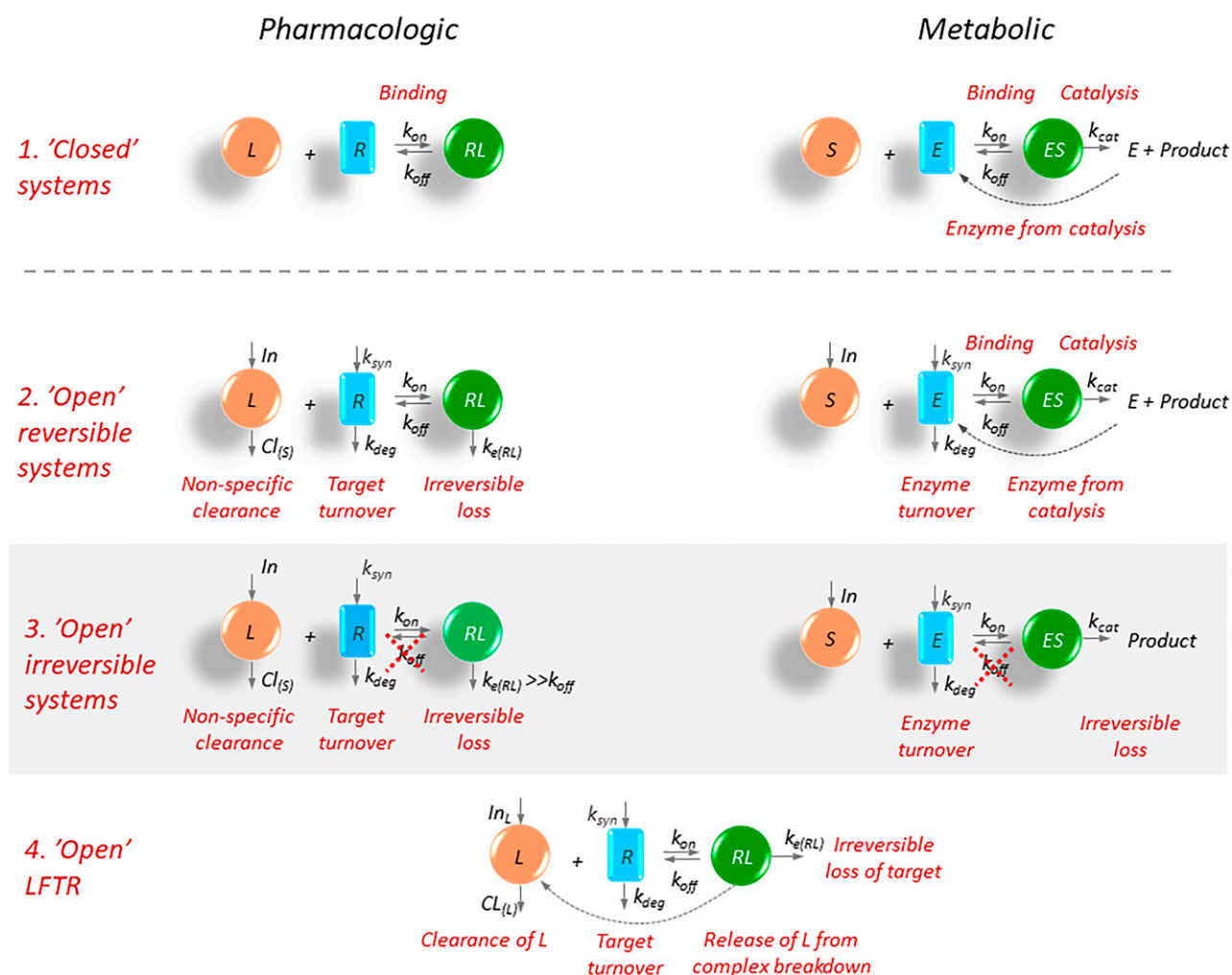
Fig. 2. (row 1) Closed pharmacodynamic (left) and metabolic (right) systems. The closed system presented in most pharmacology text books assumes a constant pool of total target (left plot, free target R (blue box representing, for example, the concentration of free binding sites) and ligand–target complex bound RL) or a constant pool of total enzyme (right plot, free enzyme E and substrate-enzyme complex bound ES). The free enzyme is regenerated after the catalytic formation of product P from ES. R, k_{on}, k_{off}, and RL represent free target, second-order complex formation rate constant, first-order complex disintegration rate constant, and complex concentration, respectively. The k_{cat} parameter denotes the first-order rate constant of the catalytic process. (Row 2) The open system has an ongoing zero-order production k_{syn} and first-order loss k_{deg} of target protein (blue box representing, for example, the concentration of free binding sites at the receptor on the left and free enzyme concentration on the right). In, L, and Cl(s) denote the input rate of ligand, ligand concentration, and ligand clearance, respectively. The k_{syn}, k_{deg}, and $k_{e(RL)}$ parameters are target synthesis and target degradation rate and the ligand–target complex elimination constants. (row 3). The open systems that are used for capturing irreversible mechanisms (row 4). The open system for LFTR, where the target is degraded and the ligand is returned to its free pool. Right-hand column: (metabolic systems) schematic comparisons of the closed (row 1) and open (rows 2–4) enzymatic systems. In and S denote the input rate of substrate and substrate concentration, respectively. k_{syn}, E, and k_{deg} are enzyme protein synthesis rate, free enzyme concentration, and enzyme degradation rate constant, respectively. k_{on}, k_{off}, ES, and k_{cat} represent second-order substrate–enzyme complex formation rate constant, first-order complex disintegration rate constant, substrate–enzyme complex, and the catabolic rate constant, respectively.

quantitative assessment of response-time courses (Nagashima et al., 1969; Dayneka et al., 1993; Gabrielsson and Peletier, 2017). In the current account, we further extend and develop this analysis with a comprehensive review of examples from the literature. Within this context, we exemplify and discuss the importance of integrating drug and target properties in reversible and irreversible pharmacodynamic systems. This provides a background to the origin of the corresponding expressions and an illustration of how changes in target turnover may affect the in vivo drug-induced response outcome. It should be noted that specific target turnover (or half-life) may be

different from the pharmacodynamic half-life (or in vivo biologic half-life, biologic half-life) as assessed from biomarker information (although related to target turnover) due to distributional or transductional delays or feedback being the rate-limiting step in vivo.

A. In Vivo Open Systems; Reversible vs. Irreversible Ligand–Target Interactions

A reversible system can exhibit both bidirectional ligand–target binding interactions and removal of the ligand–target complex. In a living organism (i.e., an in vivo open system) situation, these three key

components (free ligand L, free target receptor R, and target receptor–ligand complex RL) fluctuate over time. This is described by eq. 1, where the dynamics of the free concentrations of L (drug) and of R (i.e., free binding sites) depend on drug input In and first-order nonspecific clearance of L and on the zero-order turnover rate k_{syn} and first-order fractional turnover rate k_{deg} of free target R (Fig. 2, second row, left), respectively. The changes in RL are governed by k_{on} and k_{off} for the L in question (the second-order association and first-order dissociation rate constant, respectively) and $k_{e(RL)}$, which is the first-order rate constant for irreversible loss via all relevant routes of complex removal (such as degradation, internalization, interstitial fluid turnover, etc.).

$$
\begin{cases}
\dfrac{dL}{dt} = \dfrac{In}{V} - \dfrac{Cl_{(L)}}{V} \cdot L - k_{on} \cdot L \cdot R + k_{off} \cdot RL \\[2mm]
\dfrac{dR}{dt} = k_{syn} - k_{deg} \cdot R - k_{on} \cdot L \cdot R + k_{off} \cdot RL \\[2mm]
\dfrac{dRL}{dt} = k_{on} \cdot L \cdot R - k_{off} \cdot RL - k_{e(RL)} \cdot RL
\end{cases} \tag{1}
$$

Thus, as evident from the previous discussion, the overall pharmacodynamic outcome in the in vivo context will depend not only on drug (ligand; i.e., L) levels versus input and elimination thereof (Cl) as well as affinity (i.e., k_{off}/k_{on}) for its target R but also on the actual levels, production (k_{syn}), and removal (k_{deg}) of R and of the target–ligand complex RL. From an in vivo biomarker or clinical response perspective, three key stages in the formation of a pharmacological effect may be discerned: (i) the input and loss of the drug, which is only captured by the open model (Fig. 2, row 2); (ii) the ligand–target binding process (k_{off}/k_{on}), captured by both the closed in vitro and open in vivo models; target turnover k_{deg}; and complex kinetics $k_{e(RL)}$, captured exclusively by the open in vivo model (Fig. 2, rows 1 and 2); and (iii) transduction/conversion triggered by the target–ligand complex RL to a measurable in vivo (biomarker or clinical) response via a series of physiologic and mechanistic events (e.g., amplification, feedback, synergy, buffering, parallel intertwined neuronal circuit processes), described by the ρ parameter [clinical efficacy is the maximum desired target-elicited effect in the presence of a composite of integrated buffering, amplifying, and compensatory processes. Importantly, clinical efficacy is also limited to what is possible to attain regarding a specific functional response without jeopardizing patient health (safety, tox)]. (see II. Pharmacologic Systems and Ligand–Target Interactions)

At equilibrium (steady state), the relationships of free target R_{ss} (eq. 2, top line) and target–ligand complex RL_{ss} (second line) as functions of drug L_{ss}, and the in vivo potency expressions EC_{50} (third line) are described in eq. 2 (Gabrielsson and Peletier, 2017, for a detailed derivation of the equilibrium relationships from the differential equation system in eq. 1). Note that the open in vivo model derived from eq. 1 will predict the same concentration EC_{50} for a half-maximal drug-induced response of both free ligand L_{ss} and the ligand–target complex RL_{ss} at steady state (eq. 2). RL_{ss} is indirectly predicted from free ligand L_{ss} via the nonlinear term in eq. 2 (second line). However, an important observation is that the pharmacological response at steady state can be driven by a nonlinear function of free ligand concentration L_{ss}, and the model parameters E_0, E_{max}, and EC_{50} (eq. 5, bottom line), which is numerically robust, conceptually pragmatic, and transparent from a translational point of view.

$$
\begin{cases}
R_{ss} = \dfrac{k_{syn}}{k_{deg}} \cdot \dfrac{EC_{50}}{L_{ss} + EC_{50}} = R_0 \cdot \left(1 - \dfrac{L_{ss}}{L_{ss} + EC_{50}} \right) \\[3mm]
RL_{ss} = \dfrac{k_{syn}}{k_{e(RL)}} \cdot \dfrac{L_{ss}}{L_{ss} + EC_{50}} = R_0 \cdot \dfrac{k_{deg}}{k_{e(RL)}} \cdot \dfrac{L_{ss}}{L_{ss} + EC_{50}} \\[3mm]
\quad EC_{50} = \dfrac{k_{deg}}{k_{e(RL)}} \cdot \dfrac{k_{off} + k_{e(RL)}}{k_{on}} = \dfrac{k_{deg}}{k_{e(RL)}} \cdot K_m \\[3mm]
\qquad\qquad K_d = \dfrac{k_{off}}{k_{on}}
\end{cases} \tag{2}
$$

As seen from eq. 2, the open system expressions now contain both free target turnover (k_{deg}) and complex kinetics ($k_{e(RL)}$) in addition to drug-target binding properties (k_{on}, k_{off}). Target turnover and complex kinetics are in vivo properties, therefore making eq. 2 (third row) more versatile for translation across different species, particularly when species-specific terms for these parameters have been defined. The generic form of the open in vivo potency expression EC_{50} in eq. 2 allows predictions of efficacious concentrations of agonists, antagonists, inverse agonists, and enzyme inhibition provided k_{on}, k_{off}, k_{deg}, and $k_{e(RL)}$ are known. The bottom row in eq. 2 shows the expression of the ligand–target dissociation constant K_d. A graphical presentation of the in vivo potency EC_{50} expression in eq. 2 is shown in Fig. 3, A–D).

As shown in the contour plots of in vivo potency EC_{50} (Fig. 3), changes in k_{deg} and k_{off} (keeping $k_{e(RL)}$ set to 0.1 for comparisons around which k_{off} is varying) impact in vivo potency EC_{50}. Note the apparent plateau (ceiling effect) when $k_{off} < k_{e(RL)}$ (Fig. 3, A). In this situation, EC_{50} may be approximated by k_{deg}/k_{on} (irreversible system) and is still sensitive to changes in k_{deg}. For comparison, Fig. 3, B shows the influence of changes in k_{deg} and $k_{e(RL)}$ (with k_{off} set to 0.1) on in vivo potency EC_{50}. In contrast, when $k_{off} > k_{e(RL)}$, EC_{50} may be approximated with $(k_{deg}/k_{e(RL)}) \times (k_{off}/k_{on})$ (reversible system) and is still sensitive to changes in k_{deg}. Fig. 3, C and D, show the same simulations of eq. 2 but with EC_{50} presented on a log scale.

The exponential increase in in vivo potency EC_{50} stemming from concurrent higher values of k_{deg} and smaller values of $k_{e(RL)}$ (reversible system) is because of the multiplicative effect of changes in k_{deg} and $k_{e(RL)}$. The graphical presentation of in vivo potency
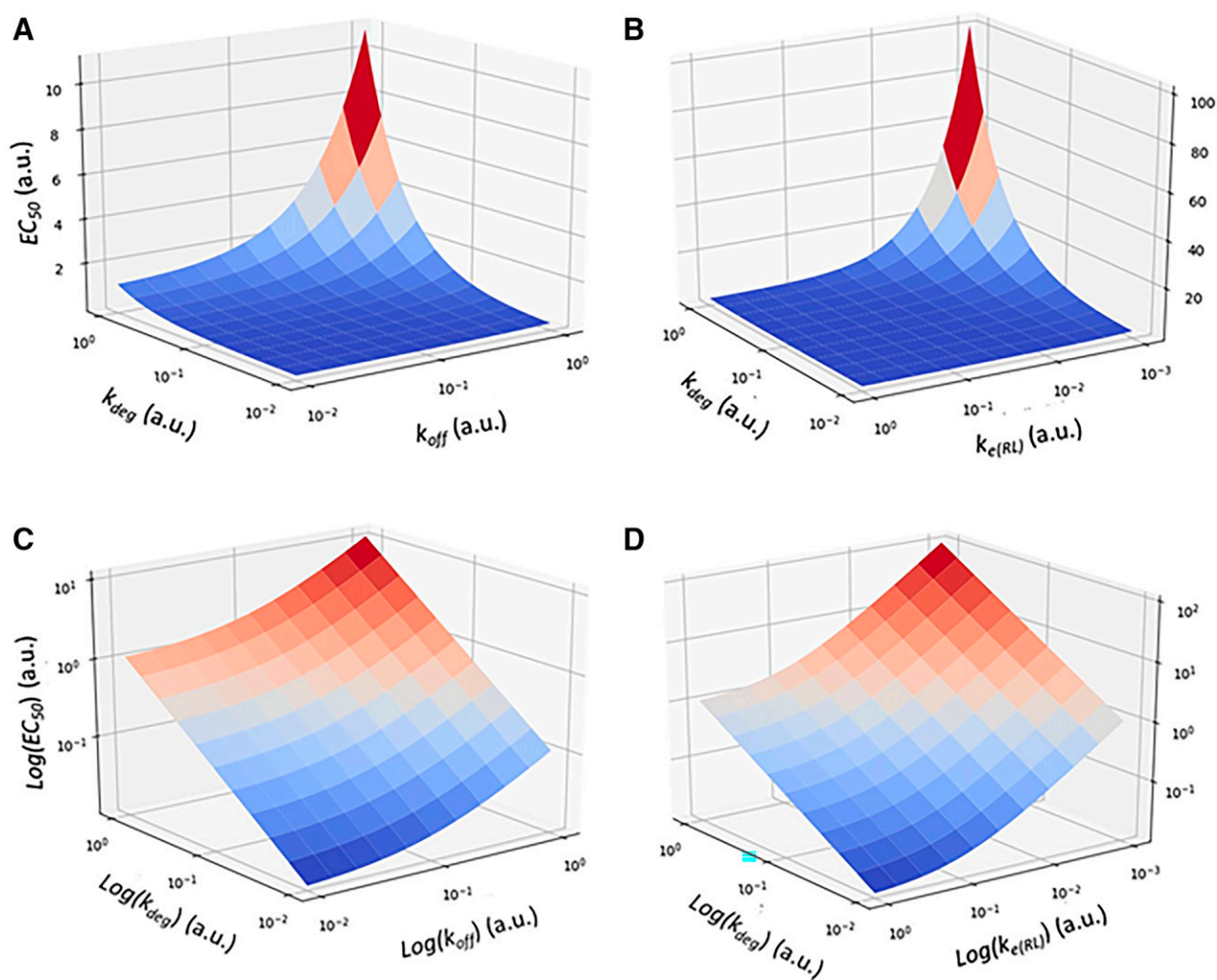
Fig. 3. Impact of changes in the parameters of in vivo potency in eq. 2. (A) In vivo potency vs. target degradation rate k_{deg} and complex dissociation rate k_{off} constants. The complex elimination rate constant $k_{e(RL)}$ is set to 0.1 time^{-1}. In vivo EC_{50} moves toward infinity when $k_{e(RL)}$ approaches zero. The system approaches an irreversible behavior when $k_{e(RL)}$ is (much) greater than k_{off}. (B) In vivo potency vs. target degradation rate k_{deg} and complex elimination rat $k_{e(RL)}$ constants. The complex dissociation rate constant k_{off} is set to 0.1 time^{-1}. In vivo EC_{50} moves toward infinity when $k_{e(RL)}$ approaches zero. The system approaches an irreversible behavior when $k_{e(RL)}$ is (much) greater than k_{off}. EC_{50} is plotted on a linear scale in (A) and (B) and on a logarithmic scale in (C) and (D). The multiplicative effect of changes in k_{deg} and $k_{e(RL)}$ are shown in (B) and (D) and therefore requires a larger range of scale.

EC_{50} in eq. 2 thus (i) distinguish between irreversible and reversible systems; (ii) demonstrates individual contributions of k_{off}, $k_{e(RL)}$, and k_{deg}; (iii) illustrates determinants of necessary exposure; (iv) gives the complex-to-free target ratio in k_{deg}-to-$k_{e(RL)}$; and (v) demonstrates that target turnover k_{deg} is always an important factor of EC_{50} and, hence, duration of pharmacological response. A typical example of the latter is proton-pump inhibitors, where the duration of action (suppression of acid secretion) is governed by the de novo synthesis ($t_{1/2kdeg}$) of proton pumps rather than by the (irreversible) drug–target interaction per se. Other examples include COX-1- and MAO-B- inhibitors. Eq. 2 is therefore applicable to both small (Smith et al., 2018) and large (Gabrielsson et al., 2018a) molecule pharmacology.

As demonstrated in the previous discussion, in vivo potency thus contains information about the route of target elimination, either via direct catabolism k_{deg} or internalization $k_{e(RL)}$ as a ligand–target complex. Increasing ligand concentrations pushes equilibrium further toward the complex formation. The higher the ligand concentration, the more target is eliminated via the ligand-complex route ($k_{e(RL)}$). Hence, the higher the potency (i.e., the lower its numerical value), the lower the necessary ligand (drug) concentration needed to drive target elimination via the complex route. At a ligand concentration equal to EC_{50}, when the ligand impacts the free target and complex equally (50%), the steady-state concentrations of free target R_{ss} and complex RL_{ss} are expressed as in eq. 3.

$$\begin{cases} R_{ss} = \dfrac{k_{syn}}{k_{deg}} \cdot 0.5 \\[2mm] RL_{ss} = \dfrac{k_{syn}}{k_{e(RL)}} \cdot 0.5 \\[2mm] \dfrac{RL_{ss}}{R_{ss}} = \dfrac{k_{deg}}{k_{e(RL)}} \end{cases} \qquad (3)$$

As evident from eq. 3 (bottom row), the steady-state concentration ratio of RL_{ss}-to-R_{ss} is governed by the $k_{deg}/k_{e(RL)}$ ratio. Therefore, this makes said parameters interesting also from a potency point of view (eq. 2). The intimate interdependence of pharmacology- and clearance-associated target dynamics factors is illustrated in Fig. 2 and by the accompanying eqs. 1 to 3.

In certain situations, the ligand binds to the target, serves as a facilitator of target removal (Chaparro-Riggers et al., 2012) and then returns to the free ligand pool. It is based on the catch and release mechanism in which the ligand is caught by the target and subsequently released when the ligand–target complex is cleared, resulting in the loss of the target (Sarkar et al., 2002). The conceptual model for this process is referred to as ligand-facilitated target removal (LFTR), which may be viewed as a form of ligand recycling (Peletier et al., 2021). A similar process is involved in the mechanism of tocilizumab (Igawa et al., 2010), where a fraction of the ligand is returned to the free ligand pool, and the remaining fraction is cleared via irreversible loss of complex. Other illustrative examples of LFTR include the selective estrogen receptor degrader group of agents (e.g., giredestrant) (Liang et al., 2021) and PCSK9 inhibitors (Hess et al., 2018), as well as an emerging number of drug classes aimed, for example, at cancer indications (Mullard, 2021).

B. Assessment of Target Turnover Under Different Conditions

It is clear from the reasoning in the previous sections that states with alterations of the target turnover will affect the observed in vivo potency of a drug. In the current account, we have chosen to focus on G protein-coupled receptor (GPCR) and enzyme targets, as these classes together dominate human targets for drugs in clinical use (Rask-Andersen et al., 2011).

While over time, a number of novel methodological approaches to assess target turnover have emerged (e.g., pulse–chase, proteomic analyses, protein synthesis inhibitors), it appears that these have mostly been applied in a closed system context and have different pros and cons (Morey et al., 2021). Regardless of the assessment method, it is also evident that the lifetimes of proteins vary widely between types and entities, depending on, for example, cellular environment and composition, subcellular fraction, function (e.g., scaffolding, structural, synaptic), and abundance in different pathways, organelles, tissues, organs, or cells (Price et al., 2010; Dörrbaum et al., 2018; Fornasiero et al., 2018). More recent methodological paths include developments in the organs-on-a-chip area (Sosa-Hernandez et al., 2018), which may potentially further extend information gathering relevant to assess drug targets and pharmacokinetic (PK) features, but still within a closed system frame.

Notwithstanding the previous discussion, with few exceptions, we find very little information derived from such methodologies pertaining to GPCRs–targets to a therapeutically dominant class of drugs (Hauser et al., 2017; Sriram and Insel, 2018). For comparison, there is a relative abundance of target half-life data for the latter type of agents using irreversible drug inactivation methods followed by monitoring of the time course of receptor recovery in vivo. Therefore, this ample literature source represents a useful alternative approach to assess rates of target synthesis and degradation within the open system setting (the target recovery half-lives presented in Tables 1, 2, and 3 are used as an in vivo proxy that may also encompass processes other than de novo target synthesis and degradation). Agents used for the purpose include, for example, N-ethoxycarbonyl-2-ethoxy-1,2-dihydroquinoline (EEDQ) (Belleau et al., 1968; Hamblin and Creese, 1983), phenoxybenzamine (Nickerson and Goodman, 1947), benextramine (Bodenstein et al., 2005), bromoacetyl-alprenolol menthane (Pitha et al., 1982), and clocinnamox (Burke et al., 1994), as well as a number of different irreversible enzyme and transporter inhibitors (e.g., clorgyline, deprenyl, RTI-76).

The formation of permanent target complexes means that the normal recycling/trafficking process cannot impact k_{off}, as drug dissociation from the target does not occur under these conditions (Norman et al., 1987). Indeed, the protein synthesis inhibitor cycloheximide prevented the recovery of dopamine D2 receptors (D2R) after EEDQ treatment (Leff et al., 1984), in line with the view that the contribution from recycled target receptors was negligible. Therefore, the irreversible target inactivation approach gives direct and useful information on the actual rate of recovery derived from newly formed GPCR molecules, a view supported by reports on corresponding increases at the mRNA transcription level (Raghupathi et al., 1996a,b). In addition, most literature studies use antagonist agents to label and monitor receptor sites to follow the rate of recovery. This avoids the potential confounding of shifts between low- and high-affinity states of one and the same target protein, as antagonists are considered to label the entire population indiscriminately. Indeed, there are data to suggest that recovery rates followed by means of agonist- versus antagonist-labeled binding may not necessarily result in exactly the same figures (Nelson et al., 1986; Ribas et al., 1998).

1. Age vs. Target Turnover. It is well known that aging impacts drug dosing and responses (Tumer et al., 1992; Turnheim, 2003; Andres et al., 2019; Thürmann, 2020) (Table 1). The inevitable gradual decay of bodily function from adulthood to older age results in altered PK (Rowland and Tozer, 2011) but also PD characteristics. Age-related changes in drug uptake, distribution, metabolism, and elimination processes thus often necessitate adjustments relative to standard prescription dosages (Andres et al., 2019). Several age-elicited physiologic function modifications likewise contribute to this (Tumer et al., 1992). However, less is known regarding shifts in target/transduction, circuit, and system homeostatic properties that may also influence the pharmacological treatment outcome in older as compared with younger adults (Levy, 1998).

Studies using irreversible target inactivation strategies in the rat and mouse suggest that turnover rates for receptor proteins normally become slower with age across targets and tissues alike (the possible exception is hippocampal 5-HT1A sites) (Keck and Lakoski, 1996a, 2000), tentatively due to decreasing

plasticity (e.g., (Dorszewska, 2013; Mateos-Aparicio and Rodriguez-Moreno, 2019) in older compared with young subjects (Table 1). Thus, for example, following the annihilation of dopamine D2 receptors (D2R), the recovery rate is roughly 70% slower in senescent/aged as compared with young and mature rats (Leff et al., 1984; Norman et al., 1987; Kula et al., 1992); likewise, recovery half-life of striatal D1 receptors (D1R) after EEDQ was approximately65% slower in senescent than in mature rats (Battaglia et al., 1988). In fact, the rat cerebral D1R and D2R appear to follow an almost identical log-linear correlation trajectory between age and turnover rate, with gradually slower rates from young to senescent animals (Fig. 4). Similar observations have also been reported from rat studies of α- and β-adrenoceptor subtypes in heart, lung, and brain tissue regions (Pitha et al., 1982; Zhou et al., 1984) and of 5-HT2 (Battaglia et al., 1987) and mouse GABAA receptors (Miller et al., 1991a) in different brain subregions. This is in accord with the key role of altered protein synthesis and degradation with age and senescence (Ryazanov and

TABLE 1
Target half-life vs. age in the rat or mouse (GABAA receptor/Bz site)

Target	Inactivating treatment	Organ/ tissue	Subregion	Age, months	Recovery half-life	Reference
Dopamine D1 receptor	EEDQ	Brain	Striatum	4	3.5 d (84 h)	(Battaglia et al., 1988)
	EEDQ	Brain	Striatum	4	3.1-3.3 d (74-80 h)	(Giorgi et al., 1991)
	EEDQ	Brain	Striatum	23	6.1 d (146 h)	(Giorgi et al., 1992)
	EEDQ	Brain	Striatum	28	5.8 d (138 h)	(Battaglia et al., 1988)
	EEDQ	Brain	N. accumbens	4	2.7 d (64 h)	(Giorgi et al., 1991; Giorgi et al., 1992)
	EEDQ	Brain	N. accumbens	23	4.5 d (108 h)	(Giorgi et al., 1992)
	EEDQ	Brain	Subst. nigra	4	7.6-8.3 d (182-200 h)	(Giorgi et al., 1991)
	EEDQ	Brain	Subst. nigra	23	9.6 d (230 h)	(Giorgi et al., 1992)
	EEDQ	Eye	Retina	4	2.2-2.3 d (53-56 h)	(Giorgi et al., 1991)
	EEDQ	Eye	Retina	23	2.9 d (70 h)	(Giorgi et al., 1992)
Dopamine D2 receptor	EEDQ	Brain	Striatum	1	1.9 d (45 h)	(Leff et al., 1984)
	EEDQ	Brain	Striatum	4	3.3 d (79 h)	(Norman et al., 1987)
	EEDQ	Brain	Striatum	9	5.0 d (120 h)	(Norman et al., 1987)
	EEDQ	Brain	Striatum	9-12	5.0 d (119 h)	(Leff et al., 1984)
	EEDQ	Brain	Striatum	28	5.7 d (136 h)	(Norman et al., 1987)
Alpha1-adrenoceptor	PBZ	Brain	Cortex	3	7 d (168 h)	(Zhou et al., 1984)
	PBZ	Brain	Cortex	24	14 d (336 h)	(Zhou et al., 1984)
	PBZ	Brain	Hypothalamus	3	8 d (192 h)	(Zhou et al., 1984)
	PBZ	Brain	Hypothalamus	24	15 d (360 h)	(Zhou et al., 1984)
Alpha2-adrenoceptor	PBZ	Brain	Cortex	3	5 d (120 h)	(Zhou et al., 1984)
	PBZ	Brain	Cortex	24	20 d (480 h)	(Zhou et al., 1984)
Beta1-adrenoceptor	BAAM	Heart	—	1-2	approximately 3.8 d (approximately 90 h)[*]	(Baker and Pitha, 1982; Pitha et al., 1982)
	BAAM	Heart	—	28	approximately 13.3 d (approximately 320 h)[*]	(Baker and Pitha, 1982; Pitha et al., 1982)
Beta2-adrenoceptor	BAAM	Lung	—	1-2	approximately 10 d (approximately 250 h)[*]	(Baker and Pitha, 1982; Pitha et al., 1982)
	BAAM	Lung	—	28	approximately 16.7 d (approximately 400 h)[*]	(Baker and Pitha, 1982; Pitha et al., 1982)
5-HT1A receptor	EEDQ	Brain	Hippocampus	3	6.3 d (151 h)	(Keck and Lakoski, 2000)
	EEDQ	Brain	Hippocampus	approximately 6–12	1.8 d (43 h)	(Keck and Lakoski, 1996a)
	EEDQ	Brain	Hippocampus	22	2.2 d (53 h)	(Keck and Lakoski, 2000)
	EEDQ	Brain	Cortex	approximately 6–12	7.7 d (185 h)	(Keck and Lakoski, 1996a)
5-HT2 receptor	EEDQ	Brain	Cortex	4	1.9 d (45 h)	(Battaglia et al., 1987)
	EEDQ	Brain	Cortex	28	4.1 d (98 h)	(Battaglia et al., 1987)
GABAA receptor/Bz site	EEDQ	Brain	Cortex	2	1.1 d (25 h)	(Miller et al., 1991a)
	EEDQ	Brain	Cortex	20	3.1 d (75 h)	(Miller et al., 1991a)

PBZ, phenoxybenzamine.
[*]Estimated from data in Baker and Pitha (1982) and Pitha et al. (1982).

TABLE 2
Target half-life vs. species and organ/tissue

Target	Inactivating agent	Comment	Parameter	Species	Organ/tissue	Subregion	Recovery half-life	Reference
Dopamine D1 receptor	EEDQ	Young (1.5 months)		Rat	Brain	Striatum	1.4 d (34 h)	Fuxe et al. (1987)
	EEDQ	Young (1.5 months)		Rat	Brain	Claustrum	1.8 d (43 h)	Fuxe et al. (1987)
	EEDQ	Young (1.5 months)		Rat	Brain	Olfactory tubercle	1.0 d (25 h)	Fuxe et al. (1987)
	EEDQ	Young (1.5 months)		Rat	Brain	N. accumbens	0.9 d (22 h)	Fuxe et al. (1987)
Alpha1-adrenoceptor	PBZ			Rat	Brain	Cortex	5 d (120 h)	McKernan and Campbell (1982)
	PBZ			Rat	Brain	Brain stem	6 d (144 h)	McKernan and Campbell (1982)
	PBZ			Rabbit	Brain	Forebrain	10.8 d (259 h)	Hamilton and Reid (1985)
	PBZ			Rabbit	Brain	Hindbrain	13.3 d (319 h)	Hamilton and Reid (1985)
	PBZ			Rabbit	Spleen	—	3.6 d (86 h)	Hamilton et al. (1984)
	PBZ			Rat	Submaxillary gland	—	1.4 d (33 h)	Sladeczek and Bockaert (1983)
	PBZ			Rat	Liver	—	1.8 d (42 h)	Lynch et al. (1983)
Alpha2-adrenoceptor	Benextramine			Golden hamster	Kidney	—	1.3 d (31 h)	Taouis et al. (1987)
	Benextramine			Golden hamster	Adipose tissue	—	1.9 d (46 h)	Taouis et al. (1987)
	PBZ			Rabbit	Brain	Forebrain	6.1 d (146 h)	Hamilton and Reid (1985)
	PBZ			Rabbit	Brain	Hindbrain	4.6 d (110 h)	Hamilton and Reid (1985)
	PBZ			Rabbit	Spleen	—	1.6 d (38 h)	Hamilton and Reid (1985)
	EEDQ			Rat	Brain	Cortex	4.1 d (98 h)	Adler et al. (1985)
	EEDQ	Ex vivo slices	Agonist inhibition of NA release	Rat	Brain	Cortex	2.4 d (58 h)	Adler et al. (1985)
	EEDQ	Ex vivo slices	Agonist inhibition of 5-HT release	Rat	Brain	Cortex	4.6 d (110 h)	Adler et al. (1985)
	EEDQ	Antagonist-labeled		Rat	Brain	Cortex	4.9 d (118 h)	Ribas et al. (1998)
	EEDQ	Agonist-labeled		Rat	Brain	Cortex	7.4 d (178 h)	Ribas et al. (1998)
	EEDQ			Rat	Brain	Cortex	3.9 d (94 h)	Barturen and Garcia-Sevilla (1992)
	EEDQ			Rat	Brain	Locus coeruleus	1.5 d (37 h)	Pineda et al. (1997)
	EEDQ		NA neuronal cell firing in vivo	Rat	Brain	Locus coeruleus	0.6 d (14 h)	Pineda et al. (1997)
	EEDQ			Rat	Brain	Brain stem	2.6 d (62 h)	Barturen and Garcia-Sevilla (1992)
	EEDQ			Rat	Brain	Hippocampus	4.3 d (103 h)	Barturen and Garcia-Sevilla (1992)
	EEDQ			Rat	Brain	Hypothalamus	2.1 d (50 h)	Barturen and Garcia-Sevilla (1992)
	EEDQ			Rat	Brain	Striatum	2.1 d (50 h)	Barturen and Garcia-Sevilla (1992)
	EEDQ	Ex vivo slices		Rat	Brain	Cortex	18.5 d (445 h)	Agneter et al. (1993)
	EEDQ	Ex vivo slices		Rat	Brain	Cortex	0.8-2.7 d (20-64 h)	

(continued)

TABLE 2—Continued

Target	Inactivating agent	Comment	Parameter	Species	Organ/tissue	Subregion	Recovery half-life	Reference
	EEDQ		Agonist inhibition of NA release	Mouse	Brain	—		Agneter et al. (1993)
	EEDQ				Brain		5.3 d (126 h)	Durcan et al. (1994)
Beta2-adrenoceptor	BAAM			Guinea-pig	Lung	—	3.8-5 d (90–120 h)*	Nelson et al. (1986)
5-HT1A receptor	EEDQ	Young (approximately 2 months)		Rat	Brain	Cortex	7.7 d (185 h)	Keck and Lakoski (1996a)
	EEDQ	Mature-Aged (approximately 6–12 months)		Rat	Brain	Cortex	5.2 d (124 h)	Pinto and Battaglia (1994)
	EEDQ			Rat	Brain	Cortex	2.8 d (67 h)	Vinod et al. (2001)
	EEDQ			Rat	Brain	Cortex layers	3.9-4.3 d (94–103 h)	Raghupathi et al. (1996a)
	EEDQ	Mature-Aged (approximately 6–12 months)		Rat	Brain	Hippocampus	1.8 d (43 h)	Keck and Lakoski (1996b)
	EEDQ			Rat	Brain	Hippocampus	4.7 d (113 h)	Gozlan et al. (1994)
	EEDQ			Rat	Brain	Hippocampus	5.3 d (127 h)	Vinod et al. (2001)
	EEDQ			Rat	Brain	Hippocampus	2.7 d (65 h)	Bolanos et al. (1991)
	EEDQ			Rat	Brain	Lateral septum	4.0 d (96 h)	Gozlan et al. (1994)
	EEDQ			Rat	Brain	Dentate gyrus	4.2 d (101 h)	Gozlan et al. (1994)
	EEDQ			Rat	Brain	Parietal cortex	3.9 d (94 h)	Gozlan et al. (1994)
	EEDQ			Rat	Brain	Hippocampal subareas	2.3-3.6 d (55–86 h)	Raghupathi et al. (1996a)
	EEDQ			Rat	Brain	Dorsal raphe	3.2 d (77 h)	Gozlan et al. (1994)
	EEDQ			Rat	Brain	Dorsal raphe	2.7 d (69 h)	Bolanos et al. (1991)
	EEDQ			Rat	Brain	Dorsal raphe	2.8 d (67 h)	Raghupathi et al. (1996a)
5-HT1B receptor	EEDQ			Rat	Brain	Cortex	8.9 d (213 h)	Pinto and Battaglia (1994)
5-HT2 receptor	EEDQ			Rat	Brain	Cortex	approximately 4.5 d (approximately 108 h)	Battaglia et al. (1986)
5-HT2A receptor	EEDQ			Rat	Brain	Cortex	2.9 d (70 h)	Gozlan et al. (1994)
	EEDQ			Rat	Brain	Cortex	2.5 d (58.9 h)	Pinto and Battaglia (1994)
	EEDQ			Rat	Brain	Cortex	2.6-3.3 d (62–79 h)	Raghupathi et al. (1996b)
	EEDQ			Rat	Brain	Caudate-Putamen	9.0 d (216 h)	Raghupathi et al. (1996b)
MOP	Clocinnamox			Mouse	Brain	—	2.7-4.2 d (65–101 h)	Burke et al. (1994); Zernig et al. (1996)
	Clocinnamox	Thermal heat pain in vivo		Rhesus monkey	N/A	N/A	6.3-6.6 d (151–158 h)	Zernig et al. (1994)
DAT	RTI-76			Rat	Brain	Striatum	2.1-2.9 d (50–70 h)	

(continued)

TABLE 2—*Continued*

Target	Inactivating agent	Comment	Parameter	Species	Organ/tissue	Subregion	Recovery half-life	Reference
	RTI-76			Rat	Brain	Nucleus accumbens	1.9-2.0 d (46–48 h)	Kimmel et al. (2000)
	RTI-76	Intrastriatal RTI-76		Rat	Brain	Striatum	6.3 d (151 h)	Kimmel et al. (2000)
	DEEP-NCS		V_{max} & K_m change	Rat	Brain	Striatum	6.1 d (146 h)	Fleckenstein et al. (1996)
	DEEP-NCS	Intrastriatal DEEP-NCS	Ex vivo DA reuptake	Rat	Brain	Striatum	5.3 d (127 h)	Rego et al. (1999)
	DEEP-NCS	Intrastriatal DEEP-NCS	Receptor number	Rat	Brain	Striatum	5.8 d (138 h)	Rego et al. (1999)
	DEEP-NCS	Intrastriatal DEEP-NCS		Rat	Brain	Striatum		Rego et al. (1999)
SERT	RTI-76			Rat	Brain	Hippocampus	3.4 d (82 h)	Vicentic et al. (1999)
	RTI-76			Rat	Brain	Striatum	3.8 d (91 h)	Vicentic et al. (1999)
MAO A	Clorgyline			Rat	Liver	—	2.6-3.1 d (62–74 h)	Corte and Tipton (1980)
	Clorgyline			Rat	Liver	—	3.5 d (84 h)	Egashira and Kamijo (1979)
MAO B	Deprenyl			Rat	Brain	—	7.9 d (190 h)	Felner and Waldmeier (1979)
	Deprenyl			Pig	Brain	—	6.5 d (156 h)	Oreland et al. (1990)
	Deprenyl			Baboon	Brain	—	approximately 30 d (approximately 720 h)	Arnett et al. (1987)
	Deprenyl			Human	Brain	Several regions, healthy & PD	approximately 40 d (approximately 960 h)	Fowler et al. (1994)
	Deprenyl			Rat	Brain	Caudate	9.2 d (221 h)	Youdim and Tipton (2002)
	Rasagiline			Rat	Brain	Caudate	9.6 d (230 h)	Youdim and Tipton (2002)
	Pargyline			Rat	Brain	Caudate	13 d (312 h)	Goridis and Neff (1971)
	Pargyline			Rat	Brain	Hypothalamus	10 d (240 h)	Goridis and Neff (1971)
	Pargyline			Rat	Brain	Cerebellum	9.1 d (218 h)	Goridis and Neff (1971)
	Pargyline			Rat	Brain	—	9.1 d (218 h)	Planz et al. (1972a)
	Benmoxine			Rat	Brain	—	10.3 d (247 h)	Planz et al. (1972a)
	3A2O			Rat	Brain	—	10.9 d (262 h)	Planz et al. 1972a)
	3A2O			Rat	Brain homogenate	—	10.9 d (262 h)	Planz et al. (1972b)
	3A2O			Rat	Brain mitochondria	—	10.9 d (262 h)	Planz et al. (1972b)
	Pargyline			Rat	Brain	—	9.1 d (218 h)	Planz et al. (1972b)
				Rat	Brain	—	9.6 d (230 h)	Planz et al. (1972b)
	Nialamide			Rat	Heart	—	10.4 d (250 h)	Planz et al. (1972b)
	Nialamide			Rat	Heart	—	12.9 d (310 h)	Planz et al. (1972b)
	3A2O	Leucine incorporation		Rat	Liver homogenate	—	4.1 d (98 h)	Planz et al. (1972b)
	3A2O			Rat	Liver mitochondria	—	4.0 d (96 h)	Planz et al. (1972b)

TABLE 2—Continued

Target	Inactivating agent	Comment	Parameter	Species	Organ/tissue	Subregion	Recovery half-life	Reference
	Benmoxine			Rat	Liver	—	3.9 d (94 h)	Planz et al. (1972b)
	Pargyline			Rat	Liver	—	4.3 d (103 h)	Planz et al. (1972b)
	Deprenyl			Rat	Liver	—	3.7 d (89 h)	Planz et al. (1972b)
		Leucine incorporation		Rat	Liver mitochondria	—	2.6 d (62 h)	Egashira and Kamijo (1979)
	Pargyline			Rat	Liver	—	3.5 d (84 h)	Erwin and Deitrich (1971)
	Pargyline			Rat	Liver	—	4.0 d (96 h)	Planz et al. (1972a)
	Benmoxine			Rat	Liver	—	3.9 d (94 h)	Planz et al. (1972a)
	3A2O			Rat	Liver	—	4.1 d (98 h)	Planz et al. (1972a)
	MDL72974A			Human	Platelets	—	approximately 7 d (approximately 168 h)	Hinze et al. (1990)
	Pargyline			Rat	Submaxillary gland	—	3.8 d (91 h)	Goridis and Neff (1971)
	Nialamide			Rat	Submandibular gland	—	6.0 d (144 h)	Planz et al. (1972b)
	Benmoxine			Rat	Submandibular gland	—	4.1 d (98 h)	Planz et al. (1972b)
		Leucine incorporation		Rat	Submandibular gland	—	4.2 d (101 h)	Planz et al. (1972b)
	Pargyline			Rat	Superior cervical ganglion	—	4.6 d (110 h)	Goridis and Neff (1971)
	3A2O			Rat	Small intestine	Mucus layer	4.0 d (96 h)	Planz et al. (1972a)
	3A2O			Rat	Small intestine	Muscularis layer	0.5 d (12 h)	Planz et al. (1972a)
	Deprenyl			Rat	Liver	—	2.3 d (55 h)	Youdim and Tipton (2002)
	Rasagiline			Rat	Liver	—	2.2 d (53 h)	Youdim and Tipton (2002)
AChE	—	Turnover in dermal fibroblasts		Mouse	N/A	—	3.3 d (79 h)	Swovick et al. (2018)
	—	Leucine incorporation		Rat	Brain	Cortex	2.8 d (67 h)	Wenthold et al. (1974)
	Soman		Young (approximately 1.5 months)	Rat	Brain	BLA	5.9 d (141 h)*	Prager et al. (2014)
	Soman		Young (approximately 1.5 months)	Rat	Brain	Prelimbic cortex	7.7 d (185 h)*	Prager et al. (2014)
	Soman		Young (approximately 1.5 months)	Rat	Brain	Piriform cortex	8.0 d (193 h)*	Prager et al. (2014)
	Soman		Young (approximately 1.5 months)	Rat	Brain	Hippocampus	6.6 d (159 h)*	Prager et al. (2014)

BAAM, bromoacetyl-alprenolol menthane; MOP, μ opioid receptor; DAT, dopamine reuptake transporter; SERT, serotonin reuptake transporter; TryH, tryptophan hydroxylase; PD, Parkinson's disease; MAO, monoamine oxidase; 3A2O, 3-amino-2-oxazolidinone; BLA, basolateral amygdala; PBZ, phenoxybenzamine.
*Graphically estimated.

TABLE 3
Generic expressions of open and closed pharmacological systems and their properties

Properties	Open system	Closed system
Receptor R_{ss}	$R_{ss} = R_0 \cdot \left(1 - \frac{L_{ss}}{L_{ss} + EC_{50}}\right)$	$R_{ss} = R_0 \cdot \left(1 - \frac{L_{ss}}{L_{ss} + K_d}\right)$
	$R_{ss} = \frac{k_{syn}}{k_{deg}} \cdot \left(1 - \frac{L_{ss}}{L_{ss} + EC_{50}}\right)$	
	$R_{ss} = \frac{k_{syn}}{k_{deg}} \cdot 0.5$ where $L = EC_{50}$	
Complex RL_{ss}	$RL_{ss} = R_0 \cdot \frac{k_{deg}}{k_{e(RL)}} \cdot \frac{L_{ss}}{L_{ss} + EC_{50}}$	$RL_{ss} = R_0 \cdot \frac{L_{ss}}{L_{ss} + K_d}$
	$RL_{ss} = \frac{k_{syn}}{k_{e(RL)}} \cdot \frac{L_{ss}}{L_{ss} + EC_{50}}$	
	$RL_{ss} = \frac{k_{syn}}{k_{e(RL)}} \cdot 0.5$ where $L = EC_{50}$	
K_d	$K_d = \frac{k_{off}}{k_{on}}$	$K_d = \frac{k_{off}}{k_{on}}$
K_m	$K_m = \frac{k_{off} + k_{e(RL)}}{k_{on}}$	—
Occupancy	$\frac{L_{ss}}{L_{ss} + \frac{k_{off} + k_{e(RL)}}{k_{on}}}$	$\frac{L_{ss}}{L_{ss} + K_d}$
Reversible system EC_{50}	$EC_{50} = \frac{k_{deg}}{k_{e(RL)}} \cdot \frac{k_{off} + k_{e(RL)}}{k_{on}}$	—
Irreversible system EC_{50}	$EC_{50} \propto \frac{k_{deg}}{k_{on}}$	—
	$EC_{50} \propto \frac{k_{deg}}{k_{irr}}$	
Efficacy parameter E_{max}	$E_{max} = \rho \cdot [RL_{max}] = \rho \cdot \frac{k_{syn}}{k_{e(RL)}}$	$E_{max} = B_{max}$
Efficacy parameter I_{max}	$I_{max} = -\rho \cdot [RL_{max}] = -\rho \cdot \frac{k_{syn}}{k_{e(RL)}}$	
Baseline E_0	$E_0 \propto \frac{k_{syn}}{k_{deg}}$ or constitutive activity	

R_{max} and RL_{max} are the maximum observed response *in vivo*, and maximum level of the ligand–target complex, respectively. E_0 is defined as above of an empirical function of time to capture baseline variability e.g., oscillations.

Nefsky, 2002) and may also be in line with a common, albeit not universal, increase in pharmacodynamic sensitivity seen in the elderly, which agrees with a lowering of k_{deg} and therefore a subsequent increase in in vivo potency EC_{50} (in vivo EC_{50} numerically lower) (Wanwimolruk and Levy, 1987; Bowie and Slattum, 2007; Trifiro and Spina, 2011). While changes in membrane receptor number and turnover thus represent an obvious underlying possibility here, modifications of

Fig. 4. Age vs. dopamine D1 (filled triangles) and D2 (filled circles) receptor turnover in rat striatum expressed in log-linear plot of data from Table 1; joint (D1/D2) line correlation and corresponding coefficient (R^2; inset) also shown.

intracellular transduction efficiency processes in old age may also contribute.

Consequently, it might be further predicted that depending on the afflicted organ (or subregion thereof), PD alteration-dependent drug-dosing adjustments may be required for the optimization of therapeutic benefit in elderly patients. For example, the EC_{50} for the benzodiazepine GABAA enhancing agent midazolam to induce sedation/hypnosis was reported to be at least 50% lower in elderly compared with younger individuals despite similar PK parameters in both groups (Jacobs et al., 1995; Albrecht et al., 1999), thus warranting a dose reduction. Although there may, of course, be a number of different explanations, it is interesting to note in this context the nearly three times slower turnover of the benzodiazepine GABAA receptors in brain tissue of older compared with younger mice (Table 1) (Miller et al., 1991a), a feature that if translatable may also contribute to the observations in humans. Obviously, the chain of ligand-induced events for any biologic response—from target and transduction processes, via circuit and tissue, to the whole-organism level—implicates multiple proteins. Thus, even if literature examples are sparse, it is highly likely that changes in protein turnover at one or more sites along the ligand–target response chain may underlie a requirement for age-adjusted drug dosing (either jointly or in the absence of concurrent PK alterations). For agents engaging multiple targets in their mechanism of action, the overall pharmacodynamic impact on
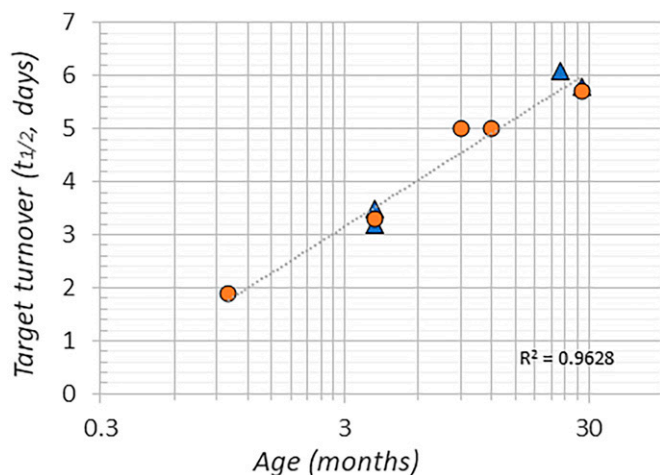
function would be expected to vary in relation not only to the affinities for the sites in question but also to the corresponding relative target turnover rates, in turn, possibly leading to altered drug profile expressions in older compared with younger subjects. Within the context of drug research and development, it is therefore evident that consideration of age as a factor in the intended clinical treatment population may affect the projection from in vitro target data toward adequate (efficacious as well as safe) in vivo exposures for desired pharmacodynamic responses in humans. Since the fractional turnover rate k_{deg} of a target is a term in the in vivo potency EC_{50} expression of both reversible and irreversible systems, it becomes evident how changes with size (body weight) in k_{deg} also impact in vivo EC_{50}.

Regrettably, very little turnover data are available for nonadults. However, intuitively, it seems likely that such states would be decidedly much more variable and dynamic across stages (embryonic, fetal, infant, child/adolescent) overall compared with adult and even aging conditions. Even if far more drugs are aimed at/used to treat adult (vs. nonadult) diseases and disorders, further detailed insights into the particular target dynamic properties of the nonadult periods remain important tasks for future study also from a drug developmental and treatment perspective.

2. Species and Tissues vs. Turnover. Any attempt to use target turnover information for drug response translation purposes inevitably needs to account for interspecies differences. While allometric predictions (for a review of allometry principles, see Boxenbaum, 1982; Boxenbaum and Ronfeld, 1983) of PK variables are commonly based on the correlation of body mass to metabolic rate (Kleiber's law) (Kleiber, 1947), it is less clear how the translation of drug PD indices relates to species-dependent target turnover properties

(Table 2). In this regard, it is notable that Swovick et al. (Swovick et al., 2018) found a negative correlation of median fractional turnover rate k_{deg} values for the global proteome with maximal lifespan (i.e., faster protein degradation with shorter lifespan) but not with the adult body mass of eight rodent species (approximately 20g $\geq$ approximately 20 kg). These authors also noticed that whereas there were clearcut species differences in the turnover across much of the proteome, turnover remained conserved for some proteins regardless of (rodent) species. Spector (Spector, 1974) further reported that there is a negative correlation between plasma protein turnover rates and animal longevity, including rodents, ruminants, and humans. The general applicability of these findings across target proteins and mammalian species remains to be established. Interestingly, and possibly concurring with the aforementioned (Spector, 1974; Swovick et al., 2018), the literature data for cerebral MAO-B protein turnover half-life (days) for five different mammalian species (Table 2) seemed to correlate better versus lifespan than versus adult body (or brain; not shown) mass (Fig. 5).

Further, even though the very same target protein may be present in several different tissues throughout the body, turnover rates can vary significantly between locations, even within the same organ or tissue (Table 2). The half-life also varies between subcategories of receptor proteins responding to the same transmitter (e.g., 5-HT1B vs. 5-HT2A) (Table 2). Although data from the same laboratory comparing rates between different organ tissues are scarce, the turnover of rat α1-adrenoceptors was reported to be approximately three to four times slower in rat and rabbit brain than in submaxillary gland and spleen, respectively (McKernan and Campbell, 1982; Sladeczek and Bockaert, 1983; Hamilton and Reid, 1985). Similarly, the half-life of MAO-B in rat brain may be
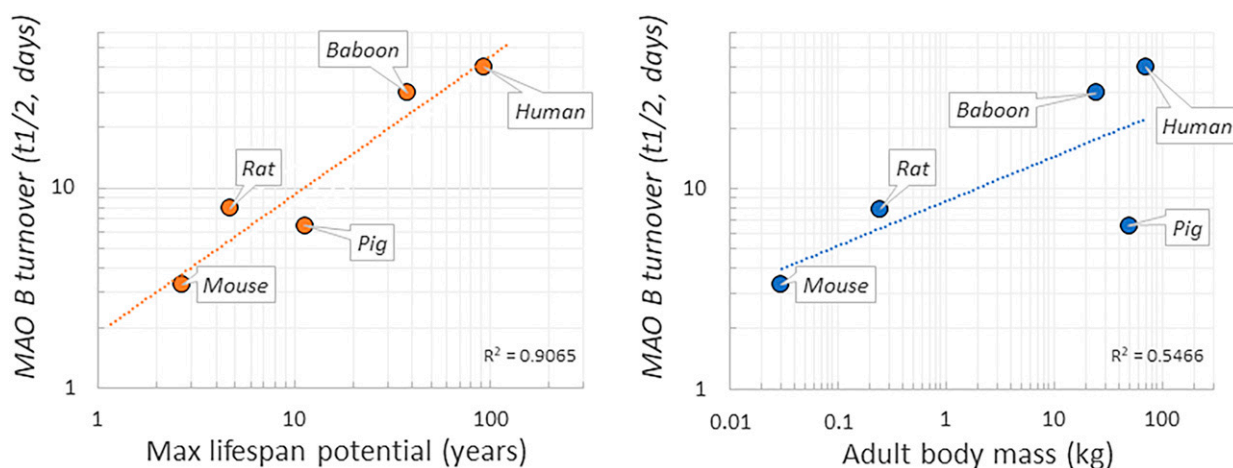

Fig. 5. Brain MAO B turnover for five mammalian species (Table 1) vs. lifespan (left) and adult body mass (right), expressed in log–log diagrams [line correlations and corresponding coefficients (R^2) shown as insets]. MAO B data were aken from references in Table 2; max lifespan potential data were taken from Boxenbaum (Boxenbaum, 1982) and AnAge [The Animal Aging & Longevity database (https://genomics.senescence.info/species/)].

approximately two to four times slower than in liver, salivary glands, and small intestinal tissue (Goridis and Neff, 1971; Planz et al., 1972a,b). It is relevant in this context that whereas cell types in the body differ in their dividing pace, the turnover of central nervous system (CNS) neuronal cells is generally slow and sustained (Savage et al., 2007) although, depending on function, the cells express a wide range of rates across the various cell constituents (e.g., vesicular vs. receptor target proteins) (Dorrbaum et al., 2018). As a likely overarching principle, the functions of the specific target protein and dynamics of the associated complexes may determine the rate of turnover. Overall, data cited in the previous discussion are consistent with the observation that target half-lives in peripheral organs and tissues are often faster than in brain (Price et al., 2010), but also that turnover rates may vary among subregions and proteins within the brain and peripheral tissue (see Table 2 for examples). Notably, Price et al. (Price et al., 2010) point out that turnover rates as determined in vitro versus in vivo correlate poorly, possibly at least partly related to more rapid proliferation and less regulatory control in cultured cell lines compared to in a living organism. This further emphasizes the importance of knowledge of in vivo target turnover rates toward drug response predictions and translation efforts. Since the fractional turnover rate k_{deg} of a target is present in the in vivo potency EC_{50} expression of both reversible and irreversible systems, it becomes evident from the compiled literature how species differences in k_{deg} also impact in vivo EC_{50}.

Most of the examples in Table 2 involve pharmacological challenge. It is, however, worth noting the correspondence to data obtained using the Leu-incorporation methodology (Planz et al., 1972b), arguing that the pharmacological perturbation per se may leave the turnover process relatively untouched.

3. Target Pool Turnover vs. Functional Recovery. For biologic responses to materialize, drugs or other ligands need to occupy molecular target proteins (e.g., GPCR, ion channels, enzymes, neurotransmitter transporters, polypeptides). However, there is a notable variation in the level of fractional occupancy (i.e., the proportion of targets occupied by a ligand) required for functional effect (Furchgott, 1966; Furchgott and Bursztyn, 1967; Grimwood and Hartig, 2009; Kenakin, 2016), and the level of receptor occupancy for a 50% response differs greatly for different agonists. What constitutes "adequate" occupancy not only differs between ligands and targets but may also vary across tissues for the same target and, depending on the type of downstream effector response assessed, even within the same tissue (Hoyer and Boddeke, 1993). In an open system context, occupancy is defined as in Table 3.

As most of the turnover data in Tables 1, 2, and 4 represent studies of agents acting at GPCRs, the

discussion in the following section focuses on this therapeutically highly prevalent target class (Garland, 2013). The intrinsic activity or efficacy of a GPCR ligand describes its ability to trigger an intracellular transduction process via its target site (i.e., defining stimulus force) expressed relative to a defined full agonist (i.e., able to elicit 100% under the same experimental conditions) (Kenakin, 2013). For example, the neurotransmitter DA (by definition, a full D2 receptor agonist) and the full D2 agonist NPA (N-n-propyl-norapomorphine) inhibit cAMP generation—one of the G-protein-mediated, immediate transduction pathways linked to the site—to a much greater extent than do partial D2 agonists like, for example, aripiprazole (Jordan et al., 2007; Beaulieu and Gainetdinov, 2011). This outcome may be envisaged in terms of ligand-induced changes in conformational states as a result of target binding, whereby agonists prompt (intracellular) second messenger amplification cascades and onward signaling more effectively than partial agonists, and antagonists fail to do so at all (intrinsic activity/efficacy = zero). However, for full (high-efficacy) agonists, there is typically a nonlinear relationship between drug–target occupancy and effect on functional output, as low receptor occupancy levels (2–30%) may suffice to trigger adequate—even near-maximal—functional responding (Grimwood and Hartig, 2009; Kenakin, 2016). In this situation, a major proportion of available target sites therefore remain functional but temporarily idle/unoccupied, which reflects the high agonist sensitivity of the signaling pathway (a.k.a. receptor reserve or spare receptors) (Neubig et al., 2003; Kenakin, 2018). For comparison, low(er)-efficacy agonists require high levels of target binding to elicit biologic responses and are often unable to reach maximal functional responding even at target saturation in a defined assay system. Thus, the definition of efficacy for a drug along the agonist–antagonist spectrum is dynamic as it is expressly reliant on the size of the available receptor pool and transduction function (Charlton, 2009). Consequently, efficacy may differ markedly, for example, between tissues (receptor amounts) and responses measured, as well as alterations induced by disease states and chronic drug treatments. As ligand efficacy is thus in part system-dependent: any given agent may behave as a full agonist for one tissue or particular readout while showing up as a partial agonist under other conditions (Kenakin, 2013). The interrelation between drug properties and the number of receptor sites—and as a corollary, influences via target turnover (see eq. 4)—in any given situation is thus a central factor in determining response efficacy to an agent within a defined context.

From the previous discussion, it follows that to reasonably gauge target turnover using functional in vivo output, an understanding of ligand efficacy in the system in question is vital (Grimwood and Hartig, 2009;

TABLE 4
Treatment vs. target half-life in the rat or mouse[a] brain

Target	Treatment	Inactivating agent	Species	Subregion	Recovery Half-life	Reference
Dopamine D1 receptor	Control (ECS)	EEDQ	Rat	Striatum	3.3 d (80 h)	Nowak and Zak (1989)
	Repeat ECS	EEDQ	Rat	Striatum	2.3 d (55 h)	Nowak and Zak (1989)
	Vehicle	EEDQ	Rat	Striatum	2.2 d (53 h)	Dewar et al. (1997)
	6-OHDA	EEDQ	Rat	Striatum	4.3 d (103 h)	Dewar et al. (1997)
	Chronic vehicle	EEDQ	Rat	Striatum	6.0 d (144 h)	Zou et al (1996)
	Chronic (-)stepholidine	EEDQ	Rat	Striatum	4.9 d (118 h)	Zou et al. (1996)
	Chronic vehicle (OVX)	EEDQ	Rat	Striatum	2.3 d (55 h)	Levesque and Di Paolo (1991)
	Chronic estradiol (OVX)	EEDQ	Rat	Striatum	4.4 d (107 h)	Levesque and Di Paolo (1991)
	Chronic vehicle (OVX)	EEDQ	Rat	Substantia nigra	1.7 d (42 h)	Morissette et al. (1992)
	Chronic estradiol (OVX)	EEDQ	Rat	Substantia nigra	1.4 d (34 h)	Morissette et al. (1992)
	Chronic vehicle (OVX)	EEDQ	Rat	Striatum (posterior)	1.7 d (41 h)	Morissette et al. (1992)
	Chronic estradiol (OVX)	EEDQ	Rat	Striatum (posterior)	3.8 d (91 h)	Morissette et al. (1992)
Dopamine D2 receptor	Chronic vehicle	EEDQ	Rat	Striatum	3.9 d (94 h)	Pich et al. (1987)
	Chronic haloperidol	EEDQ	Rat	Striatum	5.7 d (137 h)	Pich et al. (1987)
	Chronic vehicle	EEDQ	Rat	Striatum	5.9 d (141 h)	Zou et al. (1996)
	Chronic (-)stepholidine	EEDQ	Rat	Striatum	3.5 d (85 h)	Zou et al. (1996)
	Control (ECS)	EEDQ	Rat	Striatum	1.2 d (29 h)	Nowak and Zak (1991a)
	Repeat ECS	EEDQ	Rat	Striatum	2.4 d (58 h)	Nowak and Zak (1991a)
	Chronic vehicle	EEDQ	Rat	Striatum	3.0 d (73 h)[a]	Leff et al. (1984)
	Chronic reserpine	EEDQ	Rat	Striatum	5.4 d (130 h)[a]	Leff et al. (1984)
	Vehicle	EEDQ	Rat	Striatum	4.8 d (116 h)	Neve et al. (1985)
	6-OHDA	EEDQ	Rat	Striatum	5.3 d (128 h)	Neve et al. (1985)
	Vehicle	EEDQ	Rat	Striatum	3.8 d (90 h)	Dewar et al. (1997)
	6-OHDA	EEDQ	Rat	Striatum	4 d (96 h)	Dewar et al. (1997)
	Chronic vehicle (OVX)	EEDQ	Rat	Striatum (posterior)	2.4 d (58 h)	Morissette et al. (1992)
	Chronic estradiol (OVX)	EEDQ	Rat	Striatum (posterior)	4 d (95 h)	Morissette et al. (1992)
	Chronic vehicle (OVX)	EEDQ	Rat	Pituitary	0.75 d (18 h)	Levesque and Di Paolo (1991)
	Chronic estradiol (OVX)	EEDQ	Rat	Pituitary	2.1 d (51 h)	Levesque and Di Paolo (1991)
Alpha1-adrenoceptor	Control (ECS)	EEDQ	Rat	Cortex	1.6 d (39 h)	Nowak and Zak (1991b)
	Repeat ECS	EEDQ	Rat	Cortex	1.5 d (36 h)	Nowak and Zak (1991b)
Alpha2-adrenoceptor	Chronic vehicle	EEDQ	Rat	Cortex	3.9 d (94 h)	Barturen and Garcia-Sevilla, (1992)
	Chronic desipramine	EEDQ	Rat	Cortex	1.5-1.7 d (36-41 h)	Barturen and Garcia-Sevilla (1992)
	Chronic vehicle	EEDQ	Rat[b]	Cortex	4.9 d (118 h)	Ribas et al., 1993)
	Chronic clorgyline	EEDQ	Rat[b]	Cortex	3.6 d (86 h)	Ribas et al. (1993)
	Chronic vehicle	EEDQ	Rat[c]	Cortex	8.1 d (194 h)	Ribas et al. (1993)
	Chronic clorgyline	EEDQ	Rat[c]	Cortex	2.1 d (51 h)	Ribas et al. (1993)
	Chronic vehicle	EEDQ	Rat	Cortex	6.4 d (154 h)	Ribas et al. (2001)
	Chronic reserpine	EEDQ	Rat	Cortex	6.1 d (146 h)	Ribas et al. (2001)
	Chronic vehicle	EEDQ	Rat	Cortex	8.2 d (197 h)	Carbonell et al. (2004)
	Chronic lithium	EEDQ	Rat	Cortex	4.1 d (98 h)	Carbonell et al. (2004)
	Chronic vehicle	EEDQ	Rat	Cortex	4.4 d (106 h)	Gabilondo and Garcia-Sevilla (1995)
	Chronic morphine	EEDQ	Rat	Cortex	5.0 d (120 h)	Gabilondo and Garcia-Sevilla (1995)
	Morphine withdrawal	EEDQ	Rat	Cortex	2.7 d (65 h)	Gabilondo and Garcia-Sevilla (1995)
GABAA receptor /Bz site[a]	Chronic vehicle	EEDQ	Mouse	Cortex	1.3 d (31 h)	Miller et al. (1991b)
	Chronic lorazepam	EEDQ	Mouse	Cortex	0.8 d (19 h)	Miller et al. (1991b)
	Chronic vehicle	EEDQ	Mouse	Cerebellum	1.8 d (42 h)	Miller et al. (1991b)
	Chronic lorazepam	EEDQ	Mouse	Cerebellum	1.5 d (35 h)	Miller et al. (1991b)
Dopamine transporter (DAT)	Chronic vehicle	RTI-76	Rat	Striatum	2.1 d (50 h)	Kimmel et al. (2003)
	Chronic cocaine	RTI-76	Rat	Striatum	0.94 d (23 h)	Kimmel et al. (2003)

(continued)

TABLE 4—*Continued*

Target	Treatment	Inactivating agent	Species	Subregion	Recovery Half-life	Reference
	Chronic vehicle	RTI-76	Rat	Nucleus accumbens	2.2 d (53 h)	Kimmel et al. (2003)
	Chronic cocaine	RTI-76	Rat	Nucleus accumbens	2.2 d (53 h)	Kimmel et al. (2003)

ECS, electroconvulsive shock; OVX, ovariectomized; 6-OHDA, 6-hydroxydopamine.
[a]Extrapolated from data in Leff et al. (1984).
[b]SHR rats.
[c]Wistar-Kyoto rats.

Kenakin, 2017). To account for this element, the linear transduction factor ρ [the signal or stimulus triggered in the cell by the ligand–target complex; also known as the conversion of a chemical (complex concentration) or electrical (voltage) signal via amplification and/or feedback to a measurable in vivo pharmacological response (blood pressure, heart rate)] is included to separate full and partial agonists from each other and describe the efficacy parameter E_{max} (Choe and Lee, 2017). Hence, the in vivo efficacy parameter of a ligand, defined as the maximum drug-induced response by an individual ligand (E_{max} for stimulatory systems of agonists and antagonists or I_{max} for inhibitory systems such as with inverse agonism), derived from eqs. 1 and 2, becomes

$$E_{max} = \rho \cdot \frac{k_{syn}}{k_{e(RL)}} = \rho \cdot [RL_{max}] \tag{4}$$

The in vivo efficacy parameter of ligand, E_{max} (or I_{max} if derived from inverse agonism), is the maximum obtainable response, composed of maximum complex concentration (RL_{max}) derived from $k_{syn}/k_{e(RL)}$ and the transduction factor ρ (strength of the ligand–target complex RL_{max} to elicit a pharmacological response; see the previous discussion) (the in vivo efficacy parameter E_{max} is observed in response–time data; maximum ligand–target complex concentration in vivo RL_{max} may be measurable in certain instances, which allows prediction of the transduction parameter ρ from E_{max}/RL_{max}). Practically, E_{max} is the parameter obtained by fitting the Hill function (eq. 5, bottom line) to concentration–response or response–time data where E_{max} is equivalent to the maximal drug-induced response as the ligand concentration approaches infinity (Choe and Lee, 2017; Gabrielsson and Weiner, 2016). Equation 4 suggests that target synthesis k_{syn} and the degradation of ligand–target complex $k_{e(RL)}$ contribute to the overall capacity of the system (Gabrielsson and Peletier, 2017) rather than the ligand–target binding parameters per se (k_{on}, k_{off}). The elimination rate of complex $k_{e(RL)}$ is a shared parameter among in vivo potency, and efficacy parameters and hence connects these two pharmacological properties. A logistic expression of transduction ρ may, in some cases, be considered, provided supplementary information in vivo data are available and possible to access/extract.

The implications of the transduction (encompassing all steps involved in the conversion from a target–ligand complex concentration to a measurable pharmacological response in vivo) factor ρ are illustrated not only in a host of literature aimed at establishing the number of temporarily idle or "spare" receptors (a.k.a. receptor reserve) but also in some of the target inactivation–recovery studies cited in Table 4. In this regard, it was reported (Agneter et al., 1993; Pineda et al., 1997) that the recovery of α2-adrenoceptor function was significantly faster than the regain of actual target protein molecules. This is in line with the view that high-efficacy agonists may produce a regain of function already by occupying relatively few receptors; that is, even low receptor–agonist ligand (RL) complex concentrations may elicit an adequate level of functional responding (Grimwood and Hartig, 2009). For comparison, the return of target protein and functionality after inactivation of the DA transporter parallel each other (Rego et al., 1999). These latter observations agree with the high target binding required for functional responding in this target class (see the previous discussion) (Grimwood and Hartig, 2009).

A special case is when $k_{e(RL)}$ is equal to zero, which means that there is no irreversible loss of the complex as such via $k_{e(RL)}$. The ligand–target complex hence only functions as a storage pool and can only be split into its principal parts L and R via dissociation, controlled by k_{off}. The free target concentration at steady-state R_{ss} returns to its baseline value R_0 since routes of production and loss of target are governed by k_{syn} and k_{deg}, respectively (Gabrielsson and Peletier, 2017; Gabrielsson et al., 2018a). This is a situation that may be observed as functional adaptation or "fading" of the pharmacological response (i.e., tolerance). If suppression of the levels of the free target (e.g., antigen–antibody complexing) is the main goal and proportional to pharmacologic effect, it will only be accomplished during a certain amount of time until the target has returned to its baseline level and the effect vanished. It is possible that the natural behavior of such a system might reflect a disequilibrium between ligand, target, and complex rather than an example of functional adaptation. Almquist et al. (Almquist et al., 2018) demonstrated the correspondence between in vitro (functional assays) and in vivo properties (EC_{50}

by means of modeling) for a series of antilipolytic compounds (Fig. 6).

An approximate estimate of the complex kinetics $k_{e(RL)}$ term is obtained by regressing the data in Fig. 6 of the negative logarithm of in vivo potency (Y-axis) versus *the* negative logarithm of binding dissociation constant (X-axis) and inserting estimates of k_{deg} (denoted k_{out}) from Almquist et al. (Almquist et al., 2018). Unfortunately, plasma protein–binding differences across compounds were not considered in vivo, which might potentially have improved the consistency between in vitro and in vivo, as was shown for a series of opioids (Kalvass et al., 2007) in mice. Similar in vitro and in vivo correlation data have also been collected for in vitro (K_i) and in vivo potency (EC_{50}) of benzodiazepines (Visser et al., 2003). These three examples illustrate good correlations between in vitro binding properties and in vivo potency EC_{50} for reversible systems, provided k_{off} is greater than $k_{e(RL)}$ and that k_{deg}-to-$k_{e(RL)}$ in eq. 2 of in vivo potency EC_{50} is a constant term across compounds.

Predictions of exposure levels for repeated dosing in animals in vivo are typically based on target in vitro IC_{50}/EC_{50} data, with the aim to attain a specific multiple of exposure above the in vitro potency. However, the required duration of exposure needed for a therapeutic pharmacological response can vary significantly, a point generally that receives very little attention. In fact, it is often implicit that predicted exposure coverage requires 24 h/day for meaningful in vivo drug effects. Thus, based on the particular pharmacokinetic profile of a test compound, a dosing rate (often involving multiple daily doses) may be set to ensure constant drug exposure at a prespecified level of target engagement. However, if the target half-life exceeds the plasma half-life of the drug with irreversible action (e.g., proton-pump inhibitors), the duration of response will rather

Fig. 6. In vitro lipolysis negative logarithm of unbound in vivo potency (pEC_{50}) vs. unbound in vivo potency (pEC_{50}) data redrawn from Almquist et al. (2018). The gray dashed line (lower diagonal) represents the line of unity, and the red (upper diagonal) line represents the regression of all data. For all prediction models, both in vitro and in vivo potency are expressed on a logarithmic scale normalized to 1 molar (1M), according to pEC_{50} = -$\log_{10}(EC_{50}/1M)$. Note the pEC_{50} scale, meaning that compounds become more potent toward the upper right corner. The endogenous ligand nicotinic acid NiAc is specifically identified in the graph.

depend on de novo synthesis and half-life of the target protein. Conversely, if the target half-life is shorter than the plasma half-life of the drug, the duration of response will be determined primarily by the presence of the drug at the target (vide infra).

The conventional notion of 24 h/day exposure above a target concentration was recently challenged in the nicotinic acid (NiAc) treatment context (Kroon et al., 2017), emphasizing the importance of target biology integration with drug PK and PD features. Thus, these authors found that

an intermittent but not continuous NiAc dosing strategy, succeeded in retaining NiAc's ability to lower plasma FFA and improve insulin sensitivity. Furthermore, a well-defined NiAc exposure, timed to feeding-periods, but not fasting-periods, profoundly improves the metabolic phenotype of this animal model.

The discontinuous NiAc dosing approach hence minimized tolerance to the drug effect and lessened the impact with regard to counterbalancing feedback processes. Indeed, by incorporating biologic properties such as turnover of the NiAc target and of insulin, Andersson et al. (Andersson et al., 2019) succeeded in modeling and quantifying the interwoven behavior of NiAc with free fatty acid (FFA) and insulin. The target turnover aspects, as previously described, are therefore also an example of a property to be considered within the multifaceted field of chronopharmacology (for a review, see Dallmann et al., 2014).

4. Pharmacological Effect and Target Turnover: Dependency on Baseline States. In a typical closed in vitro system situation, the experimental setup determines the (static) size of the target pool (e.g., native tissue or induced expression of a target in a select cell preparation); whether the readout is affinity only or a functional (e.g., receptor binding or the magnitude of a particular biosignal, respectively); and, needless to say, disconnected from fluctuations in drug/ligand exposure across time.

From a modeling point of view, two principally different states may thus be envisaged: (i) when the baseline target occupancy and effect in vitro is zero or negligible (resting) and (ii) when the baseline activity is higher than the absolute zero, either as a consequence of endogenous ligand tone because the target is constitutively active in the absence of ligand or when there is baseline variability due to unknown factors. Compared with in vitro–controlled system assays (typically in non-native tissue or cells), the open, thermodynamically determined in vivo situation confers many more options (variable receptor conformations, temperature changes, cell and tissue nutritional fluctuations) for stimulating the receptor baseline behavior. Thus, the situations described in (ii) are more likely to be the case in vivo.

Fig. 7 shows schematically the relationship between different maximum complex concentrations and the efficacy
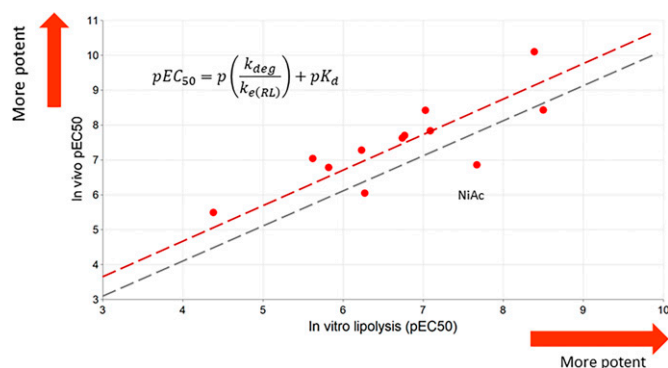
parameter E_{max}, (Fig. 7, A) and ligand concentration L and in vivo effect, free target concentration R, and ligand–target complex Fig. 7, B, solid blue line, solid red line, and dashed red line, respectively). The pharmacological effect response is a function of the baseline effect E_0 and the nonlinear E_{max} function, where the efficacy parameter E_{max} and potency EC_{50} are model parameters (eq. 5).

$$
\begin{cases}
EC_{50} = \dfrac{k_{deg}}{k_{e(RL)}} \cdot \dfrac{k_{off} + k_{e(RL)}}{k_{on}} \\[2mm]
E_{max} = \rho \cdot RL_{max} = \rho \cdot \dfrac{k_{syn}}{k_{e(RL)}} \\[2mm]
E_0 \propto \dfrac{k_{syn}}{k_{deg}} \quad \text{or constitutive activity} \\[2mm]
Response = E_0 + \dfrac{E_{max} \cdot L}{EC_{50} + L}
\end{cases}
\tag{5}
$$

We assume that the baseline effect E_0 is proportional to either an endogenous ligand–target interaction (at target baseline R_0) or a putative constitutive activity level expressed by the target in the absence of a ligand. In the former case (i.e., endogenous ligand–target interaction), the endogenous species may be readily displaced by a more potent drug ligand L. The efficacy parameter E_{max} is the absolute difference between the maximum drug- (or ligand-)induced effect response and the baseline effect E_0.

The in vivo efficacy parameter E_{max} is mathematically expressed as the product of maximum ligand complex RL_{max} ($k_{syn}/k_{e(RL)}$) and the transduction factor ρ (eq. 5) and will be ligand- and tissue-specific. Here, ρ is presented as a linear scalar, but may, in some instances, be a nonlinear expression, provided independent experimental data support that. The use of a nonlinear ρ term multiplied by a nonlinear expression of L_{ss} is challenging from a numerical (over-parameterization of embedded expressions), conceptual (which parameter contributes to what), and translational (how are products/ratios of parameters scaled across species) point of view.
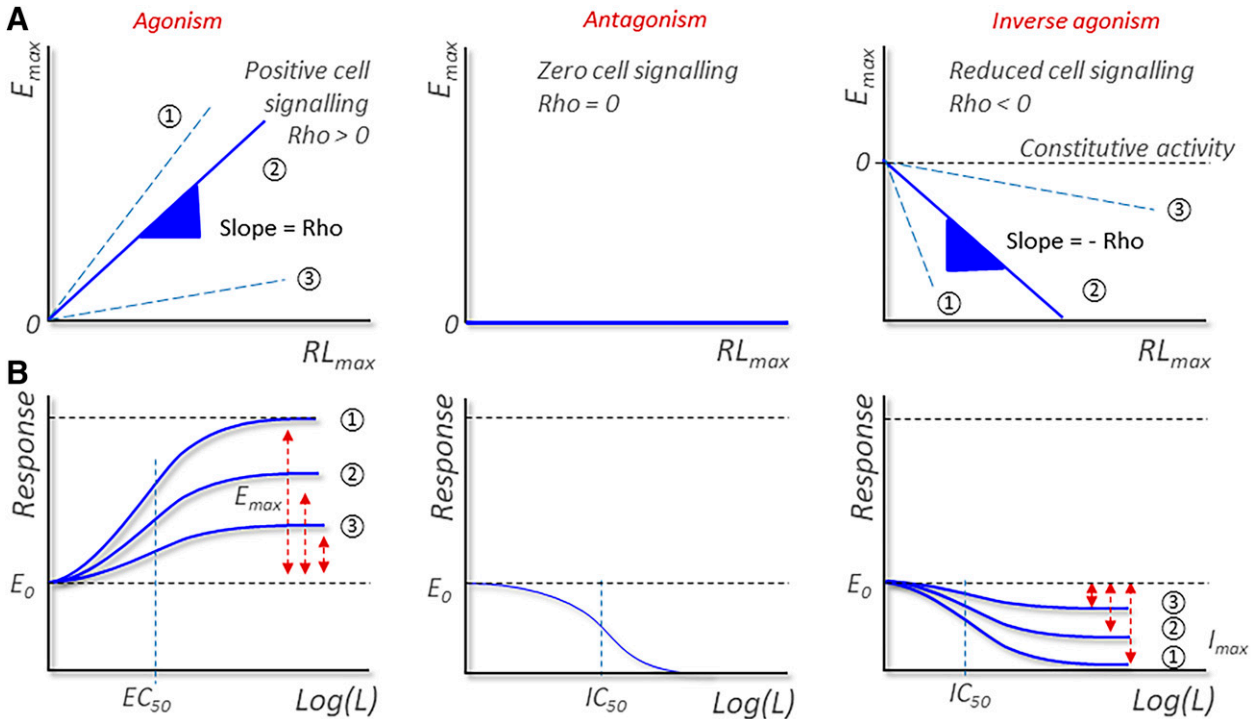

Fig. 7. (A) Efficacy parameter E_{max} vs. different maximum complex concentrations RL_{max} (eq. 4). Upper row left: Agonism: the steepness of the slope (ρ) is a correlate of the efficacy of the agonist ligand–target complex to generate a cellular response [i.e., (1) > (2) > (3)]. Assuming that (1) represents a full agonist, (2) and (3) depict partial agonists with a gradually lower efficacy. Upper row middle: Antagonism: the ligand–target complex has no intrinsic power to generate a cell response. Once bound to the target, the antagonist can, however, compete with and displace an endogenous agonist ligand from the target site (in turn, leading to a lower response; bottom middle plot). Upper row right: Inverse agonism: even in the absence of a drug–target complex, there may be a constitutive activity/cell signal. This activity diminishes upon increased amounts of inverse agonist ligand forming a complex with the available target. Similar to the classic agonist case described (upper row left), the steepness of the slope correlates with the relative efficacy of the inverse agonist ligand–target complex to alter the cellular response [(1) > (2) > (3)]. However, in contrast to the previous antagonist case, the inverse agonist ligand–target complex will weaken the baseline constitutive cell activity. NB!: Even though a neutral antagonist will not change a baseline target constitutive activity, it is able to counter the actions of classic as well as inverse agonist ligands, bringing both back to their corresponding baseline level. B,. log (ligand concentration L) vs. response. Bottom row left: Agonism: Log (ligand concentration L) vs. response is a saturable function (Model C in (Gabrielsson and Peletier, 2018; Gabrielsson et al., 2018a). With a transduction parameter $\rho > 0$, the response will increase from the baseline with increasing ligand concentrations; (1) represents a full agonist, (2) and (3) depict partial agonists with gradually lower efficacy. Bottom row middle: Antagonism: the endogenous agonist ligand is displaced by increasing concentrations of an antagonist drug ligand, thereby gradually reducing the baseline response (endogenous tone). The antagonist displacement of endogenous agonist ligand binding to target not only decreases the pharmacological response but also the concentration of free receptors available. Bottom row right: Inverse agonism: the constitutive activity of the target drops with more and more drug ligand bound to the target, forming an RL complex. L vs. RL is a nonlinear/saturable function that gives a declining, sigmoidal, L-vs.-response curve. Here, the transduction parameter ρ is < 0 and results in a progressively decremental response from the baseline as the concentration of ligand increases; (1) represents a full inverse agonist, (2) and (3) depict partial inverse agonists with a gradually lower efficacy.

ρ is an additional parameter taking stimulus into account, which corresponds to transduction of RL_{ss} complex concentration into a pharmacological response (the relative ability of a ligand–target complex to trigger downstream transduction events; i.e., a parameter defining stimulus strength of the ligand); a full agonist has a $\rho >> 0$, which is greater than that of a partial agonist $\rho > 0$ or an antagonist where $\rho = 0$ (i.e., $E_{max} = 0$). Analogously, when the ligand–target complex activity is less than the natural constitutive tone of the "naked" target in the absence of a ligand (in the case of inverse agonism), there is an attenuation of the constitutive signal eq. 6 (Fig. 7, A) thus becomes

$$\begin{cases} IC_{50} = \dfrac{k_{deg}}{k_{e(RL)}} \cdot \dfrac{k_{off} + k_{e(RL)}}{k_{on}} \\[2mm] I_{max} = \rho \cdot RL_{max} = \rho \cdot \dfrac{k_{syn}}{k_{e(RL)}} < 0 \\[2mm] Response = E_0 - \dfrac{I_{max} \cdot L}{IC_{50} + L} \end{cases} \quad (6)$$

to describe a maximum drug-induced response *lower* than the baseline activity E_0 (Fig. 7, A). The ρ is a conglomerate of multiple individual transduction processes (e.g., target signaling cascades, cellular and tissue environments, physiological amplification, dampening processes, feedback, etc.) (Cooper, 2000) across different organs, which may well be species/strain-, sex-, and disease-dependent. For an inverse agonist ligand, ρ, comprising all target-associated elements affecting the neuronal signal studied and conversion from a chemical or electrical signal to a pharmacologically measurable response, will change to a negative term in eq. 6 (I_{max}), which is analogous to E_{max} in eq. 5. Inverse agonists are therefore said to have negative intrinsic efficacy (i.e., the ability to decrease the activity of a constitutively active receptor). Such agents may display different degrees of negative intrinsic efficacy, resulting in strong and weak (partial) inverse agonists, analogous to classical agonist stimulatory intrinsic efficacy for full (strong) and partial (weaker) agonists (Costa and Herz, 1989; Berg and Clarke, 2018).

Whereas in vitro assays may quite easily be set up to discriminate pure antagonists from inverse agonist properties of drugs at various targets, it is decidedly more difficult to differentiate in the in vivo situation (Berg and Clarke, 2018). Currently, we are aware of only one drug that purports to derive its therapeutic efficacy from inverse agonism. The US Food and Drug Administration has recently approved pimavanserin as a 5-HT2A receptor inverse agonist to treat psychosis associated with Parkinson's disease (Cummings et al., 2014). Whether this is indeed the true molecular mechanism of pimavanserin remains to be further investigated, as according to a recent review, constitutive activity at 5-HT2A receptor sites may be rare in vivo (De Deurwaerdere et al., 2020).

5. Chronic Drug Treatments and Disease States vs. Turnover. Typically, the treatment of many physiologic perturbations and disease states requires repeat drug administration over shorter or longer time periods (Table 4). Although studies do not uncommonly report net changes in the target density following different periods of chronic dosing, there is relatively little data on the impact of repeated drug treatment—and withdrawal thereof—on the dynamics of target turnover rates k_{syn} and k_{deg} that underlie the changes in receptor numbers.

However, studies on D2R recovery following acute or more chronic depletion of endogenous DA, either by (6-hydroxydopamine–induced) denervation or repeated reserpine treatment, did find an acceleration of D2R reappearance (Leff et al., 1984; Neve et al., 1985), as might be expected for a compensatory process. Chronic monoamine depletion accompanying reserpine treatment likewise accelerated the return of cortical α2-adrenoceptors (Ribas et al., 2001). These reserpine-induced accelerations of turnover were reported to primarily reflect an increase in k_{syn} rather than a decrease in k_{deg}, and to result in an increased density of (high-affinity state) receptors. For comparison, chronic administration of the NA-selective reuptake-blocking antidepressant desipramine shortened the half-life of α2-adrenoceptors in rat brain tissue, mainly via increased k_{deg}, although alterations in k_{syn} were also noted (Barturen and Garcia-Sevilla, 1992). Similarly, repeat administration of the bipolar disorder medication lithium resulted in a significant reduction of α2-adrenoceptor half-life in the rat cortex (Carbonell et al., 2004), as did chronic MAO A inhibition by means of clorgyline (Ribas et al., 1993). Repeat electroconvulsive shock or citalopram treatment approximately doubled rat striatal D2R half-life, while limbic D2R turnover remained essentially unchanged (Nowak and Zak, 1991a). Repeat electroconvulsive shock treatment also enhanced striatal D1R turnover (Nowak and Zak, 1989) but did not modify the cortical α1-adrenoceptor half-life (Nowak and Zak, 1991b) in the rat. Estrogen is known to modulate central D2R, and chronic estradiol in female ovariectomized rats leads to a slowing of striatal D2R recovery (Levesque and Di Paolo, 1991). Interestingly, Kuhar and collaborators (Kuhar and Joyce, 200, 2003; Joyce et al., 2006; Kuhar, 2009) have also discussed in a series of papers the hypothesis that altered target turnover is an important contributor to the slow onset of the therapeutic as well as dependence-inducing actions of CNS-acting agents. Since the fractional turnover rate k_{deg} of a target is present in the in vivo potency EC_{50} expression of both reversible and irreversible systems, it becomes evident from the compiled literature how chronic drug treatment and disease states changes k_{deg} also impacts in vivo EC_{50}.

6. Up- and Dowregulation of Target: Impact of k_{syn}, k_{deg}, and $k_{e(RL)}$. As previously discussed, repeat drug administration may result in pharmacological target up- or downregulation. However, although an up- or

downregulation of target synthesis rate (turnover rate; k_{syn}) will impact the baseline level of the target (R_0) and therefore change the efficacy parameter E_{max} of ligand L at steady-state, it will not affect the potency, EC_{50} (Table 5; eqs. 2 and 3). The explanation for this is that efficacy will be determined by the total concentration of receptors but also by the transduction parameter ρ (eq. 4), which refers to the ligand–target complex stimulus strength if different from endogenous agonists or baseline activity (R_0).

Different from closed system predictions (Stephenson, 1956; Black and Leff, 1983), the present deliberations demonstrate that in vivo potency is not affected by the target expression level (R_0) per se. Instead, it is contingent on a conglomerate of fractional turnover rates of target and complex; hence, potency (eq. 2) is a function of binding and degradation rates (k_{deg}, $k_{e(RL)}$, k_{off}, and k_{on}). For comparison, efficacy is composed by ligand–target complex expression level (k_{syn} /$k_{e(RL)}$) and the transduction parameter (ρ). Thus, ligand–target binding properties (k_{off} and k_{on}) per se will not influence the efficacy parameter (E_{max}) in the open model. The relative impact of individual changes in the turnover parameters k_{syn}, k_{deg}, and $k_{e(RL)}$, respectively, are shown in Table 5 and Fig. 8 (see eq. 2).

A corollary of these expressions and reasoning is that an increase in the fractional turnover rate of ligand–target complex ($k_{e(RL)}$) alone results in an increased ligand potency (i.e., the numerical EC_{50} value decreases) and decreased efficacy (decrease in the efficacy parameter E_{max}). In other words, the compound is able to operate at

lower concentrations but displays less efficacy, provided transduction (ρ) remains the same.

In addition to drug-induced processes, cancerous and miscellaneous inflammatory states have also been reported to change (mainly increase) the rate of protein turnover (for a review, see Biolo et al., 2003). Alterations in synthesis, as well as breakdown, have been described, the magnitude, distribution, and allocation of which also depend on the severity of the condition (Powell-Tuck et al., 1984; Fearon et al., 1988; Biolo et al., 2003). Myasthenia gravis, an autoimmune condition, appears associated primarily with an enhanced breakdown ($k_{deg}\uparrow$) of the muscular ACh receptor protein (Appel et al., 1977; Sher and Clementi, 1984). For comparison, mice with the Ax[1] (ataxia) mutation display impaired GABAA receptor turnover, possibly associated with deficient protease activity [i.e., reduced degradation ($k_{deg}\downarrow$)] of the receptors (Lappe-Siefke et al., 2009). Other examples of likely alterations in target k_{syn} and/or k_{deg} as a consequence of the disease and associated medications include Parkinson's disease (i.e., increased levels of DA receptors, tolerance to levodopa treatment) (Antonini et al., 1997), delayed onset of antidepressant drug action in major depressive states (i.e., downregulation of 5-HT, NA autoreceptors) (Commons and Linnros, 2019), neuroleptic-induced motor and psychotic supersensitivity conditions (i.e., tardive dyskinesia, DA supersensitivity psychosis (Stahl, 2017; Thompson et al., 2020), and reversal of such alterations upon withdrawal from drug treatment.

Based on these and several other examples (Biolo et al., 2003), it appears reasonable to speculate that

TABLE 5
Impact of up- and downregulation on relevant pharmacological parameters for agonists

| Target change	Cause	Baseline R_0	Complex RL_{ss}	Potency EC_{50} (numerical value = nv)	Efficacy parameter E_{max}	Comment
Upregulation (increased concentration of target R or complex RL)	$k_{syn}\uparrow$	$\uparrow$	$\uparrow$	$\leftrightarrow$	$\uparrow$	Baseline and complex and efficacy increase since target synthesis rate impacts all (eq. 3). Potency remains unchanged (eq. 2).
	$k_{deg}\downarrow$	$\uparrow$	$\leftrightarrow$	$\uparrow$ (nv=$\downarrow$)	$\leftrightarrow$	Baseline and potency increase (lower numerical value, eq. 2) whereas complex and efficacy remain unchanged.
	$k_{e(RL)}\downarrow$	$\leftrightarrow$	$\uparrow$	$\downarrow$ (nv=$\uparrow$)	$\uparrow$	Baseline unchanged, complex and efficacy increase, but potency drops (increased numerical value (eqs. 2 and 3)
Downregulation (decreased concentration of target R or complex RL)	$k_{syn}\downarrow$	$\downarrow$	$\downarrow$	$\leftrightarrow$	$\downarrow$	Baseline, complex, and efficacy decrease since target synthesis rate impacts all (eq. 3). Potency remains unchanged (eq. 2).
	$k_{deg}\uparrow$	$\downarrow$	$\leftrightarrow$	$\downarrow$ (nv=$\uparrow$)	$\leftrightarrow$	Baseline and potency decrease (higher numerical value, eq. 2) whereas complex and efficacy remain unchanged.
	$k_{e(RL)}\uparrow$	$\leftrightarrow$	$\downarrow$	$\uparrow$ (nv=$\downarrow$)	$\downarrow$	Baseline unchanged, complex and efficacy decrease, but increased potency (decreased numerical value (eqs. 2 and 3)
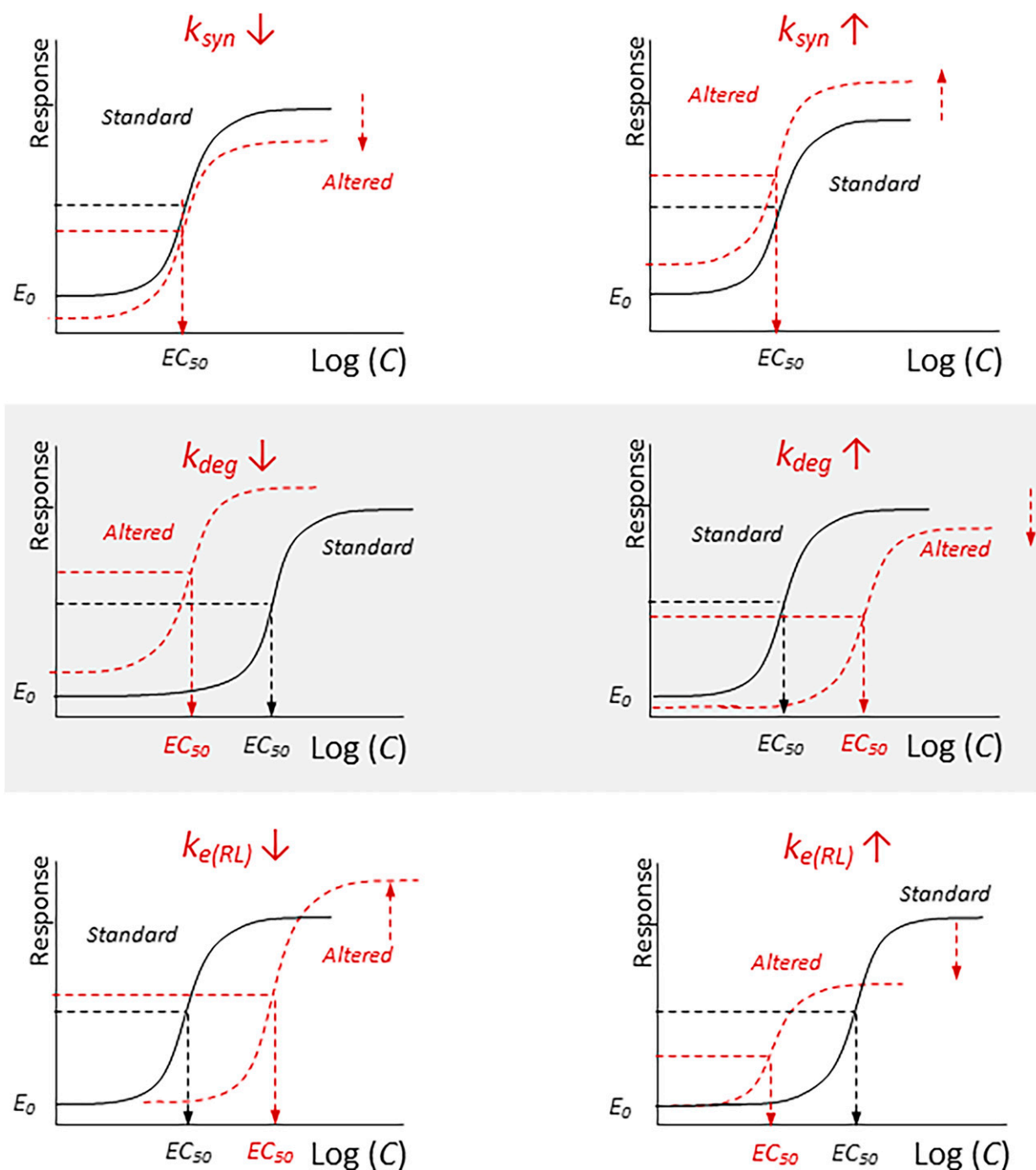
Fig. 8. Schematic illustration of ligand concentration C-response relationships following changes in target turnover rate (k_{syn}), fractional target turnover rate (k_{deg}), or ligand–target complex ($k_{e(RL)}$). Note that only $k_{e(RL)}$ impacts both in vivo potency and efficacy. Changes in k_{syn} shift intensity of the response and k_{deg} changes in vivo potency. If E_{max} is changed without any concomitant changes in baseline, it is most probably due to changes in either $k_{e(RL)}$ or ρ. Baseline response E_0 is governed by target exposure k_{syn}/k_{deg} and target constitutive activity, whereas maximum ligand-induced response E_{max} by $\rho\, k_{syn}/k_{e(RL)}$. Altered implies a new concentration–response relationship after a parameter change.

not only disease states but also numerous other less grave situations would be associated with alterations in the turnover of the whole or specific parts of the proteome, such as conditions including, for example, hormonal and nutritional state, day–night cycle, and various forms of stress (surgical, trauma, environmental, etc.), to mention a few (Richardson and Rose, 1971; Adam and Oswald, 1983; Biolo et al., 2003).

C. Summary of Target Turnover-Modifying Influences

Taken together, it is evident that the rate of target turnover is subject to modification by several factors and conditions. Distinct variations are found across organs and tissues, as well as between species and stages of the life cycle. Therefore, it is evident that any of these may impact the translation of in vitro to

in vivo pharmacodynamic outcome (viz. closed vs. open systems) and, in turn, predictions of drug responses from experimental animal work to clinical efficacy in man. Thus, to recapitulate, some key elements that may significantly influence target half-life are age, species (and strain/ethnicity), organ/tissue and region (subregion), and chronic treatment/withdrawal and disease states.

Hence, in vivo potency and efficacy should not be expected to be constant across species, ages, tissues, or chronic drug treatment. Further, it appears reasonable to hypothesize that sex differences in target turnover may also play a role in observed male versus female-related disparities in pharmacodynamic drug response, although so far such data remain scarce. In fact, barring studies addressing medications intended for female-specific conditions, most of the preclinical as well as clinical literature, in general, is still dominated by investigations carried out in the male sex. The topic of target turnover is no exception in this regard; this is indeed a limitation and one that certainly deserves more attention. Apart from scattered reports (of conceivable clinical implications (Abou Sawan et al., 2021; Farrell et al., 2021), sex differences in target turnover remain to be further documented and defined. Additionally, recent developments suggest that factors such as target genetic variants/SNPs, RNA stability, epigenetic effects, transcriptional and post-transcriptional regulation, targets existing in protein complexes, and/or in cellular subcompartments may also influence target expression, turnover, and resultant net output (Esteller, 2008; Pereira et al., 2010; Corradin et al., 2016). While not specifically addressed in the present review, it is clear that response differences may also result from diverse subcellular (micro- or nano-domains) locations of the targets and involve various post-translational modifications, possible dimeric/heteromeric coexistence, partner proteins/lipids, etc.

Needless to say, the more defined and detailed knowledge about target turnover in a particular disease condition, the more precise prediction from in vitro and in vivo animal models to in vivo clinical target response. The relative importance and implications of the aforementioned factors thus need to be considered not only within the context of the actual intended therapeutic target but also taking into account characteristics of state and trait within the intended clinical treatment population.

Obviously, observed changes in target turnover may relate to alterations in target synthesis (k_{syn}) and/or breakdown (k_{deg}) as well as in the elimination of the target–ligand complex ($k_{e(RL)}$). In the following section, these aspects will be further gauged and scrutinized, including associated examples of possible clinical relevance and impact.

D. In Vivo EC_{50} Compared to In Vitro K_d: Dependency on k_{deg}, k_{off}, and $k_{e(RL)}$

A common misconception in drug discovery contexts is that unbound therapeutic concentrations (C_u) have to be a fixed multiple greater than in vitro potency (K_d or in vitro IC_{50}) to demonstrate a satisfactory pharmacological response in vivo (Jansson-Lofmark et al., 2020). Jansson-Lofmark et al. (2020) reported that over 70% of 167 drugs across various chemical and pharmacological classes have an efficacious C_u-to-in vitro potency ratio (eq. 7) of less than unity. In fact, 30% and 50% of the compounds studied were found to have an in vivo-to-in vitro ratio of less than 0.1 and 0.3, respectively.

Occasionally, the in vivo potency of a drug exceeds the prediction from in vitro binding K_d (i.e., displaying an in vivo EC_{50} value numerically *lower* than its K_d), and vice versa. As shown in eq. 7, this depends primarily on the absolute size of k_{off} and $k_{e(RL)}$.

1. Case 1. If $k_{e(RL)}$ is greater than k_{off}, the system behaves irreversibly, and in vivo potency EC_{50} may be approximated by k_{deg}/k_{on} alone (see Fig. 9). K_d is still k_{off}/k_{on}, and therefore the relative magnitude of the EC_{50}-to-K_d (in vivo-to-in vitro) ratio is governed by k_{deg}/k_{off} as

$$
\begin{cases}
Ratio = \dfrac{EC_{50}}{K_d} = \dfrac{k_{deg}}{k_{e(RL)}} \cdot \dfrac{k_{off}+k_{e(RL)}}{k_{on}} \cdot \dfrac{1}{\frac{k_{off}}{k_{on}}} = \dfrac{k_{deg}}{k_{e(RL)}} \cdot \dfrac{k_{off}+k_{e(RL)}}{k_{on}} \cdot \dfrac{k_{on}}{k_{off}} \\[4mm]
\dfrac{EC_{50}}{K_d} = \dfrac{k_{deg}}{k_{e(RL)}} \cdot \dfrac{k_{off}+k_{e(RL)}}{k_{off}} \\[4mm]
\dfrac{EC_{50}}{K_d} = \dfrac{k_{deg}}{k_{off}} \quad when \ \ k_{off} \ll k_{e(RL)} \\[4mm]
\dfrac{EC_{50}}{K_d} = \dfrac{k_{deg}}{k_{e(RL)}} \quad when \ \ k_{off} \gg k_{e(RL)}
\end{cases}
$$

$$(7)$$

where k_{deg} represents the turnover of the target and k_{off} the dissociation rate constant of ligand–target
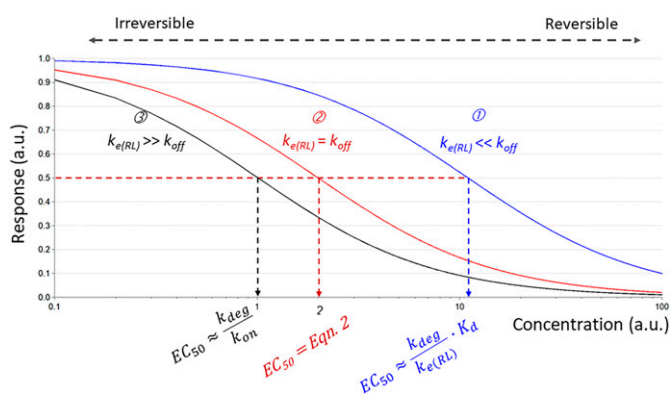

Fig. 9. Schematic depiction of response [arbitrary units (a.u.)] vs. test compound concentration (a.u.) for situations along an irreversible/reversible ligand–target interaction scale. Shown are simulations of changes in ligand—target complex elimination $k_{e(RL)}$ and the corresponding impact on in vivo potency EC_{50}. (1) Blue curve, right: A reversible system where $k_{e(RL)}$ is much less than k_{off}. Potency EC_{50} is approximately $k_{deg}/k_{e(RL)} \cdot K_d$; off-rate k_{off} from ligand–target complex binding will be an important covariate. (2) Red curve, middle: $k_{e(RL)} = k_{off}$; EC_{50} corresponds to eq. 2. (3) Black curve, left: Irreversible in the sense that there is only an infinitesimal contribution of ligand regenerated from the ligand–target complex pool since $k_{e(RL)}$ is much greater than k_{off}. Potency EC_{50} is approximately k_{deg}/k_{on}; target turnover will again be an important covariate as in eq. 2.

binding. This implies an essentially irreversible system in which the fractional turnover rate of the target becomes more important for the level of the in vivo EC_{50} than does the ligand-to-target affinity parameters per se. Examples of this situation are discussed further later in the text with proton pump inhibitors.

2. Case 2. When $k_{e(RL)}$ is smaller than k_{off}, the system behaves reversibly, and in vivo EC_{50} is approximated by $(k_{deg}/k_{e(RL)}) \times K_d$ (Fig. 9). Hence, the relative magnitude of the EC_{50}-to-K_d ratio is then governed by $k_{deg}/k_{e(RL)}$ where k_{deg} represents turnover of target and $k_{e(RL)}$ loss of the (non-dissociated) target–ligand complex. If k_{deg} is smaller than $k_{e(RL)}$, the in vivo EC_{50} will be numerically lower (potency higher) than anticipated from the in vitro binding K_d. Therefore, converse to case 1, complex loss $k_{e(RL)}$ plays a relatively greater role in the magnitude of in vivo-to-in vitro potency ratio than k_{off}. Hence, it is evident that the magnitude of the target turnover k_{deg} influences the relation between in vitro and in vivo potency in both cases and should not be ignored.

While the previous discussion clearly applies to most single therapeutic drug entities, how do you deal with the situation when a drug has an active metabolite or metabolites? A potential approach is to predict the active moiety of the parent and metabolite(s) at steady-state. For example, the M_3-muscarinic receptor antagonist tolterodine and its 5-OH-methyl metabolite have similar in vitro binding affinity (K_i 2.7 and 2.9 nM, respectively) at muscarinic receptors (Brynne et al., 1997; Nilvebrant et al., 1997). Therefore, Brynne et al. (Brynne et al., 1999) used the sum of the unbound concentrations of drug and metabolite at steady-state as the active moiety. The corresponding efficacious unbound plasma concentration of active moiety-to-K_i ratio will then be <0.1. Again, this is yet another example consistent with the finding (Jansson-Lofmark et al., 2020) that a multiple of in vitro potency *greater than* unity is not a compulsory requirement for an acceptable clinical effect.

The in vivo-to-in vitro ratio is influenced by k_{deg} and will be less than unity if the turnover of target k_{deg} is slower than either complex kinetics $k_{e(RL)}$ or dissociation rate of the complex into ligand and target k_{off} for reversible and irreversible systems, respectively. However, recall that irrespective of the efficacious concentration C_u where a drug operates, the turnover of the target will impact the ratio, as EC_{50} is an element comprising both drug and target properties (see eq. 7). Uncritical use of a ratio approach for ranking of drug candidates should thus be avoided unless a reasonable scientific foundation is at hand.

E. Examples of Irreversible and Reversible Ligand–Target Interactions

Most therapeutically used drugs interact with their corresponding target(s) in a reversible, noncovalent manner, but the pharmaceutical arsenal also contains several irreversibly acting agents of significant clinical importance. Next, we discuss examples of reversible as well as irreversible ligand–target interactions in relation to target turnover parameter impact and consequences thereof.

We define an irreversible system as one where removal of the ligand–target complex as such ($k_{e(RL)}$) dominates over first-order dissociation of ligand–target complex (k_{off}). Irreversible ligand–target interactions are indeed used pharmacologically, for example, among acetylcholine-esterase-, COX-1, H^+/K^+-ATPase-, and MAO-B inhibitors (Wallmark et al., 1985; Arnett et al., 1987; Gedda et al., 1995; Vane and Botting, 2003; Freedman et al., 2005; Mbonye et al., 2006; Kang et al., 2007; Colovic et al., 2013). In these cases, the ligand off-rate (k_{off}) from the complex is negligible compared to the elimination of the ligand–target complex such as $k_{e(RL)}$. The duration of the pharmacological effect will therefore depend on target de novo synthesis and its half-life. An example of this is the duration of the effect of gastric proton pump inhibition following a single dose of omeprazole. The pharmacokinetic half-life of omeprazole is about 1 hour in humans, whereas the half-life of the proton pump falls in the range of 15 to 20 hours, thus making once-a-day dosing a practical approach (Wallmark et al., 1985). When the half-life of the target protein is shorter, the plasma half-life and presence of the drug become more important for the dosing interval and duration of response.

Using the derived generic expression of in vivo potency (EC_{50}) valid under a wide range of circumstances, the following illustrates the performance of an *irreversible* system. Here the removal of ligand–target complex $k_{e(RL)}$ dominates over regeneration k_{off} of free ligand L and target R from the complex pool RL (see eq. 8) (Fig. 8). The route of elimination of the ligand–target complex RL will therefore indirectly be important to the elimination of both ligand and target per se.

Recall that for the irreversible system shown in Figs. 2 and 9, the expression of in vivo potency from eq. 2 can be simplified to the ratio of k_{deg}-to-k_{on} as

$$\begin{cases} EC_{50} = \dfrac{k_{deg}}{k_{e(RL)}} \cdot \dfrac{k_{off} + k_{e(RL)}}{k_{on}} \\[2mm] EC_{50} = \dfrac{k_{deg}}{k_{e(RL)}} \cdot \dfrac{k_{off} \ll k_{e(RL)}}{k_{on}} = \dfrac{k_{deg}}{k_{e(RL)}} \cdot \dfrac{k_{e(RL)}}{k_{on}} \\[2mm] EC_{50} \propto \dfrac{k_{deg}}{k_{on}} \end{cases} \quad (8)$$

The notion of drug–target residence time, defined as $1/k_{off}$ (Copeland, 2016; Copeland et al., 2006), deserves some comment in this context. Within this frame and a closed system setting, target off-rate may be an important factor in determining drug potency K_d and in vivo effect duration (Lu and Tonge, 2010; Dahl and Akerud, 2013; Copeland, 2016; Hothersall et al., 2016; Bosma et al., 2017), this but has also been questioned (Folmer, 2018). The concept of ligand–

receptor "rebinding," still based on a closed system in vitro approach, has also been introduced as a potential contributory mechanism with implications for the duration of drug action in vivo (Vauquelin, 2010; Vauquelin and Charlton, 2010) and it has further been argued that target saturation is an important component to the extended duration of a pharmacological effect (de Witte et al., 2018). However, in an open system, the loss of (non-dissociated) drug–target complex is an additional route of removal, and the drug–target residence time expression becomes $1/(k_{off} + k_{e(RL)})$. Therefore, despite a very small k_{off}—suggestive of a long drug–target residence time and an extended duration of response according to the closed system nomenclature—rapid replenishment of target (k_{deg} fast) or removal of the ligand–target complex (approximately $1/k_{e(RL)}$) can appreciably shorten the apparent residence time and hence the duration of the drug–target effect (Corzo, 2006). On the other hand, even when the size of k_{off} and $k_{e(RL)}$ confers a short residence time, the response duration may still be substantial due to a slow regeneration of free target levels in an open in vivo system [e.g., proton pump inhibitors (PPI)]. In the latter case, it is the target half-life that governs the duration of response rather than the degree of saturation of the target system, as suggested by de Witte et al. (de Witte et al., 2018) using closed model arguments.

An instructive example is a comparison of the new PPI IY-81149 and omeprazole (Kwon et al., 2001). The in vitro IC_{50} of H^+K^+-ATPase activity of IY-81149 and omeprazole were 6 μM and 100 μM, respectively, demonstrating a substantial difference in the in vitro binding affinities to the target. Based only on relative in vitro binding, IY-81149 would have been expected to be about 15 times more potent than omeprazole in vivo. However, the potency difference was more or less abolished when the effects were studied in a dog model in vivo (e.g., histamine-stimulated gastric secretion in the Heidenhain pouch (Kwon et al., 2001). No clinical differences were seen between

compounds (Wang et al., 2019). This outcome is consistent with eqs. 2 and 8 and an irreversible system, where $k_{e(RL)} >> k_{off}$ is required for irreversibility and hence in vivo potency is governed by target turnover k_{deg}; thus, basically independent of further changes in k_{off}. It is evident that the notion about drug–target residence time according to closed system nomenclature does not hold since k_{deg}, rather than k_{off}, will be the major determinant of pharmacological in vivo potency of an irreversible system (eq. 8) (Fig. 9).

If the target half-life is longer than the drug plasma half-life, the duration of response will be governed by de novo synthesis of the target and the target protein half-life. This reasoning is applicable to irreversible target interactions (e.g., H^+/K^+-ATPase, COX-1, MAO-B) (Table 6). Conversely, if the reverse is true (i.e., target half-life shorter than drug plasma half-life), the drug has to be present at adequate inhibitory concentrations throughout the desired duration of the pharmacological effect since target loss (through $k_{e(RL)}$) is quickly replenished by newly synthesized target molecules.

An interesting example is the COX-1 enzyme (prostaglandin–endoperoxide synthase) involved in the generation of prostaglandins throughout body organs and tissues. Drugs that are inhibitors of this enzyme (nonsteroidal anti-inflammatory drugs) may be acting either reversibly (ibuprofen, naproxen) or irreversibly [acetylsalicylic acid (ASA). In the case of the archetypal nonsteroidal anti-inflammatory drug, ASA, the COX-1 enzyme interaction is irreversible, and the duration of the biologic effect is thus entirely dependent on the turnover of the enzyme per se and/or the turnover of the COX-1-containing tissue. Despite a short plasma half-life of ASA (15–20 minutes), the return of platelet function to baseline thus occurs only after 72 to 96 hours as a result of irreversible COX-1 interaction (Hong et al., 2008) and the slow regeneration rate of blood platelets. For comparison, ibuprofen and naproxen are both reversible and, therefore, much more short-acting COX-1 inhibitors (Table 6). The pharmacodynamic action of these agents is thus less

TABLE 6
Response duration dependence on drug and target half-lives in irreversible and reversible conditions

Half-life	Irreversible H^+/K^+-ATPase inhibitor (omeprazole)	Irreversible COX-1 inhibitor (ASA; platelet aggregation)	Reversible COX-1 inhibitor (ibuprofen; platelet aggregation)	Reversible COX-1 inhibitor (naproxen; platelet aggregation)	Irreversible MAO-B inhibitor (rasagiline)	Reversible ACh esterase inhibitor (donepezil)	Reversible GSECR inhibitor (experimental compound)
Drug half-life	45 min	10–15 min	2 h	12–17 h	1.5–3.5 h	60–70 h	2 h
Target half-life	15–20 h[a]	33 h[b]	33 h[b]	33 h[b]	30–45 days[c]	10–11 days[d]	20 min[e]
Rate-limiting step	Target, k_{deg}	Target(/tissue), k_{deg}	Complex dissociation	$k_{deg} >> k_{off}$	Target, k_{deg}	Exposure	Exposure
Response duration	$T_{1/2, target}$	$T_{1/2, target}$	$T_{1/2, k_{off}}$	$T_{1/2, plasma}$	$T_{1/2, target}$	Presence of unbound exposure C_u	Presence of unbound exposure C_u

[a]Estimated target half–life (Wallmark et al., 1985).
[b]Estimated target half–life (Hong et al., 2008).
[c]Estimated target half–life (Fowler et al., 1994).
[d]Estimated target half–life (Moss et al., 2017).
[e]Estimated target half–life (Gabrielsson and Weiner, 2016).

dependent on fractional target turnover and more on ligand–target dissociation or ligand clearance per se. A slow off-rate (k_{off}) has been suggested to play a key role in the in vivo profiles of, for example, LABA and LAMA (e.g., tiotropium) (Disse et al., 1999) drugs for COPD treatment. However, although likely contributory, receptor kinetics may not be the full explanation for the clinical action duration and profiles of such agents (Sykes and Charlton, 2012; Sykes et al., 2012).

As discussed, previously, efforts to optimize compound affinity (in vitro binding potency) will be essentially futile if target and/or tissue turnover k_{deg} is faster than the dissociation rate k_{off}. In such a case, the duration of the response will be determined by the k_{deg} process. The open model system allows estimation of the potency of both reversible and irreversible ligand–target interactions. The open model additionally has the potential to explain the pharmacodynamic drug-interaction potential between two or more compounds.

For example, Hong et al. (Hong et al., 2008) studied the inhibition of platelet aggregation in a single-blinded, randomized, three-way crossover study. Single doses of aspirin (ASA 325 mg) and ibuprofen (400 mg) versus concomitant administration of ASA and ibuprofen were studied in patients with musculoskeletal disorders and high cardiovascular risk, with a 2-week washout between the study occasions. A substantial inhibition (77%) of platelet aggregation was seen within 2 hours and returned to baseline values within 72 to 96 hours after ASA dosing. In contrast, treatment with ibuprofen alone or together with ASA resulted in only a transient inhibition of platelet aggregation and a return of responding to baseline levels within 6 to 8 hours. The mechanism-based model of Hong et al. (2008) contains a common single parameter comprising the fractional turnover rate of the target as well as complex, denoted k_{out}. The model includes irreversible loss of free enzyme by ASA and reversible binding by ibuprofen. The estimated half-life of enzyme activity was 33 hours, which markedly differs from the first-order dissociation rate half-life of ibuprofen from the target complex (5.6 hours).

Superficially, it may seem paradoxical that there is an attenuated response (suppression of platelet aggregation) when ASA and ibuprofen were administered simultaneously as compared with when ASA is given alone. However, this may be attributed to the available target enzyme being occupied by ibuprofen binding (temporal protection as a reversible drug–target complex with slow irreversible loss of the ibuprofen–target complex per se) thereby shielding against (irreversible) simultaneous ASA interaction. This illustrates a pharmacodynamic drug–drug interaction that requires a strict dosing order of ASA (first) and ibuprofen or naproxen (later), taking into account both target recovery

time (dependent on k_{deg}) and pharmacokinetic properties (plasma half-life) of ligand.

The combined interaction at equilibrium between ibuprofen and ASA is given as (Peletier and Gabrielsson, 2018)

$$R_{ss, ASA+ibu} = R_0 \cdot \left(\frac{1}{1 + \frac{k_{irr}}{k_{out}} \cdot C_{ASA} + \frac{1}{EC_{50}} C_{ibu}} \right) \qquad (9)$$

and the second-order irreversible loss k_{irr} of ASA (denoted K in Hong et al., 2008).

What will be the outcome then if naproxen instead of ibuprofen is used together with ASA in the previously described patient category? Naproxen displays more extensive irreversibility ($k_{out} > k_{off}$) than ibuprofen and also a much longer half-life in plasma (12–17 hours), in addition to its higher potency (0.3 μM) compared with ibuprofen (12 μM) (Gierse et al., 1999).

Using eq. 9 for the interaction between ASA and ibuprofen using data from Hong (k_{irr} = 0.152 (mg · L^{-1})$^{-1}$ · h^{-1}, k_{deg} = 0.0209 hour^{-1}, Mw(ASA) = 180) yields

$$R_{SS, ASA+ibu} = R_0 \cdot \left(\frac{1}{1 + \frac{k_{irr}}{k_{deg}} \cdot C_{ASA} + \frac{1}{EC_{50, ibu}} \cdot C_{ibu}} \right)$$

$$= R_0 \cdot \left(\frac{1}{1 + 40.4 \cdot C_{ASA} + 0.083 \cdot C_{ibu}} \right) \qquad (10)$$

where $EC_{50,ibu}$ equals 12 μM (Gierse et al., 1999). The interaction model of ASA and naproxen is given as

$$R_{SS, ASA+nap} = R_0 \cdot \left(\frac{1}{1 + \frac{k_{irr}}{k_{deg}} \cdot C_{ASA} + \frac{1}{EC_{50, nap}} \cdot C_{nap}} \right)$$

$$= R_0 \cdot \left(\frac{1}{1 + 40.4 \cdot C_{ASA} + 3.3 \cdot C_{nap}} \right) \qquad (11)$$

where $EC_{50,nap}$ is 0.3 μM (Gierse et al., 1999), and all other parameters are the same as for ASA in the ibuprofen model. It is evident from eqs. 10 and 11 that ASA has the greatest inhibitory impact upon platelet aggregation per mole of the drug (40.4), followed by naproxen (3.3) and ibuprofen (0.083). The equilibrium model predicts that at fixed free plasma concentrations, the irreversible effect of ASA will be 486 (= 40.4/0.083) and 12.2 (= 40.4/3.3) times more effective than the reversible effects of ibuprofen and naproxen, respectively.

A similar model of second-order target removal, with the same rate of removal for the target and ligand–target complex ($k_{deg} = k_{e(RL)}$), was used for assessment of H$^+$/K$^+$-ATPase turnover (half-life 15–20 hours) in the dog after drug intervention of the proton pump inhibitor omeprazole (Äbelö et al., 2000).

1. Irreversible Ligand–Enzyme Target Systems. Important but less common are situations with irreversible loss of the substrate–enzyme complex and irreversible binding of substrate to the enzyme in question so that

no enzyme is regenerated from the substrate–enzyme complex after binding. Therefore, this permanent obliteration of the enzyme]affects the associated biologic response until sufficient quantities of the enzyme protein have been produced again to restore functionality. The use of acetylcholinesterase (AChE) inhibitors such as poisonous nerve gases and similar agents with intended harmful effects are illustrative, including, for example, the recent incident with the organophosphorus chemical Novichok with potentially life-threatening consequences like convulsions, asphyxiation, and cardiac arrest (Greathouse et al., 2021; Steindl et al., 2021).

However, there are also multiple instances of irreversible enzyme inhibitors with important therapeutic uses. In addition to the COX-1 and PPI drug classes discussed previously (Singh et al., 2021) and associated text portions, penicillin is perhaps one of the most immediate examples that springs to mind. Penicillins act by covalently modifying the bacterial enzyme transpeptidase, thereby preventing the synthesis of bacterial cell walls and hence becomes bactericidal (Yocum et al., 1980). The dosing of such agents is, however, typically primarily based on in vitro estimates of minimum inhibitory concentrations for bacterial growth and a set ratio of (free) in vivo plasma exposures across time (e.g., area under the plasma concentration–time curve) versus the minimum inhibitory concentration level (Mouton et al., 2018). Regarding antibiotic therapies focus is still to use simple exposure metrices (area under the plasma concentration-time curve, C_{max}, etc.) as a replacement of a more meaningful PD metric related to the mechanism(s) of action. It would be interesting to know whether a dosing approach taking into account the turnover of the actual enzyme target (i.e., transpeptidase) would improve and refine the specificity and PK–PD modeling to the benefit of treatment protocols and downstream limiting antibiotic resistance development (Khan, 2016). A related example, this time with human cells, is cancer treatment where irreversible enzyme inhibitors (e.g., 5-fluorouracil) may block certain growth-critical enzymes in cancer cells and thus act oncolytic. While drug–tissue distribution and penetrance obviously are important factors for efficiency against different tumor varieties, perhaps studies of target turnover rates might also contribute to further optimize personalized PK–PD-based cytostatic medication regimens. Irreversible GABA transaminase inhibitors are used in the treatment of epilepsy (Ben-Menachem, 2011), and covalent unselective MAO inhibitors like phenelzine and tranylcypromine are still available as (licensed) options for affective disorder (Birkenhager et al., 2004). Similar to the aforementioned antimicrobial and antiviral cases, it remains an open question if taking target turnover into account in an extended

PK–PD algorithm may help further optimize treatment schedules in these latter conditions.

In the global pharmacotherapeutic armamentarium, irreversible target ligands are relatively scarce but appear to have received renewed interest over the last decade—perhaps at least partly related to oncology indications (Bauer, 2015). The overarching issue with covalently bound agents has been the widespread view that they all carry increased safety and (on- and off-target) toxicity risks (Bauer, 2015). Nonetheless, several irreversibly acting ligands have provided therapeutically important advances in the treatment of a variety of human afflictions. Such agents include, for example, ASA, penicillin, rivastigmine, rasagiline, and a host of recent anticancer agent varieties. Furthermore, situations involving prolonged drug residence time (k_{off}) may be described as a pseudo-irreversible ligand–target interaction – thus, a variation of a strictly irreversible process where k_{off} and $k_{e(RL)}$ operate in the same time domain.

As discussed by Bauer (Bauer, 2015), some of the pros with irreversible or pseudo-irreversible agents include less frequent dosing (convenience to the patient), the potential for lower doses (due to high and prolonged efficiency against competing endogenous ligands), and less off-target issues. Naturally, these advantages need to be balanced against the theoretical risk for idiosyncratic toxicity, as well as the toxicity inherent in the reactive ligand chemistry per se. However, the irreversible drug approach should not be a priori discarded without a thorough benefit/risk analysis, particularly if the drug ligand design may produce tissue/target-directed selectivity. However, Bauer unfortunately also concluded, based on closed system reasoning, that the k_{inact}/K_i metric for compound ranking is preferred over in vivo IC_{50}. As shown in eq. 8, a better metric would be k_{deg}/k_{on} for an irreversible system. Moreover, within the present context, it is worth noting that dependent on the desired clinical outcome versus indication, conditions involving targets with rapid turnover or requiring only short-lived or partial target response modification may be less accessible for irreversible ligand treatment (Bauer, 2015). That said, when both of these target aspects (rapid turnover, partial response) coexist, an irreversible ligand may still be an option to trigger a useful clinical response.

2. Reversible Ligand–Target Interactions. In the development of therapies to treat more or less severe excess gastric acid-induced afflictions (e.g., ulcus, reflux), the historical approach relied on drugs that interact with upstream targets influencing the acid secretion, such as, for example, antihistaminergic and anticholinergic agents. These medications may now be largely obsolete for the indications mentioned, as they have been replaced by compounds such as omeprazole, lansoprazole, and the like,

the metabolites of which directly and irreversibly interact with the downstream H^+/K^+-ATPase-dependent pump in the gastric parietal cells, thereby inhibiting the final step of acid production (Wallmark et al., 1985).

In contrast with the irreversible proton pump inhibition resulting from omeprazole, as previously discussed, it may be illustrative to consider and compare with the fate of a reversible upstream treatment of the same indication. Thus, an example of reversible drug (cimetidine) interaction with an endogenous ligand (histamine) is the therapeutic effect of cimetidine mediated by the histamine H2 receptor modulating acid secretion in the stomach. Since the target protein is the same for both cimetidine and histamine, the differences in in vivo potency values are primarily due to ligand–target binding affinities of these two reversible agonists and not target turnover per se. For the open in vivo system (Peletier and Gabrielsson, 2018), the interaction model of two ligands acting on one target at equilibrium is given as

$$R_{ss,\,Cimet+Hist} = R_{\mathrm{o}}$$

$$\cdot \left(1 - \frac{C_{Cimet}}{C_{Cimet} + \theta \cdot C_{Hist} + EC_{50,\,Cimet}} - \frac{C_{Hist}}{C_{Hist} + \frac{1}{\theta} \cdot C_{Cimet} + EC_{50,\,Hist}}\right)$$

(12)

where θ equals the ratio $EC_{50,cimetidine}/EC_{50,\,Hist}$. Therapeutic plasma concentrations (C_u = 0.8 μM at a steady-state corresponding to a daily dose of 1 g of cimetidine, taking human plasma protein binding into account (f_u = 0.2), correspond to its in vitro binding affinity (K_d = 0.79 μM). Therefore, substantially lower local concentrations of cimetidine (0.80 μM as compared to histamine 165 μM) will suffice for 50% acid reduction of the free target. Since the partial agonist cimetidine exhibits a very low efficacy parameter, it will behave like an antagonist in the presence of histamine. See also Lin (Lin, 1991) for review.

A reversible process removes the free target (R) temporarily by pushing the ligand–target complex equilibrium toward complex formation (Fig. 2). This process is typically saturable and therefore requires substantial exposures beyond the potency to be efficient. Accordingly, the response duration will depend on target turnover and the ligand half-life. To achieve less frequent dosing, a long half-life (12 hours for naproxen compared to 2 hours for ibuprofen) is thus favorable. The longer half-life of naproxen also allows time for more of the complex to be (irreversibly) removed as such. When free drug (ligand) levels then decline, equilibrium starts shifting back from complex toward free target and ligand. Thereby, as a consequence of diminished complex concentration, the response begins to decline. High exposures (multiples of the potency) of ligand are therefore typically needed to fully execute suppression of that free target and a

buildup of complex to maintain a reversible drug action over longer periods of time. For example, the reversible inhibitory action by cimetidine upon gastric acid-secretion modulating H1 receptors requires high daily doses (approximately 1 g).

The reversible GSECR inhibitor (Table 6) has a plasma half-life of 2 hours in mice. Due to the shorter target half-life (20 minutes) of GSECR in mouse brain tissue, the experimental compound needs to be constantly present at substantial exposure for adequate inhibitory effect. Assuming a similar relation between drug and target half-life also in human results in a relatively large projected human daily dose (Gabrielsson and Weiner, 2016). Similar to the GSECR inhibitor, exposure is the rate-limiting factor also for the AChE inhibitor donepezil, but in this case, only low clinical doses (5–10 mg/day) are required (Doody et al., 2008). This may seem paradoxical but is explained by (i) the high bioavailability and low clearance of the latter (Lee et al., 2015) compared with the experimental GSECR inhibitor compound, which has a very short half-life, and (ii) the long target half-life of AChE versus the very short of GSECR (Table 6). That is, even if the GSECR inhibitor compound's half-life is approximately six times longer compared with its target (Table 6), a drug half-life of 2 hours is simply not sufficient to provide for low and convenient dosing within a reversible mode of target interaction where, instead, a continuous exposure would be required. In fact, even if the GSECR drug had been acting irreversibly with the same half-life, it would have been challenging to produce a very prolonged action given the rapid regeneration of its target. An interesting parallel is the pseudo-irreversible (slow k_{off}) AChE inhibitor rivastigmine, which, due to its mode of target interaction coupled with the slow target turnover, can be dosed in very low dosage (1.5–6 mg, twice daily) for clinical effect, despite a modest bioavailability (approximately 40%) and very short drug half-life (approximately 1 hour) (Jann, 2000). The previous examples again demonstrate the importance of integrating target- and drug-related (PK and PD) properties for optimization toward attaining clinically effective dosing regimens.

An irreversible process removes free target R permanently, and the newly synthesized target has to replenish the loss. This means that the duration of response will depend upon—and potentially benefit from—a long target half-life, which determines the time of return of target levels toward baseline. Therefore, a short ligand half-life does not exclude a long duration of response. An irreversible process, such as for PPIs, may also show a faster onset of action as the removal of the target is immediate. The irreversible PPI omeprazole requires low daily doses of 20 to 40 mg for effective and rapid reduction in acid secretion.

A special case of reversible or irreversible action is when the pharmacological response discloses synergistic mechanisms. Synergism may be seen with combinations of drugs or during monotherapy with agents carrying multiple mechanisms of action. An illustrative example of synergistic action in the same drug molecule on lipid metabolism is shown for the antilipolytic compound tesaglitazar (Oakes et al., 2005). The simultaneous reversible inhibition of fatty acid production (50% reduction of k_{syn}) and stimulation of plasma fatty acid loss (5.8-fold increase in k_{deg}) resulted in a dramatic synergistic (multiplicative) effect in Zucker rats after three weeks of treatment at a single-dose level. The authors concluded that thiazolidinediones ameliorate hypertriglyceridemia by lowering hepatic triglyceride production and augmenting triglyceride clearance. This highlights how a mechanism-based pharmacodynamic (open) model demonstrates its superiority over closed systems in analyzing and communicating complex pharmacodynamic processes. Similar results have also been obtained for other thiazolidinedione derivatives (Oakes et al., 2001). The assessment of drug interactions relevant to pharmacodynamic turnover models has been provided elsewhere (Gabrielsson and Weiner, 2000; Earp et al., 2004; Peletier and Gabrielsson, 2012).

To summarize, the drug efficacy parameter primarily impacts the onset and intensity, whereas potency impacts the onset and effect duration, particularly for irreversible reactions.

The examples discussed previously further emphasize the advantages of open versus closed system approaches. As shown by these cases, the inclusion of target (e.g., tissue) dynamics together with knowledge of ligand–target interaction characteristics and ligand pharmacokinetics further increases the precision in predictions of in vivo concentrations to elicit defined drug responses. Therefore, it is worth highlighting the need to assess each and every new drug candidate on a uniquely case-by-case basis, taking into account the turnover of its intended target, the type and characteristics of ligand–target interaction, and the clearance of the ligand itself. Only by doing so, improvements in the precision of projections to clinical properties and usage may be achieved.

F. Key Insights and Translational Potential of New In Vivo Potency Expression

If the major component in a pharmacological response was only derived from ligand–target binding, this alone would still not explain why two different subjects may require different doses at a steady-state, provided their bioavailability and clearance are the same. However, differences in the target turnover may help to explain differences in the actual requirement of the drug. New expressions of in vivo potency

(eq. 2) and efficacy parameters (eq. 5) show that these are inextricably linked via target turnover.

The data of Betts et al. (Betts et al., 2010) demonstrates the translational power of the open model explanatory potential in in vivo pharmacology. Table 7 shows the in vitro dissociation constant K_d for humanized prototype anti-Dickkopf-1 IgG2 antibody against osteoporosis and the corresponding in vivo potency EC_{50} values predicted from these data by means of eq. 2.

These data illustrate the discrepancy across different species with respect to target-binding affinity (> 30-fold) and in vivo potency (10-fold). Clearly, using the target affinity data of rat or monkey as guidance of human doses, in this case, will gravely misdirect predictions of dose. Even though the EC_{50}-to-K_d ratios of the rat and monkey are similar (= 64 and 66), the markedly slower target k_{off} in man is accompanied by a 10-fold higher in vivo potency and an EC_{50}-to-K_d ratio of 188. These observations unequivocally stress the important role of including target turnover in defining efficacious concentrations and, thereby, the required dose. In vitro binding affinities clearly underestimate necessary drug exposure and human dose predictions and may therefore result in (costly) late-phase project failure. In this regard, while in vitro target binding affinity (defined by the physicochemical parameters k_{off} and k_{on}) may be similar across species, they may also differ significantly, as shown in Table 7 (e.g., k_{off} varies 100-fold but k_{on} only sixfold), and thus give rise to major downstream effects on translational efforts during drug development.

TMDD captures the capacity-limited binding and/or loss of the drug via its target (receptor, enzyme, transporter, etc.), such that this interaction impacts the disposition of the drug. This phenomenon is commonly observed for antibody kinetics with high ligand specificity, where ligand and target often appear at equimolar concentrations. So far, it has received rather little attention for small molecules but might become important also in clinical studies of such entities (An, 2017, 2020; Smith et al., 2018; van Waterschoot et al., 2018). All in all, understanding the biology of the target, including expression level and target turnover properties, is, therefore, necessary in drug discovery programs for enhanced benefit/risk precision prior to delivering drug candidates to humans.

TABLE 7
Comparisons of in vitro K_d with in vivo potency EC_{50} properties
The EC_{50} values are calculated by means of eq. 2 based on the original model parameters given in (Betts et al., 2010).

Parameter	Rat	Monkey	Man
k_{off} (d^{-1})	1.72	16.2	0.1728
k_{on} (nM^{-1} d^{-1})	49.4	316	112
K_d (nM)	0.0348	0.0513	0.00154
EC_{50} (nM)	2.22	3.39	0.29
EC_{50} to K_d ratio	64	66	188

Chronic diseases imply repeated dosing and steady-state, and several therapeutic biologics agents have been developed aiming at selective and efficient treatments for, for example, inflammatory states. In a commendable aim to address unresolved issues in drug efficiency against different autoimmune diseases, a minimized physiologically based pharmacokinetic model was recently used to assess the role of tissue fluid turnover rate on the magnitude and duration of soluble target suppression by therapeutic antibodies (Li et al., 2018). In Li et al. (2018), simulations were used incorporating the fractional turnover rate of interstitial fluid (ISF) to explain and classify the therapeutic outcome in Crohn's disease versus arthritis-associated joint synovium across a series of antibody compounds. It was concluded that ISF turnover rates strongly influenced the speed of drug–target complex removal, particularly in situations with slow ligand–target binding kinetics (k_{off}). Although Lie et al. did not discuss target turnover per se, we were curious as to whether the application of our derivations of the ligand–target and ligand–complex equilibrium relationships coupled with the mechanistic expression of in vivo potency (eq. 2) could further enhance the transparency of the findings. This notwithstanding, the duration of a pharmacological response may still be rate-limited by the target half-life.

As discussed previously, in vivo potency of eq. 2 (also see Fig. 3) summarizes the interrelations of target- and drug-associated properties, covering the entire spectrum from reversible (governed by k_{off} and binding) to irreversible interactions (governed by $k_{e(RL)}$ representing all routes of first-order ligand–target complex loss) and demonstrates the importance of target turnover (k_{deg}) in both situations. Thus, eq. 2 demonstrates that for irreversible systems in vivo potency will be governed by k_{deg}/k_{on} (primarily determined by target turnover and association rate; fast k_{on} is favored), whereas the $(k_{deg}/k_{e(RL)}) \times (k_{off}/k_{on})$ relation governs reversible interactions (i.e., primarily determined by target turnover, complex loss, and binding properties; high-affinity binding will be favored). Applying eq. 2 to the data by Li et al., (2018), but with $k_{e(RL)}$ replacing the ISF turnover-based expression, we find that this may be an alternative and a transparent option to help prioritize compounds in the development of therapeutic antibodies for various diseases (see Fig. 10). Note that target loss k_{deg} is still an important factor to consider in both cases.

The use of the minimal anticipated biologic effect level (MABEL) approach is recommended for high-risk medicinal products for first-time-in-human dose predictions (EMEA, 2018). The MABEL is the anticipated dose level leading to a minimal biologic effect level in humans. The calculation of the MABEL dose should consider target binding and receptor occupancy studies in vitro in target cells from human and the relevant animal species and exposures at pharmacological
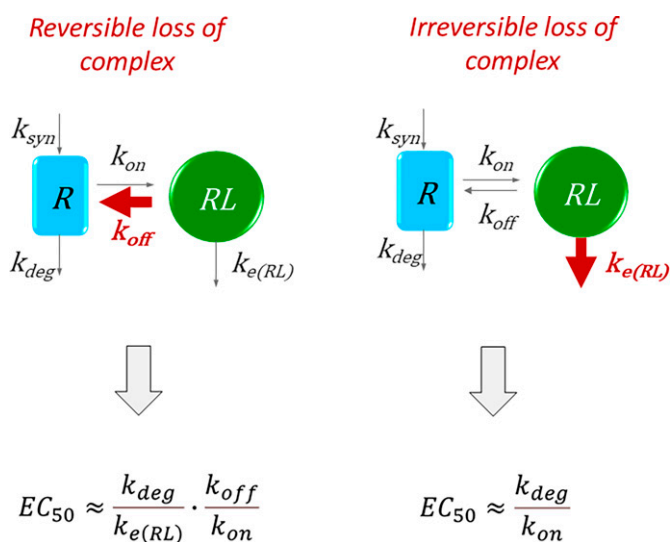

Fig. 10. Left: Schematic illustration of reversible loss of ligand–target complex where $k_{e(RL)} << k_{off}$. In vivo potency (eq. 2) may then be approximated according to the bottom row expression where ligand–target binding components as well as target turnover and ligand–target complex removal will impact in vivo potency. Right: Schematic illustration of irreversible loss of ligand–target complex where $k_{e(RL)} >> k_{off}$. In vivo potency (eq. 2) may then be approximated according to the bottom row expression where target turnover k_{deg} and ligand–target association rate k_{on} will impact in vivo potency. The $k_{e(RL)}$ parameter is the first-order loss of ligand–target complex (Gabrielsson and Peletier, 2017) corresponding to $L_T/V_T \times (1 - \sigma_v)$ in the work by Li et al. (2018). L_T, V_T, and σ_v represent lymph flow through the target tissue, interstitial flow of target tissue, and vascular reflection coefficient of the target tissue, respectively.

doses in the relevant animal species. However, the MABEL approach of human dose predictions of bispecific antibodies may not be directly applicable using binding affinity K_d (Saber et al., 2019). A tumor cell (target as such) typically has a slower turnover k_{deg} (longer half-life) than the bispecific ligand–target complex $k_{e(RL)}$. Tumor shrinkage will therefore increase via the complex since $k_{e(RL)}$ is faster than k_{deg} of the tumor cell per se. Since the k_{deg}-to-$k_{e(RL)}$ ratio in eq. 2 is less than unity, the in vivo potency EC_{50} will be higher (numerically less) than predicted from K_d (MABEL approach). Therefore, the conclusions by Saber et al. (Saber et al., 2019) indirectly support the application of the open model expression of in vivo potency (eq. 2) for first-time-in-human dose predictions of bispecifics, rather than commonly used receptor occupancy K_d.

Recently, van Waterschoot et al. (van Waterschoot et al., 2018) highlighted the poor knowledge of the actual target concentration commonly encountered in small-molecule discovery projects. The consequences of this lack of target information can range from unreliable compound potency to highly variable pharmacokinetics. Smith et al. (Smith et al., 2018) conclude that TMDD phenomena are more common for small molecules than currently appreciated and should be factored into discovery projects. Eq. 2 shows that the target properties are equally important to ligand binding characteristics (Gabrielsson and Peletier, 2017; Gabrielsson et al., 2018a,b; Gabrielsson and Hjorth, 2018). A high correlation between

in vivo potency EC_{50} and in vitro K_d relationship is not to be expected unless $k_{deg}/k_{e(RL)}$ in eq. 2 is a constant term across compounds (also see Fig. 6). It is not surprising that this correlation fails for irreversible systems since in vivo potency EC_{50} is proportional to k_{deg}/k_{on} and therefore less affected by ligand–target binding changes (Table 3).

G. Interspecies Scaling of In Vitro and In Vivo PD Properties

1. Background and Pruning of Data. Interspecies scaling of pharmacodynamic PD properties aims at the quantitative prediction of parameters responsible for the onset, intensity, and duration of a pharmacological response in different species. Following mechanism-based modeling of biomarker data, results need to be verified by extended approaches to assess factors influencing target function. To our knowledge, few studies specifically anchor their kinetic–dynamic modeling efforts to encompass properties derived from target behavior per se (e.g., turnover). This makes modeling results less reliable, particularly for interspecies scaling of pharmacodynamic PD properties. Hence, not only the origin and quality of in vitro and/or in vivo data but also the methods for PD scaling have to be scrutinized.

The pharmacological response is typically expressed by means of the Hill-function including a baseline parameter (Eq. 5, bottom) E_0 (Danhof et al., 2007; Mager et al., 2009; Gabrielsson and Weiner, 2016; Choe and Lee, 2017). The baseline E_0 may be a single parameter (constant) or function (e.g., time or an endogenous ligand concentration). E_0 may be due to biologic variation such as diurnal oscillation, endogenous ligands, stress, disease, or potentially constitutive activity. E_0 is often a conglomerate of processes that, in sum, are displayed as a baseline response. Typical biomarker responses are blood pressure, heart rate, depression scores, body weight, body temperature, etc., which all originate from a baseline time course prior to drug administration. Two additional parameters, the in vivo potency EC_{50} and the efficacy parameter E_{max} are defined in eqs. 2 to 5. One regresses the Hill function simultaneously to (two or more) response-time profiles, letting the plasma ligand concentration-time course drive the response and then simulate (with the final parameter estimates) the steady-state ligand concentration–response relationship. The efficacy parameter E_{max} (Choe and Lee, 2017) is the absolute distance between the maximum response and the baseline in a concentration–response plot. If RL_{max} is measured, it can be input as a constant and ρ as a model parameter to be estimated. If some of the target and binding properties k_{deg}, k_{off}, and k_{on} are known for a particular species (or humans), the $k_{e(RL)}$ parameter can be estimated in the in vivo potency expression.

Prior to use for comparisons across species, any confounding covariates such as plasma protein binding, active or interactive metabolites, or endogenous agonists

to a PK or PD parameter must be accounted for. As a first step, data pruning should be performed to make sure that systemic exposure (a.k.a. unbound plasma concentration) is used across species (Rolan, 1994; Benet and Hoener, 2002; Smith et al., 2010). Chronic indications and treatment imply PD and PK equilibrium between plasma and the target tissue. Under these conditions, the steady-state unbound plasma-to-unbound tissue/biophase concentration ratio will form a constant ratio. This ratio may be less than, greater than, or equal to unity but remains constant nevertheless; therefore, the unbound plasma concentration serves as a relevant proxy reference for the assessment of in vivo potency. Time-variant influences [e.g., as a consequence of (patho-)physiologic drift factors) on the biophase may include perfusion rate fluctuations, energy and protein turnover (Pich et al., 1987; Fearon et al., 1988), capillary permeability, transporters (Peletier and Gabrielsson, 2018), drug metabolism (Zanger and Schwab, 2013), disease progression (Holford and Nutt, 2008)] have to be incorporated into the prediction as complementary steps. The interplay between unbound plasma and tissue concentration is schematically illustrated for simple diffusion, active transport, clearance, etc. in Fig. 11.

Because the unbound plasma concentration is less influenced by species-dependent plasma protein binding differences, conversion from total to unbound plasma concentrations should be performed for each species. As previously discussed, the unbound plasma concentration is a proxy for the thermodynamically active exposure at the target biophase and hence indirectly drives pharmacological response at equilibrium. Unbound plasma concentrations represent both practical experimental measures (easily measured in all mammalian species, including humans) and may be used for translational purposes. Together with unbound clearance, the free drug concentrations determine the oral dose necessary for therapeutic effect and will be of importance for the assessment of safety data as well (Miida et al., 2008). In conditions with adequate knowledge of (peripherally located) targets and corresponding dysfunctional tissue, including the ability to sample actual tissue levels of the ligand, assessment of potency has to consider plasma-to-target tissue concentration differences (Kalvass et al., 2007). This situation has recently been addressed conceptually (Peletier and Gabrielsson, 2018).

The use of the equilibrium unbound drug concentration C_u in plasma coupled to a robust and meaningful PD biomarker is a good strategy for cross-compound comparisons and for developing kinetic–dynamic relationships, irrespective of reversible or irreversible mechanisms of action. An excellent review of drug concentration asymmetry in tissues versus plasma addresses this topic for small molecule-related modalities
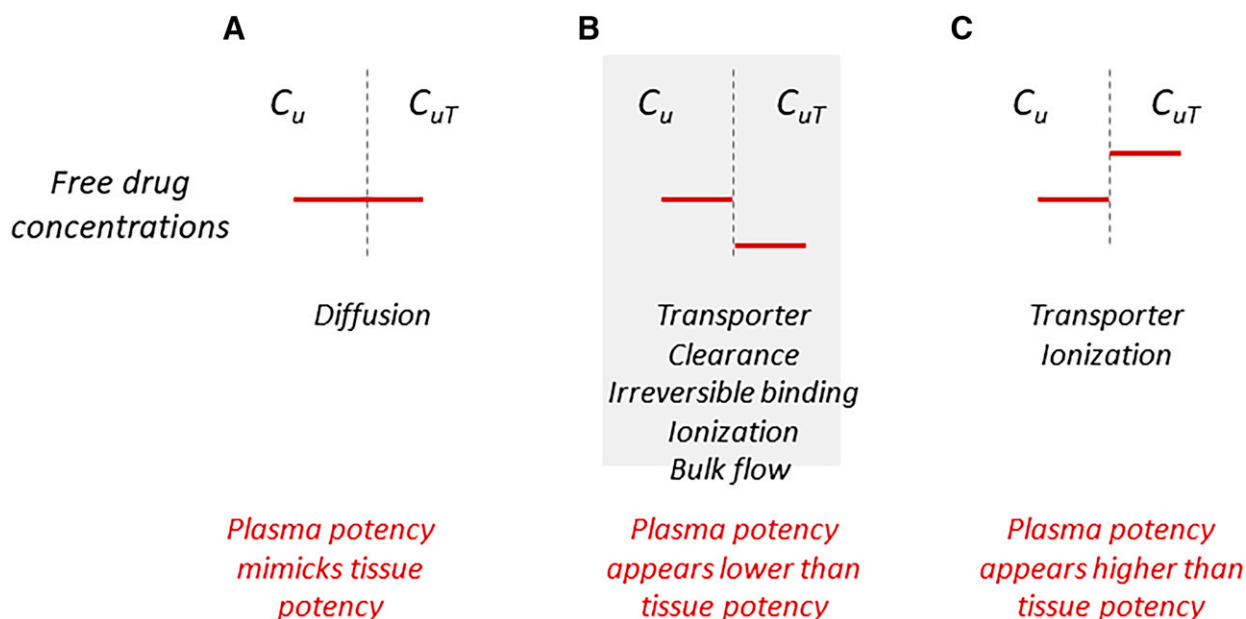
Fig. 11. Schematic illustration of unbound plasma concentration C_u and unbound tissue (target) concentration C_{uT} at steady state. Case A: Only different concentration diffusion of drug molecules is responsible for drug distribution between plasma and the target tissue. Hence, unbound concentrations in plasma are equal at steady-state. In vivo potency based on plasma or target tissue will be the same. Case B: Efflux transporters, clearance, irreversible binding, ionization (pH differences between plasma and tissue), or bulk flow are responsible for decreasing unbound concentration in the target tissue. Unbound concentrations in plasma are higher than unbound concentrations in tissue at steady-state. In vivo potency based on plasma is lower (numerically higher) than estimated from the target tissue. Case C: Uptake transporters or ionization favor increased unbound concentrations at the target tissue. Unbound concentrations in plasma are lower than unbound concentrations in tissue at steady-state. In vivo potency based on plasma is higher (numerically lower) than estimated from the target tissue.

(Zhang et al., 2019). Additional information on how endogenous ligands (Kroon et al., 2017), active or interactive metabolites (Obach, 2013), and target expression in animals and humans (Simon et al., 2013) are applied may be helpful in cross-species pruning of data (Levy, 1998).

2. Concepts of Allometry. Let us briefly review how interspecies scaling is done and then give a few recent examples related to a mechanistic interpretation of modeling output with related problems and pitfalls. We start by focusing on the most commonly used approach: allometry. Allometry, in its broadest sense, describes how the characteristics of, for example, mammals change with size. Adolph (Adolph, 1949), Boxenbaum (Boxenbaum, 1982), Kleiber (Kleiber, 1947), and Schmidt-Nielsen (Schmidt-Nielsen, 1984) provide seminal background reviews. Allometric relationships are given as power functions as

$$Y_{animal} = a \cdot BW_{animal}^b \tag{13}$$

where Y is the physiological (e.g., blood flow), pharmacokinetic (e.g., clearance), or pharmacodynamic (rate constants in the in vivo potency or efficacy expressions) variable; BW is the body weight of the particular animal (or human); and a and b are allometric parameters. When scaling properties from animals (e.g., primate) to human, the allometric relationship between the two species becomes

$$Y_{human} = Y_{primate} \cdot \left(\frac{BW_{human}}{BW_{primate}} \right)^b \tag{14}$$

where the scaling factor is the body weight ratio human-to-primate raised to the allometric exponent b. $Y_{primate}$ has to be the absolute parameter based on the total body weight and not normalized per kg. In the open model (eqs. 1, 2, and 5), we have the three important properties (k_{deg}, k_{off}, $k_{e(RL)}$) expressing in vivo potency, which guide the operating concentration range in many situations. As first-order rate constants, a practical approach is to use simple allometry (eqs. 13 and 14) or use independent (literature) data for interspecies predictions (Gabrielsson and Weiner, 2016; Gosset et al., 2017). The fractional rate constant k_{deg} of the target can be scaled according to

$$k_{deg, human} = k_{deg, animal} \cdot \left(\frac{BW_{human}}{BW_{animal}} \right)^{-b} \tag{15}$$

where BW and b (b power law with a typical range of 0.1–0.3 for first-order rate constants) (Gabrielsson and Weiner, 2016) denote body weight and the allometric exponent, respectively. Scaling the apparent synthesis rate $k_{syn,human}$ [with units amount/(volume · time)] of target is done by multiplying the target expression level in humans $R_{0,human}$ by the scaled fractional rate constant of target k_{deg}:

$$k_{syn, human} = R_{0, human} \cdot k_{deg, human} \tag{16}$$

If clearance of target $Cl_{trg,human}$ and target expression level $R_{0,human}$ are known, the corrected synthesis rate $k_{syn,human}$ (with units amount/time) of the target becomes

$$k_{syn,human} = R_{o,human} \cdot Cl_{trg,human} \qquad (17)$$

Since parameters that require energy, such as organ blood flows, clearances, and synthesis rates, often follow the 3/4 power law, the corrected synthesis rate $k_{syn,human}$ will also scale in a similar way. Hence, the target synthesis rate (amount/time) k_{syn} may be scaled from animal data according to

$$k_{syn,human} = k_{syn,animal} \cdot \left(\frac{BW_{human}}{BW_{animal}} \right)^b \qquad (18)$$

where the allometric exponent falls in the range of 0.6 to 0.9 (3/4 power law see) (Adolph, 1949; Schmidt-Nielsen, 1984) and is similar to how clearance is predicted. For practical case studies and inter-species scaling concepts, see the textbook by Gabrielsson and Weiner (Gabrielsson and Weiner, 2016).

Physiologic time (e.g., half-lives) may be scaled by means of

$$time_{human} = time_{animal} \cdot \left(\frac{BW_{human}}{BW_{animal}} \right)^b \qquad (19)$$

where the allometric exponent falls in the range of 0.2 to 0.3.

3. Literature Case Examples. The following list of interspecies scaling case examples is not intended to be exhaustive but nevertheless demonstrates some problems and solutions commonly encountered in the literature. Frequently, studies lack accounting for plasma protein–binding differences across compounds and species, resolving the contribution of active or interactive metabolites, incorporation of endogenous ligands, considerations of the link between the biomarker applied and the target function, and consolidating modeling results with independent literature data.

A recent report studied TNF_α turnover after a lipopolysaccharide (LPS) challenge, listing half-lives of the inflammatory marker TNF_α in mice, rats, and humans without reference to a specific target behavior (Larsson et al., 2021). The approach was a meta-analysis of several preclinical studies in rats comparing the anti-inflammatory activity of new compounds with roflumilast. Proper assessment of unbound plasma concentrations and active metabolites and a clear link to target function was however lacking.

Gosset et al. (Gosset et al., 2017) presented interesting data on fractional turnover rates k_{deg} (denoted k_{out}) as a function of size (body weight) of the core body temperature in mice, rats, and dogs upon intervention with PF-05105679, a moderately potent TRPM8 ion-channel blocker evaluated for the treatment of cold pain sensitivity. In this case, however, results were not validated by independent turnover data of the intended TRPM8

target, and the model also failed to account for feedback, a central mechanism in body temperature control.

In a retrospective analysis, Ito et al. (Ito et al., 1997) found a high correlation ($r^2 = 0.961$ and slope 1.038) between the unbound plasma concentration C_u and dissociation constant K_d of 19 benzodiazepines BZ when aiming at 40% to 60% occupancy at the GABA-BZ site in vivo. Visser et al. (Visser et al., 2003) compiled similar data between the EEG effects of nine prototypical $GABA_A$ receptor modulators (six benzodiazepines, one imidazopyridine, one cyclopyrrolone, and one β-carboline) and their in vivo closed model receptor affinity. Again, no quantitative information was given about the target receptor beyond drug-receptor affinities in spite of available quantitative literature data (Borden et al., 1984; Lyons et al., 2000) that might otherwise have been used for consolidating the validity of modeling results.

In a seminal paper by Kalvass et al. (Kalvass et al., 2007) results of seven opioids were presented, with a high in vitro K_i to in vivo EC_{50} correlation ($r^2 = 0.995$) when data were corrected for plasma protein binding differences across compounds and species. This suggests that the unbound plasma concentration C_u is a better predictor of PD response than total plasma concentrations. The authors discussed why in vivo EC_{50} values correlated better with receptor binding K_i values than with EC_{50} values obtained from in vitro [35S]GTPγS experiments. It should be noted that K_i measures affinity only, whereas in vitro $\acute{C}$[35S]GTPγS EC_{50} (i.e., functional) values may be contaminated by other factors in a nonsteady-state cell system.

Acute dosing estimates of the total in vivo potencies corrected for plasma protein binding of dual G-protein-coupled receptor 81/109A (GPR81/GPR109A) agonists were compared with their in vitro binding data (Almquist et al., 2018). The analysis made no efforts to dissect in vitro/in vivo differences beyond general covariates such as anesthetics. It is not clear whether experiments with compound intervention also measured and modeled active metabolites and the endogenous ligand nicotinic acid (NiAc). Simultaneous fitting of all experiments, particularly based on unbound test compound concentrations, and allowing individual efficacy parameters (I_{max}) would have allowed a more mechanistic approach.

A turnover model capturing inactive and active proton pump pools was applied to acid secretion data in cannulated Heidenhain pouch dogs (Äbelö et al., 2000). It allowed the estimation of the fractional turnover rate used for the prediction of gastric acid secretion inhibition upon repeated human dosing. Rate constants were scaled allometrically but not related to independent experiments of the target, nor was the binding dissociation rate of the complex compared with the fractional

turnover rate. The application of such reasoning might have been of importance for optimizing the ligand synthesis program.

In two seminal reviews, including interspecies scaling of pharmacodynamic data, the authors referred to binding properties based upon the closed system approach, keeping the total amount of target fixed to the baseline level (Danhof et al., 2007; Mager et al., 2009). Both reviews concluded that pharmacodynamic parameters such as potency and efficacy tend to be species independent. However, it is more likely that in vivo potency will demonstrate the opposite if system properties such as target turnover k_{deg} vary across different species (Betts et al., 2010; Gosset et al., 2017). Surprisingly, Danhof et al. (Danhof et al., 2007) state: "For drugs acting at extracellular targets, . . . binding to plasma proteins and other blood constituents can restrict distribution to the biophase," which is contrary to the well-known fact that plasma protein binding does not restrict a compound from distributing to a target site. Unbound exposure of small molecules after oral dosing is governed by dosing rate and unbound clearance (Benet and Hoener, 2002).

Interspecies scaling of the efficacy parameter E_{max} is still a challenge since transduction, denoted by ρ, may vary depending on age, sex, tissue, species, etc. Transduction contains not only the conversion of a chemical or electrical signal in the cell to physiologic action but also the cascade of events leading to downstream gene-modified amplification and/or feedback control. For example, gene expression patterns in the ischemic penumbra differed strikingly between mice and rats at both 2 and 6 hours after permanent middle cerebral artery occlusion (Wu et al., 2022). The faster cessation of penumbral oxidative stress in preclinical animal models (Nilsson et al., 1990) as compared with humans (Benveniste et al., 1984; Bullock et al., 1995a; Bullock et al., 1995b) may be an important factor that differentiates clearcut therapeutic effects in small animals but lack thereof in humans. Adjustments for differences in physiologic time (species longevity differences) (Mestas and Hughes, 2004; Dutta and Sengupta, 2016) may be a starting point when designing future human stroke studies. Positive outcomes of 3 to 5 days dosing duration in, for example, the gerbil stroke model middle cerebral artery occlusion (100 g body weight), may correspond to 3 to 4 weeks (21 days using eq. 19) treatment in humans. To our knowledge, no stroke trials have specifically addressed physiologic time differences between animals and humans. A physiologic time difference of oxidative stress was unfortunately neglected also in clinical stroke trials of the radical scavenger NXY-059, which had demonstrated good neuroprotection in several animal models (Marshall et al., 2003). Obviously, multifaceted biomarkers (such as the size of the penumbra in this case) are consequences of a host of target interactions and distributional phenomena, thus not specifically mirroring a single target turnover but rather a cascade of events. Therefore, beyond scaling determinants of ligand–target complex expression (RL), such as target synthesis rate k_{syn} and complex removal $k_{e(RL)}$, few attempts have been made to scale the transduction parameter ρ.

Kroon et al. (Kroon et al., 2017) formulated a dosing strategy based on PD findings of the highly intricate NiAc and plasma FFA interaction:

An intermittent but not continuous NiAc dosing strategy, succeeded in retaining NiAc's ability to lower plasma FFA and improve insulin sensitivity. Furthermore, a well-defined NiAc exposure, timed to feeding-periods, but not fasting-periods, profoundly improves the metabolic phenotype of this animal model.

This was concluded by refining the design of in vivo experiments (Kroon et al., 2017) and mechanistic PKPD modeling (Andersson et al., 2019), which allowed the best timing of dosing and shaping of NiAc exposure to improve therapeutic value. The authors' approach better captures what is necessary for understanding the onset, intensity, and duration of a therapeutic effect.

It appears unlikely that certain therapeutic areas, such as behavioral (CNS) effects can be reliably predicted from in vitro data per se. The symphony of interactions that impact turnover of the target systems involved (DA, 5-HT, Glu, etc.) may have entirely different time courses in vivo versus what may be predicted from on/off binding processes in vitro alone. It is also particularly challenging to generate in vitro disease models with sufficient validity for the purpose (e.g., cognitive behavioral cotreatment involved in studies of antidepressant actions of psychedelics in humans). Speculatively, a battery of in vivo behavioral (disease-related) models accompanied by robust biomarkers might be partially helpful (e.g., phenotypic drug screening approaches) (Waters et al., 2017). Overall, the mechanisms underlying psychiatric readout responses likely reflect a cascade of events through multiple circuit and target involvement greatly exceeding the duration of the initial drug–target interaction process per se. A seminal paper discussing some of the challenges in translational pharmacology was published by Green et al. (Green et al., 2011).

Human predictions of biomarker responses and PD properties from preclinical in vivo are instrumental when designing first-time-in-human studies. The aforementioned examples highlight specifically in vivo biomarker applications representing a specific target turnover, data pruning, mechanism-based PD models, and/or how interspecies predictions of PD properties are typically done. In this context, we foresee that interspecies scaling will be particularly important in pediatrics, frail

elderly, or rare diseases (de Aguiar Vallim et al., 2017), where deviating target expression levels and/or turnover rates are likely to occur. Needless to say, while the target behavior-related modeling refinements represent a clear advancement in these aims, there is still room for further mechanistic enhancements.

The following are some general points to consider with respect to the interspecies scaling of PD data:

- Target knowledge (pathophysiological conditions, rare diseases, pediatrics, frail elderly)?
- Drug mechanism(s) of action?
- Is biomarker/disease marker applicable in humans (species-specificity of targets)?
- Does biomarker/disease marker capture target behavior?
- Quality of in vitro and in vivo preclinical data available (e.g., unbound concentrations and unbound target tissue-to-plasma concentration differences)?
- Is quantitative target information available?
- Is allometry applicable to a specific parameter or expression?
- Differences in physiologic time (species longevity differences)?
- Information about robust safety marker(s)?
- Use of the model as a knowledge repository, as predictions are never better than background data used for generating predictions (uncertainty range, sensitivity analysis, etc.)?

This section has addressed how target turnover properties will affect in vivo potency and efficacy and thereby predictions of therapeutically meaningful drug dosage. The new expression of in vivo potency will be a valuable tool in experimental pharmacology and translational and regulatory sciences. In the next section, the incorporation of turnover in drug elimination enzymatic systems, new properties of clearance, time to equilibrium, and steady-state solutions of substrate, the enzyme and complex will be discussed.

III. Drug Metabolism and the Open Michaelis–Menten System

1. Background to Equations and Models

In vivo potency guides at which plasma exposure a drug is active, and clearance carries information about how efficiently the body removes the medicine. For linear (first-order) systems, clearance is assumed to be constant independently of a change in the substrate (drug) concentration over time. A robust method to estimate systemic clearance is through intravenous injection of substrate followed by dividing the intravenous dose by the observed total area under the plasma concentration-time profile. At higher substrate (drug) exposure saturation of the eliminating pathways may occur, and clearance is then often expressed by means of the classic closed Michaelis–Menten (MM) model. Since its introduction in 1913, the MM equation has become a central tenet in biomedical sciences in general and as a function of saturable processes in particular (Michaelis and Menten, 1913; Michaelis et al., 2011). The closed MM model has been applied to in vitro and in vivo systems of acute and chronic data. The limitations of the closed MM system are, however, its lack of enzyme protein synthesis and loss in parallel to its metabolic processes (Fig. 2, metabolic systems, right-hand column). This means that the total pool E_{tot} of free E and substrate-bound ES enzyme complex is constant and equal to the free baseline pool E_0 at any time. It is often assumed for closed systems that the initial substrate concentration S is initially constant and much greater than the total enzyme concentration E_0. During oral dosing, for example, both the rate and extent of substrate exposure are highly variable and do not exceed the responsible enzyme concentrations at therapeutic drug concentrations (for a review on CYP450., see Zanger and Schwab, 2013). Daily 400 mg oral doses of the anti-inflammatory drug acetaminophen (Mw = 151.16 g/mol) corresponds to a plasma peak concentration of about 10 mg/L (66 μM) (Raffa et al., 2018). The most abundant hepatic responsible enzyme, CYP3A4, for the metabolism of acetaminophen has a total amount of 60 to 150 nmol/g hepatic tissue (60–150 μmol/kg liver or 90–225 μmol/ liver) (Zanger and Schwab, 2013), which exceeds drug exposure to acetaminophen at any time.

The underlying assumptions of the open MM model are that the synthesis of free enzyme protein stays constant, but the rate of elimination of free enzyme decreases as the free enzyme concentration diminishes when temporarily occupied by substrate molecules (Gabrielsson and Peletier, 2018; Peletier and Gabrielsson, 2022). Total enzyme concentration (free and complex bound) is allowed to vary under chronic drug use, which means that it can exceed the initial enzyme level E_0. Clearance of free substrate will vary until equilibrium is established. The closed MM approach assumes that the catalytic reaction, rather than the substrate-enzyme binding process, is the rate-limiting step. This assumption is not necessary in the open model. The open model does not exclude that drug–drug metabolic interactions may affect both rate and extent of binding. By including the substrate and target turnover (i.e., opening the system) to mimic the in vivo situation, new kinetic properties of enzyme and substrate enzyme evolve. A consequence of this will be that the open MM equation of clearance [originally denoted as the specificity constant fractional catabolic rate constant (k_{cat})/K_m times the enzyme baseline concentration E_0] and rate of metabolism will take another functional form.

Studying drug metabolism outside the in vivo context is most often done in vitro. With purified enzymes, neither synthesis nor degradation of the enzyme is expected. In cell systems, the turnover of enzymes may still be an ongoing process. However, the timeframe within which this is done is important. Even though the cell system (in vitro) may have synthesis and catabolism of enzymes, studies of drug metabolism under chronic in vitro conditions are rarely performed. Synthesis and catabolism of enzyme proteins are seldom studied in parallel to drug substrate metabolism. Whereas drug metabolism is typically studied within a timeframe of a few hours or a maximum of a day, enzyme half-lives are most often much longer than that. A closed system approximation may therefore be valid for acute but not chronic situations assuming a stable enzyme level (Fig. 2) (von Bahr et al., 1998; Rostami-Hodjegan et al., 1999; Magnusson et al., 2008; Ramsden et al., 2015).

In this section, we first explore and compare the open model with the traditional closed system MM model derived by Gabrielsson and Peletier (Gabrielsson and Peletier, 2018) and recently further explored (Peletier and Gabrielsson, 2022). We derive steady-state equations of the substrate (S, drug), enzyme (E), and complex (ES) and then dissect the new relationship of *in vivo* V_{max}, K_m, and clearance Cl. Simulations are done with the open system showing its intrinsic behavior governed by experimental data. From this, conclusions about the drug–drug interaction potential are then drawn.

Let us start with the rate equations of the open system metabolic model of the free substrate (S), free enzyme €, and substrate-enzyme complex (ES), including zero-order input (*Input*) and nonspecific clearance ($Cl_{(S)}$) of the substrate, and zero-order turnover rate (k_{syn}) and first-order fractional turnover rate (k_{deg}) of enzyme shown in the following equation (Fig. 2, metabolic systems, right-hand column). The rate of formation of product (metabolite) via the substrate-enzyme complex activity (k_{cat}) is shown in eq. 19 (bottom line):

$$\begin{cases} \dfrac{dS}{dt} = \dfrac{Input}{V} - \dfrac{CL_{(S)}}{V} \cdot S - k_{on} \cdot S \cdot E + k_{off} \cdot ES \\[2mm] \dfrac{dE}{dt} = k_{syn} - k_{deg} \cdot E - k_{on} \cdot S \cdot E + (k_{off} + k_{cat}) \cdot ES \\[2mm] \dfrac{dES}{dt} = k_{on} \cdot S \cdot E - k_{off} \cdot ES - k_{cat} \cdot ES \\[2mm] \dfrac{dP}{dt} = k_{cat} \cdot ES \end{cases} \quad (20)$$

We assume that free substrate S is only eliminated via enzymatic degradation and therefore set nonspecific clearance of $Cl_{(S)}$ to zero.

2. Equilibrium States and Clearance Expression of (Reversible) Metabolic Systems

Mechanistic expressions of the substrate, free enzyme, and substrate–enzyme complex concentrations are derived by incorporating target/enzyme turnover (Table 8). In particular, we show that whereas in closed systems, there is a built-in saturation beyond which the substrate

TABLE 8
Generic expressions of the open and closed system properties of enzymes
E_0 of the closed system is fixed over time unless changes occur due to changes in synthesis (induction/inhibition) or catabolism. The closed system demonstrates saturation of free enzyme, complex, clearance and rate of elimination at equilibrium in contrast to the open system which behaves nonlinearly until equilibrium is reached.

Metabolic system	Open system	Closed system
$V_{max}(t)$	$E(t) \cdot k_{cat} \cdot V$	$E_0 \cdot k_{cat} \cdot V$
$V_{max}(t)$	$E(0) \cdot k_{cat} \cdot V$	$E_0 \cdot k_{cat} \cdot V$
K_m	$\dfrac{k_{cat} + k_{off}}{k_{on}}$	$\dfrac{k_{cat} + k_{off}}{k_{on}}$
Substrate S_{ss}	$S_{ss} = \dfrac{Input}{V \frac{V_{max}(0)}{K_m}}$	$S_{ss} = \dfrac{Input}{V \frac{V_{max}}{K_m + S_{ss}}}$
Free enzyme E_{ss}	$E_{ss} = E_0 = \dfrac{k_{syn}}{k_{deg}}$	$E_{ss} = K_m \cdot \dfrac{ES_{ss}}{S_{ss}}$
Complex ES_{ss}	$ES_{ss} = \dfrac{Input}{V \cdot k_{cat}} = \dfrac{S_{ss}}{\frac{E_0}{K_m}}$	$ES_{ss} = \dfrac{E_0 \cdot S_{ss}}{K_m + S_{ss}}$
Clearance at disequilibrium $Cl(t)$	$E(t) \cdot k_{cat} \cdot V \dfrac{1}{\frac{k_{cat} + k_{off}}{k_{on}}} = \dfrac{V \cdot V_{max}(t)}{K_m}$	$E_0 \cdot k_{cat} \cdot V \dfrac{1}{\frac{k_{cat} + k_{off}}{k_{on}} + S(t)} = \dfrac{V \cdot V_{max}}{K_m + S(t)}$
Clearance at equilibrium Cl_{ss}	$E(0) \cdot k_{cat} \cdot V \dfrac{1}{\frac{k_{cat} + k_{off}}{k_{on}}} = \dfrac{V \cdot V_{max}(0)}{K_m}$	$E_0 \cdot k_{cat} \cdot V \dfrac{1}{\frac{k_{cat} + k_{off}}{k_{on}} + S} = \dfrac{V \cdot V_{max}}{K_m + S_{ss}}$
Elimination rate at disequilibrium $v(t)$	$\dfrac{V \cdot V_{max}(t)}{K_m} \cdot S(t)$	$\dfrac{V_{max} \cdot V}{K_m + S(t)} \cdot S(t)$
Elimination rate at equilibrium v_{ss}	$\dfrac{V \cdot V_{max}(0)}{K_m} \cdot S_{ss}$	$\dfrac{V_{max} \cdot V}{K_m + S} \cdot S$

concentration keeps rising, in open systems involving enzyme turnover, this is no longer the case. However, after an initial period of disequilibrium, the expression of intrinsic clearance reduces to a linear expression. Here, clearance is assumed to be proportional to the free enzyme concentration $E(t)$ over time and therefore varies in a similar pattern to $E(t)$. At equilibrium, clearance returns to be proportional to the free baseline enzyme concentration E_0.

A revision of the closed MM system to also include enzyme turnover was recently undertaken to attain a closer resemblance to the in vivo situation (Gabrielsson and Peletier, 2018). The revised expressions of intrinsic clearance and rate of elimination at equilibrium are given in as

$$
\begin{cases}
Cl = E(t) \cdot k_{cat} \cdot V \cdot \dfrac{1}{\dfrac{k_{cat} + k_{off}}{k_{on}}} = \dfrac{V_{max}(t)}{K_m} \\[2em]
Cl_{ss} = E(\circ) \cdot k_{cat} \cdot V \cdot \dfrac{1}{\dfrac{k_{cat} + k_{off}}{k_{on}}} = \dfrac{V_{max}(\circ)}{K_m} \\[2em]
Rate = \dfrac{V_{max}(t)}{K_m} \cdot S(t) \\[1em]
Rate_{ss} = \dfrac{V_{max}(\circ)}{K_m} \cdot S_{ss}
\end{cases} \quad (21)
$$

where $E(t)$ denotes the time course of the free enzyme. Since the free enzyme level (E) changes over time and will initially decline during extended drug exposure, both $V_{max}(t)$ and clearance Cl will decrease and appear time-dependent until equilibrium [steady-state, Cl_{ss} and $V_{max}(0)$] is reached (Figs. 12 and 13). The equilibrium relationships of target substrate (S_{ss}) free enzyme (E_{ss}) and substrate-enzyme complex (ES_{ss}) are shown as follows:
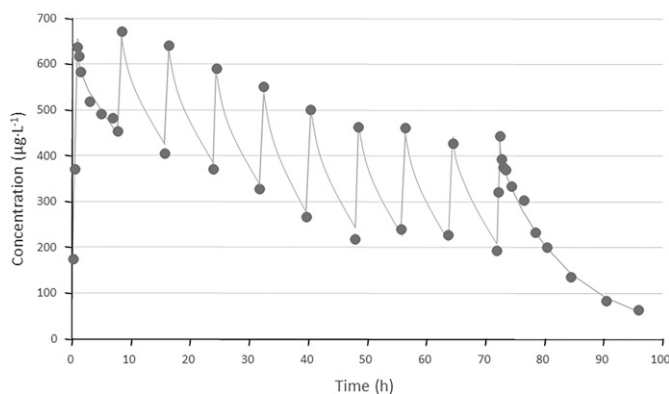

Fig. 12. Observed (solid symbols) and regressed (eq. 9, solid line) concentration-time data of compound X after 10 repeated intravenous injections. The first 120 mg intravenous injection was followed by nine 40 mg intravenous injections given every eighth hour. Concentration-time data and doses are taken from case study PK22 in Gabrielsson and Weiner (2016). This data set was included to demonstrate the flexibility of the open MM model.

$$
\begin{cases}
S_{ss} = \dfrac{Input}{Cl_{ss}} \\[1.5em]
E_{ss} = E_0 = \dfrac{k_{syn}}{k_{deg}} \\[1.5em]
ES_{ss} = \dfrac{Input}{V \cdot k_{cat}}
\end{cases} \quad (22)
$$

The substrate concentration S_{ss} increases proportionally with the $Input$ rate at steady-state since clearance is a nonsaturable term at equilibrium (steady-state) in the open model of drug metabolism, which contrasts the closed system model (Table 8).

Surprisingly, the free enzyme level at steady-state E_{ss} returns to the enzyme baseline value E_0 since it is only determined by k_{syn} and k_{deg} (Table 8; Fig. 12). The equilibrium level of the substrate–enzyme complex ES_{ss} is the ratio of substrate $Input$ to the catalytic clearance (elimination rate constant k_{cat} times distribution volume) at equilibrium. Substrate clearance Cl is determined by the biologic properties of the responsible enzyme, synthesis k'_{syn}, and degradation k_{deg}, as well as the binding and catalytic properties k_{off}, k_{on}, and k_{cat}. Cl can be simplified to $(k'_{syn}/k_{deg}) \cdot k_{on}$ when k_{cat} is much greater than k_{off}, which means that Cl is a function of free enzyme baseline expression E_0 and the second-order rate constant k_{on} at equilibrium.

Table 8 summarizes the different properties of the open and closed systems. The time courses of substrate, enzyme, complex, clearance, and elimination rates display saturable behavior akin to the closed system. All of these variables and parameters follow dose-proportional (first-order) kinetics at equilibrium of the open model. The duality of the open system is that substrate, free enzyme, and the substrate–enzyme complex also display nonlinear behavior during the time to equilibrium. Table 8 contrasts Cl derived from the closed system, which decreases with increasing substrate exposure S, and Cl of the open system, which is independent of the substrate exposure at equilibrium. This stems from the fact that while in the closed system, the total amount of enzyme E_{tot} is fixed to what it is initially, E_0 and the amount of the substrate–enzyme complex can never exceed the total amount of enzyme in closed systems. In the open system, the free enzyme is continuously synthesized and turned over via irreversible loss and complex formation.

The degree of target–ligand (substrate–enzyme) complex formation is a significant element affecting substrate metabolism rate in the open situation. Thus, as more substrate (drug)–enzyme complex is formed, the availability of free enzyme protein declines and, in turn, also the rate of elimination of free enzyme, while the rate of synthesis (replenishment) of free enzyme molecules is sustained. That is, the total concentration of enzyme (free + substrate complex-bound) will increase during the period of disequilibrium until a balance between the three entities (free and bound enzyme and
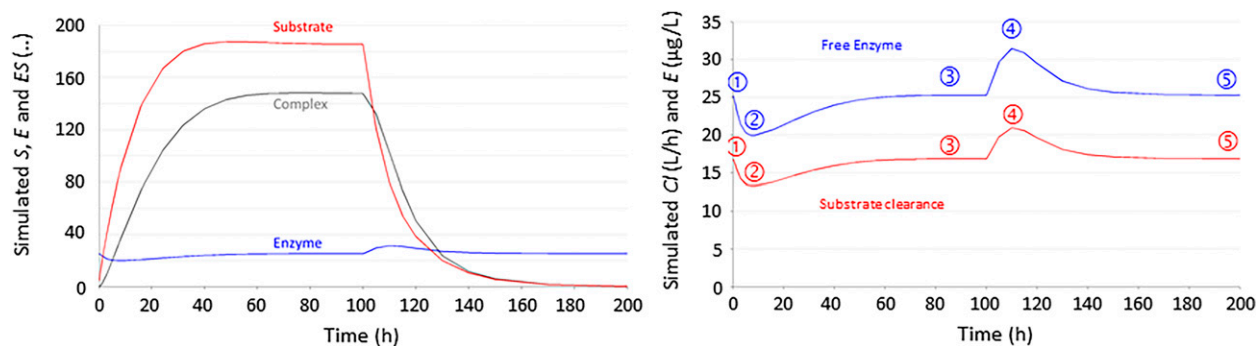
Fig. 13. Left: Model simulations of concentration-time courses of the substrate (S), free enzyme (E), and substrate-enzyme complex (ES) after a 100-hour constant-rate infusion aiming at about 200 $\mu g \cdot L^{-1}$ of test compound analyzed in Fig. 12. Therapeutic concentrations fall in the range of 100 to 500 $\mu g \cdot L^{-1}$. Right: Model simulations of concentration-time courses of free enzyme (blue line) and clearance (red line). The free enzyme level deceases transiently from its baseline value (1) to a trough (2) during the initial rise in plasma concentration of substrate since substrate will bind to free enzyme. An apparent steady state is reached between 40 to 60 hours (3) and lasts until the end of infusion. Only synthesis k_{syn} and loss k_{deg} of free enzyme governs the steady-state free enzyme concentration. There is a rapid rise in free enzyme concentrations upon stop of infusion due to stop of complex formation (no further consumption of free enzyme for complex formation) and release of the free enzyme from the substrate–enzyme complex pool (4) as the rate of substrate input stops. The free enzyme concentration returns to the equilibrium concentration terminally (5). (1)–(5) correspond to the different stages schematically shown in Fig. 14.

substrate) has been established. Typically, enzyme proteins have relatively long half-lives (von Bahr et al., 1998; Rostami-Hodjegan et al., 1999; Magnusson et al., 2008; Ramsden et al., 2015), often exceeding that of substrate per se. It follows that the time to equilibrium between free enzyme, substrate, and substrate–enzyme complex may therefore be much longer than the usual three to five substrate half-lives. The classic closed system MM model recognizes the referred disequilibrium as a nonlinear clearance [$Cl = V_{max}/(K_m + C)$] with clearance decreasing as substrate concentrations increase. However, by introducing turnover properties of the enzyme as such, this nonlinear (saturable) clearance term disappears for the equilibrium state, and clearance returns to its equilibrium state V_{max}/K_m, since free enzyme concentration (E) is determined only by the ratio of k_{syn}-to-k_{deg} at equilibrium (steady-state).

To illustrate the previous discussion, eq. 20 was fitted to rapid repeated intravenous dose data in Fig. 12. Simulations were then done with a constant intravenous infusion over 100 hours to show how the time courses of substrate S, free enzyme E, substrate-enzyme complex ES, and clearance of substrate Cl of this open system varied over time (Fig. 13).

Synthesis k_{syn} and clearance of free enzyme stays constant, but the rate of elimination of free enzyme decreases as the free enzyme concentration falls when the substrate-enzyme complex is formed. Total enzyme concentrations (free E and complex bound ES) are allowed to vary, which means that they can both exceed and become less than the initial enzyme level E_0. The time course of clearance may be easier to understand and apply than that of free enzyme and relates to actual observable values. The k_{cat}, k_{deg}, k_{off}, k_{on}, and k_{syn} were estimated at 0.151 hour^{-1}, 0.986 hour^{-1}, 0.109 hour^{-1}, 0.0082 hour$^{-1} \cdot (\mu g \cdot L^{-1})^{-1}$ and 24.9 $\mu g \cdot L^{-1} \cdot h^{-1}$, respectively, with a resulting K_m

of 32 $\mu g \cdot L^{-1}$ and clearance Cl of about 17 L $\cdot$ h^{-1}. The reasons behind the data of Figs. 12 and 13 are thus as follows: (i) an initial decrease in free enzyme concentrations as a consequence of complex formation, resulting in (ii) a decrease in the rate of elimination of free enzyme since free concentrations decrease, (iii) *since free enzyme concentrations decrease the substrate clearance will decrease (change) in parallel* [$Cl(S) = E(t) \cdot k_{cat} \cdot V$] (Table 8), and (iv) simultaneously, there is a buildup of substrate–enzyme complex (Fig. 13). Therefore, the total concentration of free and complex bound enzyme increases beyond the baseline concentration E_0.

A constant substrate clearance model would not have captured the nonlinear concentration-time data in Fig. 12. For comparison, a time-dependent change
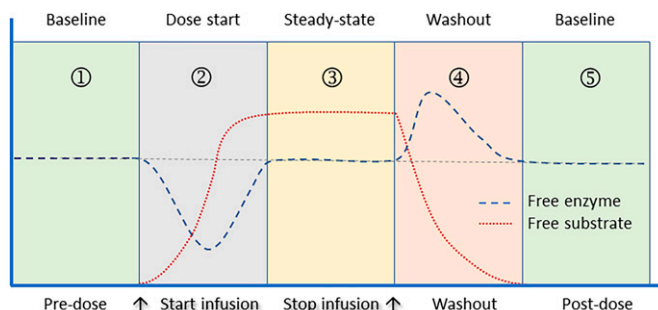

Fig. 14. Schematic presentation of free enzyme and substrate levels pre-, during, and post-dosing. The free enzyme level (dashed blue line) decreases from its baseline value [predose (1)] to a trough value [after the start of infusion (2)] during the initial rise in plasma substrate concentration (dotted red line) since substrate will allocate portions of the free enzyme during a constant rate infusion. Steady-state is reached [yellow shaded area (3)] and lasts until the stop of infusion. Only synthesis k_{syn} and loss k_{deg} of free enzyme governs the steady-state free enzyme concentration. There is a rapid rise in free enzyme concentrations upon stop of substrate infusion (4); this is due to the discharge of free enzyme from the disintegrating substrate–enzyme complex pool and no further free drug infusion to form a substrate–enzyme complex. The free enzyme concentration returns to the equilibrium concentration terminally [post-dose (5)].

in maximum metabolic capacity [closed system V_{max} (t)] (case study PK22 in Gabrielsson and Weiner, 2016) captured experimental data in Fig. 12.

The free enzyme-dependent clearance of compound A (substrate) in Fig. 14 (right) demonstrates a transient drop from baseline (1) to a trough of 20% (2) during the infusion, aiming at a substrate S concentration of about 180 μg/L. Substrate clearance then returns to its original value (E_0) at about 40 to 60 hours when the equilibrium of the whole system is reestablished (3). Substrate clearance has reached its predose value at equilibrium (3). When the infusion is stopped at 100 hours, substrate clearance rebounds (4) due to a transient rise in the free enzyme concentration. This is due to the sudden release of free enzyme from the substrate–enzyme complex as product is being formed and the lack of consumption of free enzyme due to complex formation. Substrate clearance (and free enzyme concentrations) reaches the predose equilibrium terminally (5) as all substrate is washed out. The time to equilibrium is substantially prolonged with a rise in substrate infusion rate, and vice versa. This is also shown schematically in Fig. 13.

The second example shows simulations of three different intravenous bolus doses of compound X. The substrate concentration-time courses in plasma are shown in Fig. 15, A, together with the corresponding time courses of clearance (Fig. 15, B) and substrate half-life (Fig. 15, C).

Note the dose-dependent change of substrate clearance with increasing concentrations after a bolus dose (Fig. 15, B), which exhibits the characteristics of a target-mediated drug disposition system. The transient dip in clearance over 6 to 36 hours results in a prolonged half-life (1). The dose-dependent rebound of clearance when concentrations fall below 100 μg·L^{-1} (clearance greater than its baseline value) is due to the replenishment of free enzyme from the substrate–enzyme complex, and less enzyme is used when substrate concentrations start to fall off. During the lowering of clearance below its baseline value, less free enzyme is available and can be cleared via natural catabolism k_{deg}, (rate of enzyme elimination decreases, but the rate of synthesis stays constant, which means that the total amount (free + complex) increases. The free enzyme pool is then increased by released free enzyme from the complex pool, and there is a rebound in the free enzyme concentration is seen, which then causes clearance to rebound. The temporarily increased clearance results in a decrease in half-life (2), which then increases when clearance returns to its baseline value (3) terminally. The manifestation of nonlinear plasma concentration-time courses is the archetypal signature of an open MM system at disequilibrium.
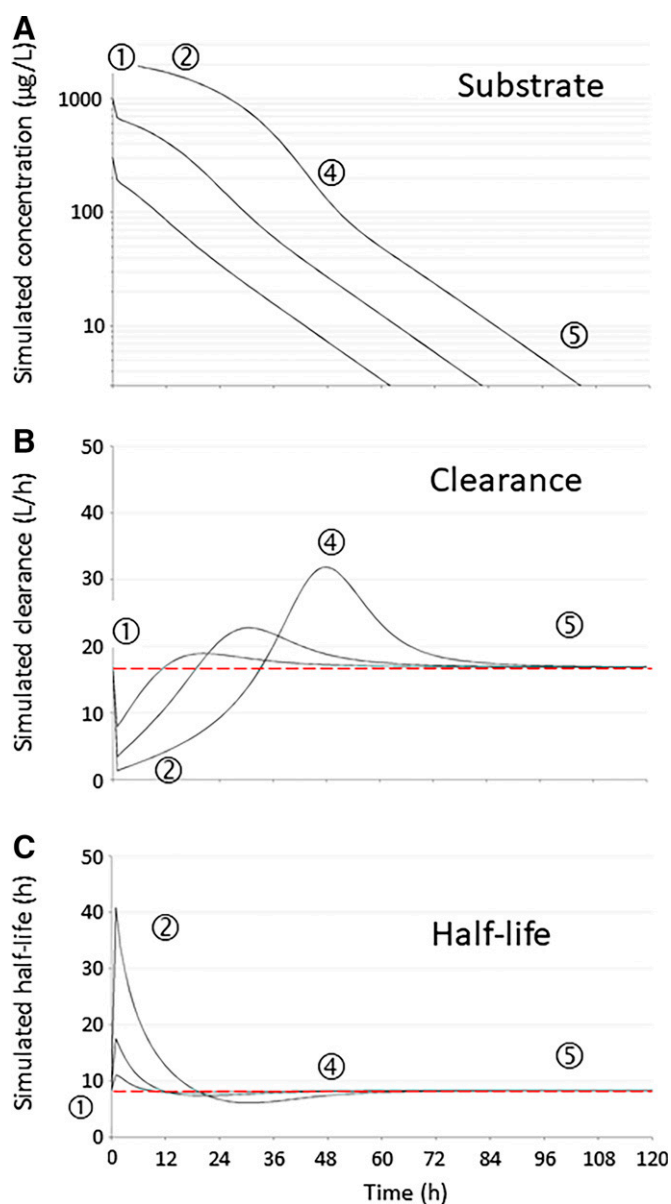

Fig. 15. (A) A semilogarithmic plot of simulated concentration-time courses of compound X after three different bolus doses. The starting concentrations are 300, 1000, and 3000 μg·L^{-1}. Therapeutic concentrations fall in the range of 100 to 500 μg·L^{-1}. (B) Simulated time courses of clearance after three bolus time courses. (C) Simulated time courses of half-life after three bolus time courses. Numbers 1 to 5 correspond to the different stages schematically shown in Fig. 14. The numbers correspond to stages in Fig. 13. Note that stage number 3 of Fig. 15 is not applicable to the bolus situation since there is no steady state during dosing, and is therefore omitted.

The dynamics of the intertwined differential equations of free substrate, free enzyme, and the substrate–enzyme complex inherently captures the disequilibrium as a nonlinearity. This is the core difference between the closed system (assuming a constant total enzyme pool) and the recently derived open system models (Figs. 2 and 14) (Gabrielsson and Peletier, 2018), which puts clearance into a new light. Until simultaneous measurement of the total enzyme concentration implicated is carried out, the possibility cannot be completely dis-

carded that, in some cases, results previously described as dose- or time-dependent kinetics may actually rather reflect a state of disequilibrium.

3. Key Insights and Translational Potential

An important advantage of using the open system approach is that an apparent temporal nonlinearity in clearance or rate of elimination does not have to be approximated using a saturable expression such as the one shown in Table 8. In open systems, the nonlinearity observed for higher intravenous bolus doses in which clearance temporarily decreases and half-life increases is an intrinsic property of the system, which results from the apparent disequilibrium between substrate S, free enzyme E, and the substrate–enzyme complex ES. Clearance behaves linearly at steady-state (Table 8, bottom row, left, V_{max}/K_m).

However, in vitro studies in general and metabolic drug–drug interaction studies in particular operate within a short timeframe, often less than 24 hours and sometimes as short as 15 to 45 minutes (Fowler and Zhang, 2008), hence totally ignoring the impact of enzyme protein turnover. Also, clearance defined by closed systems is commonly applied even in a physiologic context for translation of in vitro to in vivo metabolic data (Rostami-Hodjegan, 2010). In these cases, the nonequilibrium between the substrate (drug), free enzyme, and the complex is approximated by a nonlinear saturable function. Clearly, a better understanding is required of the biologic elements involved, including the origin of the clearance model (open or closed). Accurate in vitro-to-in vivo predictions are possible only when in vitro data are robust and the biologic structure of the clearance model is integrated. Accordingly, we therefore suggest, based on the expanded quantitative insights of the MM system presented here, that in silico MM, pharmacological, and transporter models should be built on open systems.

The tools are available to more correctly scale in vivo data from preclinical species to humans, with a reasonable mechanistic structure of the determinants of clearance. Thus, it should be appreciated that V_{max} is expressed as $E(t) \cdot k_{cat}$ (or $k_{syn} \cdot k_{cat}/k_{deg}$ at equilibrium), and K_m equals $(k_{off} + k_{cat})/k_{on}$. The k_{syn} and k_{deg} parameters represent biology and are scalable across different species. The physicochemical parameters k_{on}, k_{off}, and k_{cat} may also be species-dependent since the target properties varies across species.

The apparent clearance is determined by the free enzyme expression E and the turnover parameters k_{syn} and k_{deg} rather than its fixed baseline concentration E_0, which is contrasted by the closed system model where clearance via its V_{max} term is fixed by baseline concentration E_0. This means that two subjects with the same free enzyme expression (same E_0) will have the same clearance (provided everything else is the same).

However, the subject with the higher enzyme synthesis k_{syn} and degradation k_{deg} rates will reach enzymatic equilibrium faster. Therefore, subjects or species will, despite similar free enzyme concentrations, display different substrate time courses due to different enzyme protein turnover rates.

4. Induction or Inhibition of Enzymatic and Catalytic Processes

Since clearance of most small drug substances depends upon CYP enzymes, CYP inhibition may lead to overexposure and toxicity and CYP induction to too low exposure and deficient therapeutic effect. Understanding the cause of inhibition or induction is, therefore crucial. A practical example of the time course of heterologous drug induction is the impact of pentobarbital treatment on the disposition of nortriptyline (NT) (von Bahr et al., 1998). Pentobarbital-induced induction of NT clearance (NT clearance increases due to increased exposure to the enzyme responsible for NT

TABLE 9
Induction, inhibition or catalytic change in enzyme activity
Induction is related to the metabolic activity (increase in free enzyme E or catalytic activity k_{cat}) which means an increase in synthesis k_{syn} or decrease in loss k_{deg}, or increase in k_{cat}. *Inhibition* involves the opposite.

Observation	Cause	V_{max}	K_m	$Cl(S)$	Commentary
Induction	$k_{syn} \uparrow$	$\uparrow$	$\leftrightarrow$	$\uparrow$	If k_{syn} increases free enzyme E concentration increases. K_m is unaffected. Substrate clearance increases (von Bahr et al., 1998)
	$k_{deg} \downarrow$	$\uparrow$	$\leftrightarrow$	$\uparrow$	If k_{deg} decreases free enzyme E concentration increases. K_m is unaffected. Substrate clearance increases (Ethanol induction of CYP2E1 in (Hu et al., 1995)
Inhibition	$k_{syn} \downarrow$	$\downarrow$	$\leftrightarrow$	$\downarrow$	If k_{syn} decreases free enzyme E concentration decreases. K_m is unaffected (Ramsay and Tipton, 2017)
	$k_{deg} \uparrow$	$\downarrow$	$\leftrightarrow$	$\downarrow$	If k_{deg} increases free enzyme E concentration decreases. K_m is unaffected (Ramsay and Tipton, 2017)
Catalytic change	$k_{cat} \uparrow$	$\uparrow$	$\uparrow$	$\leftrightarrow (\uparrow)$	If k_{cat} increases V_{max} increases. K_m increases if $k_{cat} \approx k_{off}$. Substrate clearance is unaffected if V_{max} and K_m changes the same.
	$k_{cat} \downarrow$	$\downarrow$	$\downarrow$	$\leftrightarrow (\downarrow)$	If k_{cat} decreases V_{max} decreases. K_m decreases if $k_{cat} \approx k_{off}$. Substrate clearance is unaffected if V_{max} and K_m changes the same.

removal) shortened the NT half-life and time to (induced) steady-state. The plasma concentration of NT decreased by 50% during pentobarbital treatment. The reverse happens on cessation of pentobarbital treatment. The induced NT clearance decreased and half-life increased, resulting in an extended time of postinduction return of NT concentration to its pre-induced state.

Analogous to, for example, ligand–receptor target interaction, as previously discussed, the administration of agents aiming at enzyme proteins may impact the number of target molecules or their activity. An increase in the synthesis rate (turnover rate) of enzyme k_{syn} will impact the baseline value of enzyme E_0 and therefore cause an increase in clearance Cl of substrate S at steady-state. An increase in the fractional turnover rate of enzyme k_{deg} will decrease the baseline value of enzyme E_0 and, hence, decrease in clearance Cl of substrate S at steady-state (Table 9).

This section has demonstrated how enzymatic turnover properties will affect clearance, time to equilibrium, and steady-state solutions of substrate, enzyme, and the complex and, consequently, drug dose. The new expression of in vivo MM systems will be useful for quantitative analysis of clearance properties and in translational science contexts.

IV. Discussion

A. What Is the Challenge, and Why Is It a Problem?

The introductory section identified two main questions: namely, what is the challenge with today's closed system models, and why is it a challenge in pharmacology, metabolism, and even for transporter systems? These closed system models, often in vitro based, lack robust information about the target protein biology and, hence, are approximations of the in vivo situations. Closed systems models further lack the capability beyond binding to describe drug–drug interactions, time-variant induction, inhibition, or displacement (up- or downregulation of the target) of competing drug molecules or pharmacodynamic drug interactions, as previously described. Moreover, closed systems are limited to binding interactions and hence cannot explain when the duration of the drug is limited by the turnover of the target (see previous PPIs and COX-1 examples). Finally, closed systems assume a constant clearance despite the fact that the availability of free enzymes will vary for the drug (substrate), particularly during repeated dosing conditions. Mitigating these limitations is necessary for adequate assessment of in vivo potency, efficacy, and clearance.

We have shown that target turnover (k_{syn}, k_{deg}) is an important covariate to in vivo potency and effi-

cacy. Thus, the rates (k_{off}, k_{deg}, $k_{e(RL)}$, and k_{on}) or their half-lives determine potency, whereas the expression level of complex (RL_{max}) and transduction (stimulus force, ρ) determine efficacy, as in the following equation. In vivo potency and efficacy have ligand–target complex loss $k_{e(RL)}$ in common. A change in that property is therefore assumed to impact both potency and efficacy but in opposite directions. When $k_{e(RL)}$ increases, potency increases (numerical value decreases) whereas efficacy decreases, and vice versa, making the removal rate of ligand–target complex an important player.

$$\begin{cases} EC_{50} = \dfrac{k_{deg}}{k_{e(RL)}} \cdot \dfrac{k_{off} + k_{e(RL)}}{k_{on}} \\[2ex] E_{max} = \rho \cdot RL_{max} = \rho \cdot \dfrac{k_{syn}}{k_{e(RL)}} \end{cases} \quad (23)$$

Here, target biology is an important covariate of in vivo potency and may capture between species or interindividual differences. Equation 23 partly explains why in some cases target concentrations in the micromolar range only require nanomolar drug exposure, and vice versa. Still, the open model, similarly to the closed, does not take into account post-target events such as synergy, potentiation, feedback, etc. However, incorporating target properties, assessment of activities adjacent to the target will be more apparent.

Blood clearance may be expressed by means of the well-stirred physiologic model with blood flow Q_i as

$$Cl = \cfrac{Q_i \cdot \cfrac{E(t) \cdot k_{cat} \cdot V}{K_m}}{Q_i + \cfrac{E(t) \cdot k_{cat} \cdot V}{K_m}} \quad (24)$$

The determinants of free enzyme $E(t)$ concentrations are k_{syn} and k_{deg}. Again, target protein turnover plays an important role and may explain interindividual differences in the disposition of substrate S. In situations where only plasma data are available of the drug, such as in therapeutic drug monitoring TDM, $V_{max}/(K_m + C)$ gives the apparent plasma clearance rather than intrinsic clearance of eq. 23. V_{max} and K_m are typical parameters in TDM of phenytoin and salicylic acid and are based on the closed system expression of clearance (Table 8) (for a review of the clearance concept, see Benet, 2010).

B. Unifying and Separating Properties of Open Systems

The open models of pharmacological and metabolic systems have several properties (binding, target turnover and complex loss) in common that unify these systems. While not explicitly discussed in this article, it appears highly probable that similar reasoning may be applied to ligand interactions with

transport proteins as well. The open in vivo models incorporate all necessary ligand and target protein interactions, such as target binding, target protein turnover, and irreversible loss of either complex or the associated drug. By virtue of their more physiologic properties, such approaches reach beyond binding and incorporate the actual target (receptor, enzyme, or transporter protein turnover) properties, thereby encompassing physiologic means to explain within- and between-subject differences.

C. General Conclusions and Perspectives

This review endeavors to illustrate and exemplify the importance of target protein turnover as a central player in pharmacology and drug metabolism. We hope these thoughts will inspire further development of concepts of in vivo pharmacology and drug metabolism to the benefit of basic scientists as well as for drug discovery and development ventures. The introduction of protein turnover unveils the bearing of target dynamics upon pharmacologic as well as metabolic readouts—key components in determining drug responses in vivo. Specifically, we describe and provide

- The presentation of new (open model) expressions of in vivo potency, efficacy, and clearance, which notably embody target turnover, binding, and complex kinetics, as well as capturing drug-response descriptors (i.e., full, partial, and inverse agonism and antagonism)
- A detailed examination and analysis of open models to show what in vivo potency, efficacy, and clearance have in common and how they differ
- A comprehensive literature review showing that target turnover rate varies with several factors: age, species, tissue/subregion, treatment, disease state, hormonal and nutritional state, day–night cycle, and more and therefore changes in vivo potency, efficacy, and clearance

Using this new open model expression which integrates system (k_{syn} and k_{deg}) and drug (k_{on}, k_{off}, $k_{e(RL)}$, and k_{cat}) properties, we further show that

- The fractional turnover rates (k_{deg} and $k_{e(RL)}$), rather than the absolute target expression (R or RL), determine necessary drug exposure via in vivo potency EC_{50}.
- The absolute ligand–target expression (RL) determines the need for the drug based on in vivo efficacy parameter (E_{max}) and the transduction parameter ρ.
- The free enzyme concentration E determines clearance and the fractional turnover rate (k_{deg}), the time to equilibrium between the substrate, free enzyme, and the substrate–enzyme complex.

- Clearance is not a constant term but is driven by the free enzyme concentration.
- The properties of substrate, target, and complex demonstrate nonsaturable metabolic behavior at equilibrium within reasonable substrate/ligand concentration ranges.
- Nonlinear processes previously referred to as capacity- and time-dependent kinetics may have been disequilibria, which the open model handles as an intrinsic property.
- The open model may pinpoint why some subjects differ in their demand for the drug, thus defining what makes the outlier an outlier, an issue important to scrutinize from a clinical but also a regulatory point of view.

All of these results need to be considered within the framework of projecting potency, efficacy, and clearance from in vitro, via in vivo animal model work, to clinically efficacious exposures in man.

The usefulness of the open model approach has attracted increased attention—directly or indirectly—in several recent publications, demonstrating its applicability in the assessment of different compounds, targets, and systems (Oakes et al., 2001; Oakes et al., 2005; Hong et al., 2008; Gabrielsson et al., 2018a, b, 2019; Smith et al., 2018; van Waterschoot et al., 2018; Cardilin et al., 2019; Held et al., 2019; Jansson-Lofmark et al., 2020; Li et al., 2020; Choi, 2020; Webster et al., 2020; Baquero and Levin, 2021; Saganuwan, 2021; Song et al., 2021; Tang and Cao, 2021).

To understand and approach the dynamics of target biology in an open system, we present new avenues to vastly different areas beyond pharmacology, drug metabolism, or cellular (transport) systems. Open systems capture in vivo disequilibria previously categorized as capacity- and time-dependent kinetics. Open systems increase the capability to capture these processes correctly and underpin the interpretation of data, translate functionality across species, and explain clinical and preclinical variability.

Only by continued integration of the multiple levels of biologic and pharmacological insight will the precision be further improved of translational predictions across the drug development process. It is our hope that the current account may be of value to that end, as it emphasizes the importance of *in* vivo veritas principles in such endeavors.

References

Abelö A, Eriksson UG, Karlsson MO, Larsson H, and Gabrielsson J (2000) A turnover model of irreversible inhibition of gastric acid secretion by omeprazole in the dog. *J Pharmacol Exp Ther* **295**:662–669.

Abou Sawan S, Hodson N, Tinline-Goodfellow C, West DWD, Malowany JM, Kumbhare D, and Moore DR (2021) Incorporation of dietary amino acids into myofibrillar and sarcoplasmic proteins in free-living adults is influenced by sex, resistance exercise, and training status. *J Nutr* **151**:3350–3360.

Adam K and Oswald I (1983) Protein synthesis, bodily renewal and the sleep-wake cycle. *Clin Sci (Lond)* **65**:561–567.

Adler CH, Meller E, and Goldstein M (1985) Recovery of alpha 2-adrenoceptor binding and function after irreversible inactivation by N-ethoxycarbonyl-2-ethoxy-1,2-dihydroquinoline (EEDQ). *Eur J Pharmacol* **116**:175–178.

Adolph EF (1949) Quantitative relations in the physiological constitutions of mammals. *Science* **109**:579–585.

Agneter E, Drobny H, and Singer EA (1993) Central alpha 2-autoreceptors: agonist dissociation constants and recovery after irreversible inactivation. *Br J Pharmacol* **108**:370–375.

Albrecht S, Ihmsen H, Hering W, Geisslinger G, Dingemanse J, Schwilden H, and Schüttler J (1999) The effect of age on the pharmacokinetics and pharmacodynamics of midazolam. *Clin Pharmacol Ther* **65**:630–639.

Almquist J, Hovdal D, Ahlström C, Fjellström O, Gennemark P, and Sundqvist M (2018) Overexpressing cell systems are a competitive option to primary adipocytes when predicting in vivo potency of dual GPR81/GPR109A agonists. *Eur J Pharm Sci* **114**:155–165.

An G (2017) Small-molecule compounds exhibiting Target-Mediated Drug Disposition (TMDD): A minireview. *J Clin Pharmacol* **57**:137–150.

An G (2020) Concept of pharmacologic Target-Mediated Drug Disposition in large-molecule and small-molecule compounds. *J Clin Pharmacol* **60**:149–163.

Andersson R, Jirstrand M, Almquist J, and Gabrielsson J (2019) Challenging the dose-response-time data approach: Analysis of a complex system. *Eur J Pharm Sci* **128**:250–260.

Andres TM, McGrane T, McEvoy MD, and Allen BFS (2019) Geriatric pharmacology: An update. *Anesthesiol Clin* **37**:475–492.

Antonini A, Schwarz J, Oertel WH, Pogarell O, and Leenders KL (1997) Long-term changes of striatal dopamine D2 receptors in patients with Parkinson's disease: a study with positron emission tomography and [11C]raclopride. *Mov Disord* **12**:33–38.

Appel SH, Anwyl R, McAdams MW, and Elias S (1977) Accelerated degradation of acetylcholine receptor from cultured rat myotubes with myasthenia gravis sera and globulins. *Proc Natl Acad Sci USA* **74**:2130–2134.

Arnett CD, Fowler JS, MacGregor RR, Schlyer DJ, Wolf AP, Långström B, and Halldin C (1987) Turnover of brain monoamine oxidase measured in vivo by positron emission tomography using L-[11C]deprenyl. *J Neurochem* **49**:522–527.

Baker SP and Pitha J (1982) Irreversible blockade of beta adrenoreceptors and their recovery in the rat heart and lung in vivo. *J Pharmacol Exp Ther* **220**:247–251.

Baquero F and Levin BR (2021) Proximate and ultimate causes of the bactericidal action of antibiotics. *Nat Rev Microbiol* **19**:123–132.

Barturen F and Garcia-Sevilla JA (1992) Long term treatment with desipramine increases the turnover of alpha 2-adrenoceptors in the rat brain. *Mol Pharmacol* **42**:846–855.

Battaglia G, Norman AB, and Creese I (1987) Differential serotonin2 receptor recovery in mature and senescent rat brain after irreversible receptor modification: effect of chronic reserpine treatment. *J Pharmacol Exp Ther* **243**:69–75.

Battaglia G, Norman AB, and Creese I (1988) Age-related differential recovery rates of rat striatal D-1 dopamine receptors following irreversible inactivation. *Eur J Pharmacol* **145**:281–290.

Battaglia G, Norman AB, Newton PL, and Creese I (1986) In vitro and in vivo irreversible blockade of cortical S2 serotonin receptors by N-ethoxycarbonyl-2-ethoxy-1,2-dihydroquinoline: a technique for investigating S2 serotonin receptor recovery. *J Neurochem* **46**:589–593.

Bauer RA (2015) Covalent inhibitors in drug discovery: from accidental discoveries to avoided liabilities and designed therapies. *Drug Discov Today* **20**:1061–1073.

Beaulieu JM and Gainetdinov RR (2011) The physiology, signaling, and pharmacology of dopamine receptors. *Pharmacol Rev* **63**:182–217.

Belleau B, Martel R, Lacasse G, Ménard M, Weinberg NL, and Perron YG (1968) N-carboxylic acid esters of 1,2- and 1,4-dihydroquinolines. A new class of irreversible inactivators of the catecholamine alpha receptors and potent central nervous system depressants. *J Am Chem Soc* **90**:823–824.

Ben-Menachem E (2011) Mechanism of action of vigabatrin: correcting misperceptions. *Acta Neurol Scand Suppl* **192**:5–15.

Benet LZ (2010) Clearance (née Rowland) concepts: a downdate and an update. *J Pharmacokinet Pharmacodyn* **37**:529–539.

Benet LZ and Hoener BA (2002) Changes in plasma protein binding have little clinical relevance. *Clin Pharmacol Ther* **71**:115–121.

Benveniste H, Drejer J, Schousboe A, and Diemer NH (1984) Elevation of the extracellular concentrations of glutamate and aspartate in rat hippocampus during transient cerebral ischemia monitored by intracerebral microdialysis. *J Neurochem* **43**:1369–1374.

Berg KA and Clarke WP (2018) Making Sense of Pharmacology: Inverse Agonism and Functional Selectivity. *Int J Neuropsychopharmacol* **21**:962–977.

Betts AM, Clark TH, Yang J, Treadway JL, Li M, Giovanelli MA, Abdiche Y, Stone DM, and Paralkar VM (2010) The application of target information and preclinical pharmacokinetic/pharmacodynamic modeling in predicting clinical doses of a Dickkopf-1 antibody for osteoporosis. *J Pharmacol Exp Ther* **333**:2–13.

Biolo G, Antonione R, Barazzoni R, Zanetti M, and Guarnieri G (2003) Mechanisms of altered protein turnover in chronic diseases: a review of human kinetic studies. *Curr Opin Clin Nutr Metab Care* **6**:55–63.

Birkenhäger TK, van den Broek WW, Mulder PG, Bruijn JA, and Moleman P (2004) Efficacy and tolerability of tranylcypromine versus phenelzine: a double-blind study in antidepressant-refractory depressed inpatients. *J Clin Psychiatry* **65**:1505–1510.

Black JW and Leff P (1983) Operational models of pharmacological agonism. *Proc R Soc Lond B Biol Sci* **220**:141–162.

Bodenstein J, Venter DP, and Brink CB (2005) Phenoxybenzamine and benextramine, but not 4-diphenylacetoxy-N-[2-chloroethyl]piperidine hydrochloride, display irreversible noncompetitive antagonism at G protein-coupled receptors. *J Pharmacol Exp Ther* **314**:891–905.

Boisvert FM, Ahmad Y, Gierlinski M, Charriere F, Lamont D, Scott M, Barton G and Lamond AI (2012) A quantitative spatial proteomics analysis of proteome turnover in human cells. *Mol Cell Proteomics* **11**:M111 011429.

Bolaños FJ, Schechter LE, Laporte AM, Hamon M, and Gozlan H (1991) Recovery of 5-HT 1A receptors after irreversible blockade by N-ethoxycarbonyl-2-ethoxy-1,2-dihydroquinoline (EEDQ). *Proc West Pharmacol Soc* **34**:387–393.

Borden LA, Czajkowski C, Chan CY, and Farb DH (1984) Benzodiazepine receptor synthesis and degradation by neurons in culture. *Science* **226**:857–860.

Bosma R, Witt G, Vaas LAI, Josimovic I, Gribbon P, Vischer HF, Gul S, and Leurs R (2017) The target residence time of antihistamines determines their antagonism of the G Protein-Coupled histamine H1 receptor. *Front Pharmacol* **8**:667.

Bowie MW and Slattum PW (2007) Pharmacodynamics in older adults: a review. *Am J Geriatr Pharmacother* **5**:263–303.

Boxenbaum H (1982) Interspecies scaling, allometry, physiological time, and the ground plan of pharmacokinetics. *J Pharmacokinet Biopharm* **10**:201–227.

Boxenbaum H and Ronfeld R (1983) Interspecies pharmacokinetic scaling and the Dedrick plots. *Am J Physiol* **245**:R768–R775.

Brynne N, Forslund C, Hallén B, Gustafsson LL, and Bertilsson L (1999) Ketoconazole inhibits the metabolism of tolterodine in subjects with deficient CYP2D6 activity. *Br J Clin Pharmacol* **48**:564–572.

Brynne N, Stahl MM, Hallén B, Edlund PO, Palmér L, Höglund P, and Gabrielsson J (1997) Pharmacokinetics and pharmacodynamics of tolterodine in man: a new drug for the treatment of urinary bladder overactivity. *Int J Clin Pharmacol Ther* **35**:287–295.

Bullock R, Zauner A, Myseros JS, Marmarou A, Woodward JJ, and Young HF (1995a) Evidence for prolonged release of excitatory amino acids in severe human head trauma. Relationship to clinical events. *Ann N Y Acad Sci* **765**:290–297, discussion 298.

Bullock R, Zauner A, Woodward J, and Young HF (1995b) Massive persistent release of excitatory amino acids following human occlusive stroke. *Stroke* **26**:2187–2189.

Burke TF, Woods JH, Lewis JW, and Medzihradsky F (1994) Irreversible opioid antagonist effects of clocinnamox on opioid analgesia and mu receptor binding in mice. *J Pharmacol Exp Ther* **271**:715–721.

Carbonell L, Cuffi ML, and Forn J (2004) Effect of chronic lithium treatment on the turnover of alpha2-adrenoceptors after chemical inactivation in rats. *Eur Neuropsychopharmacol* **14**:497–502.

Cardilin T, Almquist J, Jirstrand M, Zimmermann A, Lignet F, El Bawab S, and Gabrielsson J (2019) Modeling long-term tumor growth and kill after combinations of radiation and radiosensitizing agents. *Cancer Chemother Pharmacol* **83**:1159–1173.

Chaparro-Riggers J, Liang H, DeVay RM, Bai L, Sutton JE, Chen W, Geng T, Lindquist K, Casas MG, Boustany LM, et al. (2012) Increasing serum half-life and extending cholesterol lowering in vivo by engineering antibody with pH-sensitive binding to PCSK9. *J Biol Chem* **287**:11090–11097.

Charlton SJ (2009) Agonist efficacy and receptor desensitization: from partial truths to a fuller picture. *Br J Pharmacol* **158**:165–168.

Choe S and Lee D (2017) Parameter estimation for sigmoid E_{max} models in exposure-response relationship. *Transl Clin Pharmacol* **25**:74–84.

Choi YH (2020) Interpretation of drug interaction using systemic and local tissue exposure changes. *Pharmaceutics* **12**:417.

Colović MB, Krstić DZ, Lazarević-Pašti TD, Bondžić AM, and Vasić VM (2013) Acetylcholinesterase inhibitors: pharmacology and toxicology. *Curr Neuropharmacol* **11**:315–335.

Commons KG and Linnros SE (2019) Delayed antidepressant efficacy and the desensitization hypothesis. *ACS Chem Neurosci* **10**:3048–3052.

Cooper GM (2000) Pathways of Intracellular Signal Transduction, in *The Cell: A Molecular Approach*, Sinauer Associates, Sunderland MA.

Copeland RA (2016) The drug-target residence time model: a 10-year retrospective. *Nat Rev Drug Discov* **15**:87–95.

Copeland RA, Pompliano DL, and Meek TD (2006) Drug-target residence time and its implications for lead optimization. *Nat Rev Drug Discov* **5**:730–739.

Corradin O, Cohen AJ, Luppino JM, Bayles IM, Schumacher FR, and Scacheri PC (2016) Modeling disease risk through analysis of physical interactions between genetic variants within chromatin regulatory circuitry. *Nat Genet* **48**:1313–1320.

Corte LD and Tipton KF (1980) The turnover of the A- and B-forms of monoamine oxidase in rat liver. *Biochem Pharmacol* **29**:891–895.

Corzo J (2006) Time, the forgotten dimension of ligand binding teaching. *Biochem Mol Biol Educ* **34**:413–416.

Costa T and Herz A (1989) Antagonists with negative intrinsic activity at delta opioid receptors coupled to GTP-binding proteins. *Proc Natl Acad Sci USA* **86**:7321–7325.

Cummings J, Isaacson S, Mills R, Williams H, Chi-Burris K, Corbett A, Dhall R, and Ballard C (2014) Pimavanserin for patients with Parkinson's disease psychosis: a randomised, placebo-controlled phase 3 trial. *Lancet* **383**:533–540.

Dahl G and Akerud T (2013) Pharmacokinetics and the drug-target residence time concept. *Drug Discov Today* **18**:697–707.

Dallmann R, Brown SA, and Gachon F (2014) Chronopharmacology: new insights and therapeutic implications. *Annu Rev Pharmacol Toxicol* **54**:339–361.

Danhof M, de Jongh J, De Lange EC, Della Pasqua O, Ploeger BA, and Voskuyl RA (2007) Mechanism-based pharmacokinetic-pharmacodynamic modeling: biophase distribution, receptor theory, and dynamical systems analysis. *Annu Rev Pharmacol Toxicol* **47**:357–400.

Dayneka NL, Garg V, and Jusko WJ (1993) Comparison of four basic models of indirect pharmacodynamic responses. *J Pharmacokinet Biopharm* **21**:457–478.

de Aguiar Vallim TQ, Lee E, Merriott DJ, Goulbourne CN, Cheng J, Cheng A, Gonen A, Allen RM, Palladino END, Ford DA, et al. (2017) ABCG1 regulates pulmonary surfactant metabolism in mice and men. *J Lipid Res* **58**:941–954.

De Deurwaerdère P, Bharatiya R, Chagraoui A, and Di Giovanni G (2020) Constitutive activity of 5-HT receptors: Factual analysis. *Neuropharmacology* **168**:107967.

de Witte WEA, Danhof M, van der Graaf PH, and de Lange ECM (2018) The implications of target saturation for the use of drug-target residence time. *Nat Rev Drug Discov* **18**:82–84.

Dewar KM, Paquet M, and Reader TA (1997) Alterations in the turnover rate of dopamine D1 but not D2 receptors in the adult rat neostriatum after a neonatal dopamine denervation. *Neurochem Int* **30**:613–621.

Disse B, Speck GA, Rominger KL, Witek Jr TJ, and Hammer R (1999) Tiotropium (Spiriva): mechanistic considerations and clinical profile in obstructive lung disease. *Life Sci* **64**:457–464.

Doody RS, Corey-Bloom J, Zhang R, Li H, Ieni J, and Schindler R (2008) Safety and tolerability of donepezil at doses up to 20 mg/day: results from a pilot study in patients with Alzheimer's disease. *Drugs Aging* **25**:163–174.

Dörrbaum AR, Kochen L, Langer JD, and Schuman EM (2018) Local and global influences on protein turnover in neurons and glia. *eLife* **7**:e34202.

Dorszewska J (2013) Cell biology of normal brain aging: synaptic plasticity-cell death. *Aging Clin Exp Res* **25**:25–34.

Durcan MJ, Morgan PF, Van Etten ML, and Linnoila M (1994) Covariation of alpha 2-adrenoceptor density and function following irreversible antagonism with EEDQ. *Br J Pharmacol* **112**:855–860.

Dutta S and Sengupta P (2016) Men and mice: Relating their ages. *Life Sci* **152**:244–248.

Earp J, Krzyzanski W, Chakraborty A, Zamacona MK, and Jusko WJ (2004) Assessment of drug interactions relevant to pharmacodynamic indirect response models. *J Pharmacokinet Pharmacodyn* **31**:345–380.

Egashira T and Kamijo K (1979) Synthetic rates of monoamine oxidase in rat liver after clorgyline or deprenyl administration. *Jpn J Pharmacol* **29**:677–680.

European Medicines Agency(2017) Guideline on strategies to identify and mitigate risks for first-in-human and early clinical trials with investigational medicinal products. EMEA/CHMP/SWP/28367/07 Rev. 1. European Medicines Agency, Amsterdam.

Erwin VG and Deitrich RA (1971) The labeling in vivo of monoamine oxidase by 14 C-pargyline: a tool for studying the synthesis of the enzyme. *Mol Pharmacol* **7**:219–228.

Esteller M (2008) Epigenetics in cancer. *N Engl J Med* **358**:1148–1159.

Farrell K, Musaus M, Navabpour S, Martin K, Ray WK, Helm RF, and Jarome TJ (2021) Proteomic analysis reveals sex-specific protein degradation targets in the amygdala during fear memory formation. *Front Mol Neurosci* **14**:716284.

Fearon KC, Hansell DT, Preston T, Plumb JA, Davies J, Shapiro D, Shenkin A, Calman KC, and Burns HJ (1988) Influence of whole body protein turnover rate on resting energy expenditure in patients with cancer. *Cancer Res* **48**:2590–2595.

Felner AE and Waldmeier PC (1979) Cumulative effects of irreversible MAO inhibitors in vivo. *Biochem Pharmacol* **28**:995–1002.

Fleckenstein AE, Pögün S, Carroll FI, and Kuhar MJ (1996) Recovery of dopamine transporter binding and function after intrastriatal administration of the irreversible inhibitor RTI-76 [3 beta-(3p-chlorophenyl) tropan-2 beta-carboxylic acid p-isothiocyanatophenylethyl ester hydrochloride]. *J Pharmacol Exp Ther* **279**:200–206.

Folmer RHA (2018) Drug target residence time: a misleading concept. *Drug Discov Today* **23**:12–16.

Fornasiero EF, Mandad S, Wildhagen H, Alevra M, Rammner B, Keihani S, Opazo F, Urban I, Ischebeck T, Sakib MS, et al. (2018) Precisely measured protein lifetimes in the mouse brain reveal differences across tissues and subcellular fractions. *Nat Commun* **9**:4230.

Fowler JS, Volkow ND, Logan J, Wang GJ, MacGregor RR, Schyler D, Wolf AP, Pappas N, Alexoff D, Shea C, et al. (1994) Slow recovery of human brain MAO B after L-deprenyl (Selegiline) withdrawal. *Synapse* **18**:86–93.

Freedman NM, Mishani E, Krausz Y, Weininger J, Lester H, Blaugrund E, Ehrlich D, and Chisin R (2005) In vivo measurement of brain monoamine oxidase B occupancy by rasagiline, using (11)C-l-deprenyl and PET. *J Nucl Med* **46**:1618–1624.

Furchgott RF (1966) The use of beta-halo alkylamines in the differentiation of receptors and in the determination of dissociation constants of receptor-agonist complexes. *Adv Drug Res* **3**:21–55.

Furchgott RF and Bursztyn P (1967) Comparison of dissociation constants and of relative efficacies of selected agonists acting on parasympathetic receptors. *Ann N Y Acad Sci* **144**:882–889.

Fuxe K, Agnati LF, Merlo Pich E, Meller E, and Goldstein M (1987) Evidence for a fast receptor turnover of D1 dopamine receptors in various forebrain regions of the rat. *Neurosci Lett* **81**:183–187.

Gabilondo AM and García-Sevilla JA (1995) Spontaneous withdrawal from long-term treatment with morphine accelerates the turnover of alpha 2-adrenoceptors in the rat brain: up-regulation of receptors associated with increased receptor appearance. *J Neurochem* **64**:2590–2597.

Gabrielsson J, Andersson R, Jirstrand M, and Hjorth S (2019) Dose-response-time data analysis: An underexploited trinity. *Pharmacol Rev* **71**:89–122.

Gabrielsson J and Peletier LA (2017) Pharmacokinetic steady-states highlight interesting target-mediated disposition properties. *AAPS J* **19**:772–786.

Gabrielsson J and Peletier LA (2018) Michaelis-Menten from an in vivo perspective: Open versus closed systems. *AAPS J* **20**:102.

Gabrielsson J, Peletier LA, and Hjorth S (2018a) In vivo potency revisited - Keep the target in sight. *Pharmacol Ther* **184**:177–188.

Gabrielsson J, Peletier LA, and Hjorth S (2018b) Lost in translation: What's in an EC₅₀? Innovative PK/PD reasoning in the drug development context. *Eur J Pharmacol* **835**:154–161.

Gabrielsson J and Weiner D (2000) *Pharmacokinetic and Pharmacodynamic Data Analysis: Concepts and Applications*, 2nd ed, Sw. Pharmaceutical Press, Stockholm, Sweden.

Gabrielsson J and Weiner D (2016) *Pharmacokinetic and Pharmacodynamic Data Analysis: Concepts and Applications.*, 5th ed, Sw. Pharmaceutical Press, Stockholm, Sweden.

Gabrielsson JG and Hjorth S (2018) Integration of pharmacokinetic and pharmacodynamic reasoning and its importance in drug discovery, in *Early Drug Development: Bringing a Preclinical Candidate to the Clinic* (Giordanetto F, ed) pp 369–400, Wiley-VCH, Weinheim, Germany.

Garland SL (2013) Are GPCRs still a source of new targets? *J Biomol Screen* **18**:947–966.

Gedda K, Scott D, Besancon M, Lorentzon P, and Sachs G (1995) Turnover of the gastric H+,K(+)-adenosine triphosphatase alpha subunit and its effect on inhibition of rat gastric acid secretion. *Gastroenterology* **109**:1134–1141.

Gierse JK, Koboldt CM, Walker MC, Seibert K, and Isakson PC (1999) Kinetic basis for selective inhibition of cyclo-oxygenases. *Biochem J* **339**:607–614.

Giorgi O, Pibiri MG, and Biggio G (1991) Differential turnover rates of D1 dopamine receptors in the retina and in distinct areas of the rat brain. *J Neurochem* **57**:754–759.

Giorgi O, Pibiri MG, Dal Toso R, and Ragatzu G (1992) Age-related changes in the turnover rates of D1-dopamine receptors in the retina and in distinct areas of the rat brain. *Brain Res* **569**:323–329.

Goridis C and Neff NH (1971) Monoamine oxidase: an approximation of turnover rates. *J Neurochem* **18**:1673–1682.

Gosset JR, Beaumont K, Matsuura T, Winchester W, Attkins N, Glatt S, Lightbown I, Ulrich K, Roberts S, Harris J, et al. (2017) A cross-species translational pharmacokinetic-pharmacodynamic evaluation of core body temperature reduction by the TRPM8 blocker PF-05105679. *Eur J Pharm Sci* **109S**:S161–S167.

Gozlan H, Laporte AM, Thibault S, Schechter LE, Bolaños F, and Hamon M (1994) Differential effects of N-ethoxycarbonyl-2-ethoxy-1,2-dihydroquinoline (EEDQ) on various 5-HT receptor binding sites in the rat brain. *Neuropharmacology* **33**:423–431.

Greathouse B, Zahra F, and Brady MF(2021) Acetylcholinesterase inhibitors toxicity, in *StatPearls*, Treasure Island, FL.

Green AR, Gabrielsson J, and Fone KC (2011) Translational neuropharmacology and the appropriate and effective use of animal models. *Br J Pharmacol* **164**:1041–1043.

Grimwood S and Hartig PR (2009) Target site occupancy: emerging generalizations from clinical and preclinical studies. *Pharmacol Ther* **122**:281–301.

Hamblin MW and Creese I (1983) Behavioral and radioligand binding evidence for irreversible dopamine receptor blockade by N-ethoxycarbonyl-2-ethoxy-1,2-dihydroquinoline. *Life Sci* **32**:2247–2255.

Hamilton CA, Dalrymple HW, Reid JL, and Sumner DJ (1984) The recovery of alpha-adrenoceptor function and binding sites after phenoxybenzamine. An index of receptor turnover? *Naunyn Schmiedebergs Arch Pharmacol* **325**:34–41.

Hamilton CA and Reid JL (1985) The effects of phenoxybenzamine on specific binding and function of central alpha-adrenoceptors in the rabbit. *Brain Res* **344**:89–95.

Hauser AS, Attwood MM, Rask-Andersen M, Schiöth HB, and Gloriam DE (2017) Trends in GPCR drug discovery: new agents, targets and indications. *Nat Rev Drug Discov* **16**:829–842.

Held F, Hoppe E, Cvijovic M, Jirstrand M, and Gabrielsson J (2019) Challenge model of TNFₐ turnover at varying LPS and drug provocations. *J Pharmacokinet Pharmacodyn* **46**:223–240.

Hess CN, Low Wang CC, and Hiatt WR (2018) PCSK9 inhibitors: Mechanisms of action, metabolic effects, and clinical outcomes. *Annu Rev Med* **69**:133–145.

Hinze C, Harland D, Zreika M, Dulery B, and Hardenberg J (1990) A double-blind, placebo-controlled study of the tolerability and effects on platelet MAO-B activity of single oral doses of MDL 72.974A in normal volunteers. *J Neural Transm Suppl* **32**:203–209.

Holford N and Nutt JG (2008) Disease progression, drug action and Parkinson's disease: why time cannot be ignored. *Eur J Clin Pharmacol* **64**:207–216.

Hong Y, Gengo FM, Rainka MM, Bates VE, and Mager DE (2008) Population pharmacodynamic modelling of aspirin- and Ibuprofen-induced inhibition of platelet aggregation in healthy subjects. *Clin Pharmacokinet* **47**:129–137.

Hothersall JD, Brown AJ, Dale I, and Rawlins P (2016) Can residence time offer a useful strategy to target agonist drugs for sustained GPCR responses? *Drug Discov Today* **21**:90–96.

Hoyer D and Boddeke HW (1993) Partial agonists, full agonists, antagonists: dilemmas of definition. *Trends Pharmacol Sci* **14**:270–275.

Hu Y, Ingelman-Sundberg M, and Lindros KO (1995) Induction mechanisms of cytochrome P450 2E1 in liver: interplay between ethanol treatment and starvation. *Biochem Pharmacol* **50**:155–161.

Igawa T, Ishii S, Tachibana T, Maeda A, Higuchi Y, Shimaoka S, Moriyama C, Watanabe T, Takubo R, Doi Y, et al. (2010) Antibody recycling by engineered pH-dependent antigen binding improves the duration of antigen neutralization. *Nat Biotechnol* **28**:1203–1207.

Ito K, Asakura A, Yamada Y, Nakamura K, Sawada Y, and Iga T (1997) Prediction of the therapeutic dose for benzodiazepine anxiolytics based on receptor occupancy theory. *Biopharm Drug Dispos* **18**:293–303.

Jacobs JR, Reves JG, Marty J, White WD, Bai SA, and Smith LR (1995) Aging increases pharmacodynamic sensitivity to the hypnotic effects of midazolam. *Anesth Analg* **80**:143–148.

Jann MW (2000) Rivastigmine, a new-generation cholinesterase inhibitor for the treatment of Alzheimer's disease. *Pharmacotherapy* **20**:1–12.

Jansson-Löfmark R, Hjorth S, and Gabrielsson J (2020) Does in vitro potency predict clinically efficacious concentrations? *Clin Pharmacol Ther* **108**:298–305.

Jordan S, Regardie K, Johnson JL, Chen R, Kambayashi J, McQuade R, Kitagawa H, Tadori Y, and Kikuchi T (2007) In vitro functional characteristics of dopamine D2 receptor partial agonists in second and third messenger-based assays of cloned human dopamine D2Long receptor signalling. *J Psychopharmacol* **21**:620–627.

Joyce AR, Easterling K, Holtzman SG, and Kuhar MJ (2006) Modeling the onset of drug dependence: a consideration of the requirement for protein synthesis. *J Theor Biol* **240**:531–537.

Kalvass JC, Olson ER, Cassidy MP, Selley DE, and Pollack GM (2007) Pharmacokinetics and pharmacodynamics of seven opioids in P-glycoprotein-competent mice: assessment of unbound brain EC50,u and correlation of in vitro, preclinical, and clinical data. *J Pharmacol Exp Ther* **323**:346–355.

Kang YJ, Mbonye UR, DeLong CJ, Wada M, and Smith WL (2007) Regulation of intracellular cyclooxygenase levels by gene transcription and protein degradation. *Prog Lipid Res* **46**:108–125.

Keck BJ and Lakoski JM (1996b) Region-specific serotonin1A receptor turnover following irreversible blockade with EEDQ. *Neuroreport* **7**:2717–2721.

Keck BJ and Lakoski JM (2000) Regional heterogeneity of serotonin(1A) receptor inactivation and turnover in the aging female rat brain following EEDQ. *Neuropharmacology* **39**:1237–1246.

Keck J and Lakoski JM (1996a) Age-related assessment of central 5-HT1A receptors following irreversible inactivation by N-ethoxycarbonyl-2-ethoxy-1,2-dihydroquinoline (EEDQ). *Brain Res* **728**:130–134.

Kenakin T (2013) New concepts in pharmacological efficacy at 7TM receptors: IUPHAR review 2. *Br J Pharmacol* **168**:554–575.

Kenakin T (2016) The mass action equation in pharmacology. *Br J Clin Pharmacol* **81**:41–51.

Kenakin T (2018) *A Pharmacology Primer: Techniques for More Effective and Strategic Drug Discovery*, Academic Press, Amsterdam.

Kenakin TP (2017) *Pharmacology in Drug Discovery and Development*, Academic Press.

Khan DD (2016) Pharmacokinetic-Pharmacodynamic modeling and prediction of antibiotic effects. Ph.D. thesis. Uppsala University, Uppsala, Sweden.

Kimmel HL, Carroll FI, and Kuhar MJ (2000) Dopamine transporter synthesis and degradation rate in rat striatum and nucleus accumbens using RTI-76. *Neuropharmacology* **39**:578–585.

Kimmel HL, Carroll FI, and Kuhar MJ (2003) Withdrawal from repeated cocaine alters dopamine transporter protein turnover in the rat striatum. *J Pharmacol Exp Ther* **304**:15–21.

Kleiber M (1947) Body size and metabolic rate. *Physiol Rev* **27**:511–541.

Kroon T, Baccega T, Olsén A, Gabrielsson J, and Oakes ND (2017) Nicotinic acid timed to feeding reverses tissue lipid accumulation and improves glucose control in obese Zucker rats. *J Lipid Res* **58**:31–41.

Kuhar MJ (2009) On the use of protein turnover and half-lives. *Neuropsychopharmacology* **34**:1172–1173.

Kuhar MJ and Joyce AR (2001) Slow onset of CNS drugs: can changes in protein concentration account for the delay? *Trends Pharmacol Sci* **22**:450–456.

Kuhar MJ and Joyce AR (2003) Is the onset of psychoactive drug effects compatible with a protein-synthesis mechanism? *Neuropsychopharmacology* **28** (Suppl 1):S94–S97.

Kula NS, George T, and Baldessarini RJ (1992) Rate of recovery of D1 and D2 dopaminergic receptors in young vs. adult rat striatal tissue following alkylation with ethoxycarbonyl-ethoxy-dihydroquinoline (EEDQ). *Brain Res Dev Brain Res* **66**:286–289.

Kwon D, Chae JB, Park CW, Kim YS, Lee SM, Kim EJ, Huh IH, Kim DY, and Cho KD (2001) Effects of IY-81149, a newly developed proton pump inhibitor, on gastric acid secretion in vitro and in vivo. *Arzneimittelforschung* **51**:204–213.

Lappe-Siefke C, Loebrich S, Hevers W, Waidmann OB, Schweizer M, Fehr S, Fritschy JM, Dikic I, Eilers J, Wilson SM, et al. (2009) The ataxia (axJ) mutation causes abnormal GABAA receptor turnover in mice. *PLoS Genet* **5**:e1000631.

Larsson J, Hoppe E, Gautrois M, Cvijovic M, and Jirstrand M (2021) Second-generation TNFα turnover model for improved analysis of test compound interventions in LPS challenge studies. *Eur J Pharm Sci* **165**:105937.

Lee JH, Jeong SK, Kim BC, Park KW, and Dash A (2015) Donepezil across the spectrum of Alzheimer's disease: dose optimization and clinical relevance. *Acta Neurol Scand* **131**:259–267.

Leff SE, Gariano R, and Creese I (1984) Dopamine receptor turnover rates in rat striatum are age-dependent. *Proc Natl Acad Sci USA* **81**:3910–3914.

Lévesque D and Di Paolo T (1991) Dopamine receptor reappearance after irreversible receptor blockade: effect of chronic estradiol treatment of ovariectomized rats. *Mol Pharmacol* **39**:659–665.

Levy G (1998) Predicting effective drug concentrations for individual patients. Determinants of pharmacodynamic variability. *Clin Pharmacokinet* **34**:323–333.

Li X, Jusko WJ, and Cao Y (2018) Role of interstitial fluid turnover on target suppression by therapeutic biologics using a minimal physiologically based pharmacokinetic model. *J Pharmacol Exp Ther* **367**:1–8.

Li Z, Radin A, Li M, Hamilton JD, Kajiwara M, Davis JD, Takahashi Y, Hasegawa S, Ming JE, DiCioccio AT, et al. (2020) Pharmacokinetics, pharmacodynamics, safety, and tolerability of dupilumab in healthy adult subjects. *Clin Pharmacol Drug Dev* **9**:742–755.

Liang J, Zbieg JR, Blake RA, Chang JH, Daly S, DiPasquale AG, Friedman LS, Gelzleichter T, Gill M, Giltnane JM, et al. (2021) GDC-9545 (giredestrant): a potent and orally bioavailable selective estrogen receptor antagonist and degrader with an exceptional preclinical profile for ER+ breast cancer. *J Med Chem* **64**:11841–11856.

Lin JH (1991) Pharmacokinetic and pharmacodynamic properties of histamine H2-receptor antagonists. Relationship between intrinsic potency and effective plasma concentrations. *Clin Pharmacokinet* **20**:218–236.

Lu H and Tonge PJ (2010) Drug-target residence time: critical information for lead optimization. *Curr Opin Chem Biol* **14**:467–474.

Lynch CJ, Deth RC, and Steer ML (1983) Simultaneous loss and reappearance of alpha 1-adrenergic responses and [3H]prazosin binding sites in rat liver after irreversible blockade by phenoxybenzamine. *Biochim Biophys Acta* **757**:156–163.

Lyons HR, Gibbs TT, and Farb DH (2000) Turnover and down-regulation of GABA(A) receptor alpha1, beta2S, and gamma1 subunit mRNAs by neurons in culture. *J Neurochem* **74**:1041–1048.

Mager DE, Woo S, and Jusko WJ (2009) Scaling pharmacodynamics from in vitro and preclinical animal studies to humans. *Drug Metab Pharmacokinet* **24**:16–24.

Magnusson MO, Dahl ML, Cederberg J, Karlsson MO, and Sandström R (2008) Pharmacodynamics of carbamazepine-mediated induction of CYP3A4, CYP1A2, and Pgp as assessed by probe substrates midazolam, caffeine, and digoxin. *Clin Pharmacol Ther* **84**:52–62.

Marshall JW, Cummings RM, Bowes LJ, Ridley RM, and Green AR (2003) Functional and histological evidence for the protective effect of NXY-059 in a primate model of stroke when given 4 hours after occlusion. *Stroke* **34**:2228–2233.

Mateos-Aparicio P and Rodríguez-Moreno A (2019) The Impact of Studying Brain Plasticity. *Front Cell Neurosci* **13**:66.

Mbonye UR, Wada M, Rieke CJ, Tang HY, Dewitt DL, and Smith WL (2006) The 19-amino acid cassette of cyclooxygenase-2 mediates entry of the protein into the endoplasmic reticulum-associated degradation system. *J Biol Chem* **281**:35770–35778.

McKernan RM and Campbell IC (1982) Measurement of alpha-adrenoceptor "turnover' using phenoxybenzamine. *Eur J Pharmacol* **80**:279–280.

Mestas J and Hughes CC (2004) Of mice and not men: differences between mouse and human immunology. *J Immunol* **172**:2731–2738.

Michaelis L and Menten ML (1913) Die Kinetik der Invertinwirkung. *Biochem Z* **49**:333–369.

Michaelis L, Menten ML, Johnson KA, and Goody RS (2011) The original Michaelis constant: translation of the 1913 Michaelis-Menten paper. *Biochemistry* **50**:8264–8269.

Miida H, Arakawa S, Shibaya Y, Honda K, Kiyosawa N, Watanabe K, Manabe S, Takasaki W, and Ueno K (2008) Toxicokinetic and toxicodynamic analysis of clofibrate based on free drug concentrations in nagase analbuminemia rats (NAR). *J Toxicol Sci* **33**:349–361.

Miller LG, Lumpkin M, Galpern WR, Greenblatt DJ, and Shader RI (1991a) Modification of gamma-aminobutyric acidA receptor binding and function by N-ethoxycarbonyl-2-ethoxy-1,2-dihydroquinoline in vitro and in vivo: effects of aging. *J Neurochem* **56**:1241–1247.

Miller LG, Lumpkin M, Greenblatt DJ, and Shader RI (1991b) Accelerated benzodiazepine receptor recovery after lorazepam discontinuation. *FASEB J* **5**:93–97.

Morey TM, Esmaeili MA, Duennwald ML, and Rylett RJ (2021) SPAAC Pulse-Chase: A novel click chemistry-based method to determine the half-life of cellular proteins. *Front Cell Dev Biol* **9**:722560.

Morissette M, Lévesque D, and Di Paolo T (1992) Effect of chronic estradiol treatment on brain dopamine receptor reappearance after irreversible blockade: an autoradiographic study. *Mol Pharmacol* **42**:480–488.

Moss DE, Perez RG, and Kobayashi H (2017) Cholinesterase inhibitor therapy in Alzheimer's Disease: The limits and tolerability of irreversible CNS-selective acetylcholinesterase inhibition in primates. *J Alzheimers Dis* **55**:1285–1294.

Mouton JW, Muller AE, Canton R, Giske CG, Kahlmeter G, and Turnidge J (2018) MIC-based dose adjustment: facts and fables. *J Antimicrob Chemother* **73**:564–568.

Mullard A (2021) Targeted protein degraders crowd into the clinic. *Nat Rev Drug Discov* **20**:247–250.

Nagashima R, O'Reilly RA, and Levy G (1969) Kinetics of pharmacologic effects in man: the anticoagulant action of warfarin. *Clin Pharmacol Ther* **10**:22–35.

Nelson CA, Muther TF, Pitha J, and Baker SP (1986) Differential recovery of beta adrenoreceptor antagonist and agonist high affinity binding sites in the guinea-pig lung after irreversible blockade. *J Pharmacol Exp Ther* **237**:830–836.

Neubig RR, Spedding M, Kenakin T, and Christopoulos A; International Union of Pharmacology Committee on Receptor Nomenclature and Drug Classification (2003) International Union of Pharmacology Committee on Receptor Nomenclature and Drug Classification. XXXVIII. Update on terms and symbols in quantitative pharmacology. *Pharmacol Rev* **55**:597–606.

Neve KA, Loeschen S, and Marshall JF (1985) Denervation accelerates the reappearance of neostriatal D-2 receptors after irreversible receptor blockade. *Brain Res* **329**:225–231.

Nickerson M and Goodman LS (1947) Pharmacological properties of a new adrenergic blocking agent: N,N-dibenzyl-beta-chloroethylamine (dibenamine). *J Pharmacol Exp Ther* **89**:167–185.

Nilsson P, Hillered L, Pontén U, and Ungerstedt U (1990) Changes in cortical extracellular levels of energy-related metabolites and amino acids following concussive brain injury in rats. *J Cereb Blood Flow Metab* **10**:631–637.

Nilvebrant L, Hallén B, and Larsson G (1997) Tolterodine–a new bladder selective muscarinic receptor antagonist: preclinical pharmacological and clinical data. *Life Sci* **60**:1129–1136.

Norman AB, Battaglia G, and Creese I (1987) Differential recovery rates of rat D2 dopamine receptors as a function of aging and chronic reserpine treatment following irreversible modification: a key to receptor regulatory mechanisms. *J Neurosci* **7**:1484–1491.

Nowak G and Zak J (1989) Repeated electroconvulsive shock (ECS) enhances striatal D-1 dopamine receptor turnover in rats. *Eur J Pharmacol* **167**:307–308.

Nowak G and Zak J (1991a) Effect of repeated treatment with antidepressant drugs and electroconvulsive shock (ECS) on the D2 dopaminergic receptor turnover in the rat brain. *Pharmacol Toxicol* **69**:87–89.

Nowak G and Zak J (1991b) The turnover of rat cortical alpha 1-adrenoceptors is not modified by repeated electroconvulsive treatment. *J Neurochem* **56**: 2004–2006.

Oakes ND, Thalén P, Hultstrand T, Jacinto S, Camejo G, Wallin B, and Ljung B (2005) Tesaglitazar, a dual PPARalpha/gamma agonist, ameliorates glucose and lipid intolerance in obese Zucker rats. *Am J Physiol Regul Integr Comp Physiol* **289**:R938–R946.

Oakes ND, Thalén PG, Jacinto SM, and Ljung B (2001) Thiazolidinediones increase plasma-adipose tissue FFA exchange capacity and enhance insulin-mediated control of systemic FFA availability. *Diabetes* **50**:1158–1165.

Obach RS (2013) Pharmacologically active drug metabolites: impact on drug discovery and pharmacotherapy. *Pharmacol Rev* **65**:578–640.

Oreland L, Jossan SS, Hartvig P, Aquilonius SM, and Långström B (1990) Turnover of monoamine oxidase B (MAO-B) in pig brain by positron emission tomography using 11C-L-deprenyl. *J Neural Transm Suppl* **32**:55–59.

Peletier LA and Gabrielsson J (2012) Dynamics of target-mediated drug disposition: characteristic profiles and parameter identification. *J Pharmacokinet Pharmacodyn* **39**:429–451.

Peletier LA and Gabrielsson J (2018) New equilibrium models of drug-receptor interactions derived from Target-Mediated Drug Disposition. *AAPS J* **20**:69.

Peletier LA and Gabrielsson J (2022) Impact of enzyme turnover on the dynamics of the Michaelis-Menten model. *Math Biosci* **346**:108795.

Peletier LA, Jansson-Löfmark R, and Gabrielsson J (2021) Comparisons of basic target-mediated drug disposition (TMDD) and ligand facilitated target removal (LFTR). *Eur J Pharm Sci* **162**:105835.

Pereira ER, Liao N, Neale GA, and Hendershot LM (2010) Transcriptional and post-transcriptional regulation of proangiogenic factors by the unfolded protein response. *PLoS One* **5**:e12521.

Pich EM, Benfenati F, Farabegoli C, Fuxe K, Meller E, Aronsson M, Goldstein M, and Agnati LF (1987) Chronic haloperidol affects striatal D2-dopamine receptor reappearance after irreversible receptor blockade. *Brain Res* **435**:147–152.

Pineda J, Ruiz-Ortega JA, and Ugedo L (1997) Receptor reserve and turnover of alpha-2 adrenoceptors that mediate the clonidine-induced inhibition of rat locus coeruleus neurons in vivo. *J Pharmacol Exp Ther* **281**:690–698.

Pinto W and Battaglia G (1994) Comparative recovery kinetics of 5-hydroxytryptamine 1A, 1B, and 2A receptor subtypes in rat cortex after receptor inactivation: evidence for differences in receptor production and degradation. *Mol Pharmacol* **46**:1111–1119.

Pitha J, Hughes BA, Kusiak JW, Dax EM, and Baker SP (1982) Regeneration of beta-adrenergic receptors in senescent rats: a study using an irreversible binding antagonist. *Proc Natl Acad Sci USA* **79**:4424–4427.

Planz G, Quiring K, and Palm D (1972a) Rates of recovery of irreversibly inhibited monoamine oxidases: a measure of enzyme protein turnover. *Naunyn Schmiedebergs Arch Pharmacol* **273**:27–42.

Planz G, Quiring K, and Palm D (1972b) Turnover rates of monoamine oxidases: recovery of the irreversibly inhibited enzyme activity and the influence of isoproterenol. *Life Sci I* **11**:147–160.

Powell-Tuck J, Garlick PJ, Lennard-Jones JE, and Waterlow JC (1984) Rates of whole body protein synthesis and breakdown increase with the severity of inflammatory bowel disease. *Gut* **25**:460–464.

Prager EM, Aroniadou-Anderjaska V, Almeida-Suhett CP, Figueiredo TH, Apland JP, Rossetti F, Olsen CH, and Braga MF (2014) The recovery of acetylcholinesterase activity and the progression of neuropathological and pathophysiological alterations in the rat basolateral amygdala after soman-induced status epilepticus: relation to anxiety-like behavior. *Neuropharmacology* **81**:64–74.

Price JC, Guan S, Burlingame A, Prusiner SB, and Ghaemmaghami S (2010) Analysis of proteome dynamics in the mouse brain. *Proc Natl Acad Sci USA* **107**:14508–14513.

Raffa RB, Pawasauskas J, Pergolizzi JV Jr, Lu L, Chen Y, Wu S, Jarrett B, Fain R, Hill L, and Devarakonda K (2018) Pharmacokinetics of oral and intravenous paracetamol (acetaminophen) when co-administered with intravenous morphine in healthy adult subjects. *Clin Drug Investig* **38**:259–268.

Raghupathi RK, Artymyshyn R, and McGonigle P (1996b) Regional variability in changes in 5-HT2A receptor mRNA levels in rat brain following irreversible inactivation with EEDQ. *Brain Res Mol Brain Res* **39**:198–206.

Raghupathi RK, Brousseau DA, and McGonigle P (1996a) Time-course of recovery of 5-HT1A receptors and changes in 5-HT1A receptor mRNA after irreversible inactivation with EEDQ. *Brain Res Mol Brain Res* **38**:233–242.

Ramsay RR and Tipton KF (2017) Assessment of enzyme inhibition: a review with examples from the development of monoamine oxidase and cholinesterase inhibitory drugs. *Molecules* **22**:1192.

Ramsden D, Zhou J, and Tweedie DJ (2015) Determination of a degradation constant for CYP3A4 by direct suppression of mRNA in a novel human hepatocyte model, HepatoPac. *Drug Metab Dispos* **43**:1307–1315.

Rask-Andersen M, Almén MS, and Schiöth HB (2011) Trends in the exploitation of novel drug targets. *Nat Rev Drug Discov* **10**:579–590.

Régo JC, Syringas M, Leblond B, Costentin J, and Bonnet JJ (1999) Recovery of dopamine neuronal transporter but lack of change of its mRNA in substantia nigra after inactivation by a new irreversible inhibitor characterized in vitro and ex vivo in the rat. *Br J Pharmacol* **128**:51–60.

Ribas C, Miralles A, Busquets X, and García-Sevilla JA (2001) Brain alpha(2)-adrenoceptors in monoamine-depleted rats: increased receptor density, G coupling proteins, receptor turnover and receptor mRNA. *Br J Pharmacol* **132**:1467–1476.

Ribas C, Miralles A, Escribá PV, and García-Sevilla JA (1998) Effects of the alkylating agent EEDQ on regulatory G proteins and recovery of agonist and antagonist alpha2-adrenoceptor binding sites in rat brain. *Eur J Pharmacol* **351**:145–154.

Ribas C, Miralles A, and García-Sevilla JA (1993) Acceleration by chronic treatment with clorgyline of the turnover of brain alpha 2-adrenoceptors in normotensive but not in spontaneously hypertensive rats. *Br J Pharmacol* **110**:99–106.

Richardson K and Rose SP (1971) A diurnal rhythmicity in incorporation of lysine into rat brain regions. *Nat New Biol* **233**:182–184.

Rolan PE (1994) Plasma protein binding displacement interactions–why are they still regarded as clinically important? *Br J Clin Pharmacol* **37**:125–128.

Rostami-Hodjegan A (2010) Translation of in vitro metabolic data to predict in vivo drug-drug interactions: IVIVE and Modeling and Simulation, in *Enzyme- and Transporter-Based Drug-Drug Interactions: Progress and Future Challenges* (Pang PS, Rodrigues AD, and Peter RM, eds) pp 317–341, Springer, New York.

Rostami-Hodjegan A, Wolff K, Hay AW, Raistrick D, Calvert R, and Tucker GT (1999) Population pharmacokinetics of methadone in opiate users: characterization of time-dependent changes. *Br J Clin Pharmacol* **48**:43–52.

Rowland M and Tozer TN (2011) *Clinical Pharmacokinetics and Pharmacodynamics: Concepts and Applications*, Wolters Kluwer/Lippincott Williams & Wilkins, Philadelphia.

Ryazanov AG and Nefsky BS (2002) Protein turnover plays a key role in aging. *Mech Ageing Dev* **123**:207–213.

Saber H, Simpson N, Ricks TK, and Leighton JK (2019) An FDA oncology analysis of toxicities associated with PBD-containing antibody-drug conjugates. *Regul Toxicol Pharmacol* **107**:104429.

Saganuwan SA (2021) Application of modified Michaelis - Menten equations for determination of enzyme inducing and inhibiting drugs. *BMC Pharmacol Toxicol* **22**:57.

Sarkar CA, Lowenhaupt K, Horan T, Boone TC, Tidor B, and Lauffenburger DA (2002) Rational cytokine design for increased lifetime and enhanced potency using pH-activated "histidine switching". *Nat Biotechnol* **20**:908–913.

Savage VM, Allen AP, Brown JH, Gillooly JF, Herman AB, Woodruff WH, and West GB (2007) Scaling of number, size, and metabolic rate of cells with body size in mammals. *Proc Natl Acad Sci USA* **104**:4718–4723.

Schmidt-Nielsen K (1984) *Scaling: Why is animal size so important?* Cambridge University Press, Cambridge, UK.

Sher E and Clementi F (1984) Effect of specific antibodies on acetylcholine receptor turnover: increased degradation controls low density of cell surface receptor. *Neurology* **34**:208–211.

Simon GM, Niphakis MJ, and Cravatt BF (2013) Determining target engagement in living systems. *Nat Chem Biol* **9**:200–205.

Singh K, Hotchkiss KM, Mohan AA, Reedy JL, Sampson JH, and Khasraw M (2021) For whom the T cells troll? Bispecific T-cell engagers in glioblastoma. *J Immunother Cancer* **9**:e003679.

Sladeczek F and Bockaert J (1983) Turnover in vivo of alpha 1-adrenergic receptors in rat submaxillary glands. *Mol Pharmacol* **23**:282–288.

Smith DA, Di L, and Kerns EH (2010) The effect of plasma protein binding on in vivo efficacy: misconceptions in drug discovery. *Nat Rev Drug Discov* **9**:929–939.

Smith DA, van Waterschoot RAB, Parrott NJ, Olivares-Morales A, Lavé T, and Rowland M (2018) Importance of target-mediated drug disposition for small molecules. *Drug Discov Today* **23**:2023–2030.

Song Y, Jeong H, Kim SR, Ryu Y, Baek J, Kwon J, Cho H, Kim KN, and Lee JJ (2021) Dissecting the impact of target-binding kinetics of protein binders on tumor localization. *iScience* **24**:102104.

Sosa-Hernández JE, Villalba-Rodríguez AM, Romero-Castillo KD, Aguilar-Aguila-Isaías MA, García-Reyes IE, Hernández-Antonio A, Ahmed I, Sharma A, Parra-Saldívar R, and Iqbal HMN (2018) Organs-on-a-chip module: A review from the development and applications perspective. *Micromachines (Basel)* **9**:536.

Spector IM (1974) Animal longevity and protein turnover rate. *Nature* **249**:66.

Sriram K and Insel PA (2018) G Protein-Coupled Receptors as targets for approved drugs: How many targets and how many drugs? *Mol Pharmacol* **93**:251–258.

Stahl SM (2017) Neuronal traffic signals in tardive dyskinesia: not enough "stop" in the motor striatum. *CNS Spectr* **22**:427–434.

Steindl D, Boehmerle W, Körner R, Praeger D, Haug M, Nee J, Schreiber A, Scheibe F, Demin K, Jacoby P, et al. (2021) Novichok nerve agent poisoning. *Lancet* **397**:249–252.

Stephenson RP (1956) A modification of receptor theory. *Br J Pharmacol Chemother* **11**:379–393.

Swovick K, Welle KA, Hryhorenko JR, Seluanov A, Gorbunova V, and Ghaemmaghami S (2018) Cross-species comparison of proteome turnover kinetics. *Mol Cell Proteomics* **17**:580–591.

Sykes DA and Charlton SJ (2012) Slow receptor dissociation is not a key factor in the duration of action of inhaled long-acting β2-adrenoceptor agonists. *Br J Pharmacol* **165**:2672–2683.

Sykes DA, Dowling MR, Leighton-Davies J, Kent TC, Fawcett L, Renard E, Trifilieff A, and Charlton SJ (2012) The Influence of receptor kinetics on the onset and duration of action and the therapeutic index of NVA237 and tiotropium. *J Pharmacol Exp Ther* **343**:520–528.

Tang Y and Cao Y (2021) Modeling pharmacokinetics and pharmacodynamics of therapeutic antibodies: progress, challenges, and future directions. *Pharmaceutics* **13**:1423.

Taouis M, Berlan M, and Lafontan M (1987) Alpha 2-adrenergic receptor turnover in adipose tissue and kidney: irreversible blockade of alpha 2-adrenergic receptors by benextramine. *Mol Pharmacol* **31**:89–96.

Thompson IA, de Vries EFJ, and Sommer IEC (2020) Dopamine D2 up-regulation in psychosis patients after antipsychotic drug treatment. *Curr Opin Psychiatry* **33**:200–205.

Thürmann PA (2020) Pharmacodynamics and pharmacokinetics in older adults. *Curr Opin Anaesthesiol* **33**:109–113.

Trifirò G and Spina E (2011) Age-related changes in pharmacodynamics: focus on drugs acting on central nervous and cardiovascular systems. *Curr Drug Metab* **12**:611–620.

Tumer N, Scarpace PJ, and Lowenthal DT (1992) Geriatric pharmacology: basic and clinical considerations. *Annu Rev Pharmacol Toxicol* **32**:271–302.

Turnheim K (2003) When drug therapy gets old: pharmacokinetics and pharmacodynamics in the elderly. *Exp Gerontol* **38**:843–853.

van Waterschoot RAB, Parrott NJ, Olivares-Morales A, Lavé T, Rowland M, and Smith DA (2018) Impact of target interactions on small-molecule drug disposition: an overlooked area. *Nat Rev Drug Discov* **17**:299.

Vane JR and Botting RM (2003) The mechanism of action of aspirin. *Thromb Res* **110**:255–258.

Vauquelin G (2010) Rebinding: or why drugs may act longer in vivo than expected from their in vitro target residence time. *Expert Opin Drug Discov* **5**:927–941.

Vauquelin G and Charlton SJ (2010) Long-lasting target binding and rebinding as mechanisms to prolong in vivo drug action. *Br J Pharmacol* **161**:488–508.

Vicentic A, Battaglia G, Carroll FI, and Kuhar MJ (1999) Serotonin transporter production and degradation rates: studies with RTI-76. *Brain Res* **841**:1–10.

Vinod KY, Subhash MN, and Srinivas BN (2001) Differential protection and recovery of 5-HT1A receptors from N-ethoxycarbonyl-2-ethoxy-1,2-dihydroquinoline (EEDQ) inactivation in regions of rat brain. *Neurochem Res* **26**:113–120.

Visser SA, Huntjens DR, van der Graaf PH, Peletier LA, and Danhof M (2003) Mechanism-based modeling of the pharmacodynamic interaction of alphaxalone and midazolam in rats. *J Pharmacol Exp Ther* **307**:765–775.

von Bahr C, Steiner E, Koike Y, and Gabrielsson J (1998) Time course of enzyme induction in humans: effect of pentobarbital on nortriptyline metabolism. *Clin Pharmacol Ther* **64**:18–26.

Wallmark B, Lorentzon P, and Larsson H (1985) The mechanism of action of omeprazole–a survey of its inhibitory actions in vitro. *Scand J Gastroenterol Suppl* **108**:37–51.

Wang H, Shao F, Liu X, Xu W, Ou N, Qin X, Liu F, Hou X, Hu H, and Jiang J (2019) Efficacy, safety and pharmacokinetics of ilaprazole infusion in healthy subjects and patients with esomeprazole as positive control. *Br J Clin Pharmacol* **85**:2547–2558.

Wanwimolruk S and Levy G (1987) Effect of age on the pharmacodynamics of phenobarbital and ethanol in rats. *J Pharm Sci* **76**:503–507.

Waterlow JC (1984) Protein turnover with special reference to man. *Q J Exp Physiol* **69**:409–438.

Waters S, Svensson P, Kullingsjö J, Pontén H, Andreasson T, Sunesson Y, Ljung E, Sonesson C, and Waters N (2017) In Vivo Systems Response Profiling and Multivariate Classification of CNS Active Compounds: A Structured Tool for CNS Drug Discovery. *ACS Chem Neurosci* **8**:785–797.

Webster L, Gudin J, Raffa RB, Kuchera J, Rauck R, Fudin J, Adler J, and Mallick-Searle T (2020) Understanding buprenorphine for use in chronic pain: Expert opinion. *Pain Med* **21**:714–723.

Wenthold RJ, Mahler HR, and Moore WJ (1974) The half-life of acetylcholinesterase in mature rat brain. *J Neurochem* **22**:941–943.

Wu QJ, Sun X, Teves L, Mayor D, and Tymianski M (2022) Mice and rats exhibit striking inter-species differences in gene response to acute stroke. *Cell Mol Neurobio* **42**:2773–2789.

Yocum RR, Rasmussen JR, and Strominger JL (1980) The mechanism of action of penicillin. Penicillin acylates the active site of Bacillus stearothermophilus D-alanine carboxypeptidase. *J Biol Chem* **255**:3977–3986.

Youdim MB and Tipton KF (2002) Rat striatal monoamine oxidase-B inhibition by l-deprenyl and rasagiline: its relationship to 2-phenylethylamine-induced stereotypy and Parkinson's disease. *Parkinsonism Relat Disord* **8**:247–253.

Zanger UM and Schwab M (2013) Cytochrome P450 enzymes in drug metabolism: regulation of gene expression, enzyme activities, and impact of genetic variation. *Pharmacol Ther* **138**:103–141.

Zernig G, Burke T, Lewis JW, and Woods JH (1996) Mechanism of clocinnamox blockade of opioid receptors: evidence from in vitro and ex vivo binding and behavioral assays. *J Pharmacol Exp Ther* **279**:23–31.

Zernig G, Butelman ER, Lewis JW, Walker EA, and Woods JH (1994) In vivo determination of mu opioid receptor turnover in rhesus monkeys after irreversible blockade with clocinnamox. *J Pharmacol Exp Ther* **269**:57–65.

Zhang D, Hop CECA, Patilea-Vrana G, Gampa G, Seneviratne HK, Unadkat JD, Kenny JR, Nagapudi K, Di L, Zhou L, et al. (2019) Drug concentration asymmetry in tissues and plasma for small molecule-related therapeutic modalities. *Drug Metab Dispos* **47**:1122–1135.

Zhou LW, Weiss B, Freilich JS, and Greenberg LH (1984) Impaired recovery of alpha 1- and alpha 2-adrenergic receptors in brain tissue of aged rats. *J Gerontol* **39**:538–546.

Zou LL, Cai ST, and Jin GZ (1996) Chronic treatment with (-)-stepholidine alters density and turnover of D1 and D2 receptors in striatum. *Zhongguo Yao Li Xue Bao* **17**:485–489.